Investigating the role of TELOMERE REPEAT BINDING FACTORS (TRBs) in epigenetic regulatory complexes

Doctoral thesis

for

the award of the doctoral degree

of the Faculty of Mathematics and Natural Sciences

of the University of Cologne

submitted by

Maik Marius Mendler

accepted in the year 2026

1 Table of content

Table 1, List of Abbreviations

ABA	**Ab**scisic **A**cid
ARC	Annotated Research Context
BiFC	**Bi**molecular **F**luorescence **C**omplementation
BP	**B**iological **P**rocess
CC	**C**ellular **C**ompartment
ChIP-Seq	**Ch**romatin **I**mmuno**p**recipitation-**Seq**uencing
DBS	**D**ifferentially **B**ound **S**ites
DEG	**D**ifferentially **E**xpressed **G**ene
DEX	Dexamethasone
EAR	**E**RF-associated **A**mphiphilic **R**epression
FISH	**F**luorescence ***in situ*** **H**ybridization
GFP	**G**reen **F**luorescent **P**rotein
GO	**G**ene **O**ntology
H1/5-like	Histone H1/H5-like
H2AK121ub	Monoubiquitination of Lysine 121 of Histone H2A
H3K27me3	Trimethylation of Lysine 27 of Histone H3
H3K36me3	Trimethylation of Lysine 36 of Histone H3
H3K4me3	Trimethylation of Lysine 4 of Histone H3
H3S28P	Phosphorylation of Serin 28 of Histone H3
H4K5ac	Acetylation of Lysine 5 of Histone H4
HDA	**H**istone **Dea**cetylases
IGV	**I**ntegrative **G**enomics **V**iewer
IP-MS	**I**mmuno**p**recipitation coupled with **M**ass **S**pectrometry
LD	**L**ong **D**ay Photoperiod (16 h Light)
LLPS	**L**iquid-**L**iquid **P**hase **S**eparation
MD	**M**id-**D**ay Photoperiod (12 h Light)
MF	**M**olecular **F**unction
NuA4	**Nu**cleosome **A**cetyltransferase of H**4**
p35S	Cauliflower Mosaic Virus 35S promoter
PcG	**P**oly**c**omb **G**roup
PEAT	**P**WWP-**E**PCR-**A**RID-**T**RB Complex
PRC1	**P**olycomb **R**epressive **C**omplex 1
PRC2	**P**olycomb **R**epressive **C**omplex 2
SAGA	**S**pt-**A**da-**G**cn5 **A**cetyltransferase Complex
SMH	**S**ingle **M**yb **H**istone Protein Family
SWR1	**SW**I2/SNF2-**R**elated **1** Chromatin Remodeling Complex
TF	**T**ranscription **F**actor
TINTIN	**T**rimer **I**ndependent of **N**uA4 involved in **T**ranscription **I**nteractions with **N**ucleosomes
TRHD	**TR**B1/2/3-**H**ISTONE-**D**EMETHYLASE Complex
TRHT	**TR**B1/2/3-**H**ELIX-**T**URN-HELIX-PROTEIN Complex
UTR	**Un**translated **R**egion
WT	Wild-Type (Col-0 for *Arabidopsis thaliana*)
Y2H	**Y**east **Two**-**H**ybrid

Abstract

In plants, gene expression is tightly controlled through multiple epigenetic regulatory complexes that establish, modify, and maintain the epigenetic landscape. Many of these complexes rely on DNA-binding proteins for motif-specific genomic site recognition. In *Arabidopsis thaliana* these proteins include five paralogs of TELOMERE REPEAT BINDING FACTORs (TRBs). TRBs serve as transcription factors guiding epigenetic regulatory complexes to telo-box DNA motifs. Remarkably, TRBs were found to interact with both the repressive Polycomb Repressive Complex 2 (PRC2) as well as the activating PEAT complex. Recently, it was found that both complexes can act in a bi-functional manner, modulating the epigenetic landscape through two respective behaviors: repression-coupled with deactivation for PRC2, and activation coupled with the removal of repression for PEAT.

Using protein-protein interaction data generated in our lab, I investigated whether TRBs are involved in additional bi-functional epigenetic regulatory complexes. I hypothesized the existence of a complex containing PRC2, TRBs, a novel group of proteins named UTIs, and the histone demethylase ICU11. Through CRISPR-Cas9 mediated mutagenesis I generated multiple loss-of-function mutants of *UTI1* in different *trb* backgrounds, exhibiting various flowering time phenotypes. I subsequently employed transcriptomics and ChIP-Seq to further investigate these mutants and uncovered further evidence of the connection between TRBs and ICU11.

This work includes one submitted manuscript I co-authored. For this study, I contributed an analysis of eleven ChIP-Seq datasets of various epigenetic regulatory proteins. We showed that TRBs also participate in the activating NuA4 complex, as well as an undescribed repressive JMJ14-containing complex. Furthermore, we showed that these epigenetic regulatory complexes appear to be largely mutually exclusive at their genomic binding sites. Lastly, we discovered that three TRB paralogs, previously thought to be redundant, exhibit divergent molecular behavior. In addition to their differing DNA-binding affinities and enriched DNA-motifs, they also appear to favor different epigenetic regulatory complexes.

Overall, this work offers insight into the role of TRBs in epigenetic gene regulation, provides evidence of TRBs participating in at least two additional regulatory complexes, and disproves the notion of perfect redundancy between TRB paralogs.

Zusammenfassung

In Pflanzen wird die Genexpression durch mehrere epigenetische Regulationskomplexe streng kontrolliert, welche die epigenetische Landschaft aufbauen, modifizieren und aufrechterhalten. Viele dieser Komplexe sind auf DNA-bindende Proteine angewiesen, um bestimmte Motive im Genom zu erkennen. In *Arabidopsis thaliana* gehören zu diesen Proteinen fünf Paraloge der TELOMERE REPEAT BINDING FACTORS (TRBs). TRBs dienen als Transkriptionsfaktoren, die epigenetische Regulationskomplexe zu Telo-Box-DNA-Motive rekrutieren. Bemerkenswerterweise wurde festgestellt, dass TRBs sowohl mit dem repressiven Polycomb Repressive Complex 2 (PRC2) als auch mit dem aktivierenden PEAT-Komplex interagieren. Kürzlich wurde entdeckt, dass beide Komplexe bifunktional wirken können und die epigenetische Landschaft durch zwei gleichzeitige Verhaltensweisen verändern: Repression in Verbindung mit Deaktivierung für PRC2 und Aktivierung in Verbindung mit der Aufhebung der Repression für PEAT.

Anhand von Protein-Protein-Interaktionsdaten, die in unserem Labor generiert wurden, untersuchte ich, ob TRBs an weiteren bifunktionalen epigenetischen Regulationskomplexen beteiligt sind. Ich stellte die Hypothese auf, dass es einen Komplex gibt, der PRC2, TRBs, eine neue Gruppe von Proteinen namens UTIs und die Histon-Demethylase ICU11 enthält. Durch CRISPR-Cas9-vermittelte Mutagenese erzeugte ich mehrere Funktionsverlustmutanten von *UTI1* in verschiedenen *trb*-Hintergründen, die verschiedene Blütezeitphänotypen aufwiesen. Anschließend untersuchte ich diese Mutanten mit Hilfe von Transkriptomik und ChIP-Seq weiter und fand zusätzliche Hinweise auf den Zusammenhang zwischen TRBs und ICU11.

Zu dieser Arbeit gehört auch ein eingereichtes Manuskript, das ich mitverfasst habe. Für die Studie habe ich eine Analyse von elf ChIP-Seq-Datensätzen verschiedener epigenetischer Regulationsproteine beigesteuert. Wir haben gezeigt, dass TRBs auch am aktivierenden NuA4-Komplex sowie an einem bisher nicht beschriebenen repressiven Komplex mit JMJ14 beteiligt sind. Darüber hinaus haben wir gezeigt, dass diese epigenetischen Regulationskomplexe an ihren genomischen Bindungsstellen weitgehend gegenseitig exklusiv zu sein scheinen. Abschließend haben wir entdeckt, dass drei TRB-Paraloge, die zuvor als redundant angesehen wurden, ein divergentes molekulares Verhalten aufweisen. Zusätzlich zu ihren unterschiedlichen DNA-Bindungsaffinitäten und angereicherten DNA-Motiven scheinen sie auch unterschiedliche epigenetische Regulationskomplexe zu bevorzugen.

Insgesamt bietet diese Arbeit Einblicke in die Rolle von TRBs bei der epigenetischen Genregulation, liefert Hinweise darauf, dass TRBs an mindestens zwei weiteren Regulationskomplexen beteiligt sind, und widerlegt die Vorstellung einer vollständigen Redundanz zwischen TRB-Paralogen.

1 Introduction

1.1 Epigenetic Regulatory Complexes

In multicellular organisms, all cells share the same DNA. The emergence of specialized cells is therefore controlled not through presence or absence of genes, but through gene expression levels (Campbell 2008). The mechanisms through which gene expression is controlled without changes to the underlying DNA sequence are collectively referred to as epigenetics (Willbanks et al. 2016). The sessile nature of plants, paired with their lifecycle and lack of nervous systems, renders precise control of gene expression particularly vital (Feng and Jacobsen 2011; Pikaard and Mittelsten Scheid 2014). Epigenetic gene regulation plays a crucial part in plant developmental biology, contributing to the remarkable plasticity observed in plant development. (Goodrich et al. 1997; Xiao and Wagner 2015). While epigenetic regulation takes many forms (e.g., DNA methylation or RNA-mediated gene silencing), this work focuses on histone modifications. In line with the precision necessary to control gene expression, the enzymes that control the deposition, recognition, and removal of histone modifications are part of elaborate protein complexes (Tresas et al. 2025) . Each epigenetic regulatory complex recognizes its target sites *via* a combination of DNA-motifs, pre-existing epigenetic marks, and other external signals (Yuan et al. 2016). These factors are collectively referred to as the epigenetic landscape. Additionally, epigenetic regulatory complex complexes often consist of a variety of optional subunits and/or subunits available as multiple paralogs (Baile et al. 2022). These factors lead to a diversity of epigenetic regulatory complexes in plants that is unmatched in other kingdoms of eukaryotes (Pikaard and Mittelsten Scheid 2014).

1.1.1 Polycomb Repressive Complexes

Poly**c**omb **G**roup (PcG) proteins represent one of the most thoroughly studied group of epigenetic regulators in plants (Xiao and Wagner 2015; Pu and Sung 2015; Baile and Calonje 2024; Almeida, Bowness, and Brockdorff 2020; Baile, Gómez-Zambrano, and Calonje 2022). They form two protein complexes: **P**olycomb **R**epressive **C**omplex 1 (PRC1) and **P**olycomb **R**epressive **C**omplex 2 (PRC2). Although the activities of both complexes ultimately lead to gene repression, they deposit different epigenetic marks and only a limited number of accessory proteins is shared between the two (Derkacheva et al. 2013; Calonje et al. 2008).

PRC1

At its target sites, PRC1 is responsible for the deposition of monoubiquitination around lysine 121 of histone H2A (H2AK121ub). This results primarily in gene repression (Bratzel et al. 2010; C. Yang et al. 2013). Like many epigenetic regulatory complexes, PRC1 is conserved across eukaryotic life and was first described in *Drosophila melanogaster* (Shao et al. 1999; Merini and Calonje 2015; Cao, Tsukada, and Zhang 2005). Both in insects and vertebrates, several variant PRC1 complexes are described alongside their canonical PRC1 (Lagarou et al. 2008; de Potter et al. 2023). These canonical PRC1 complexes contain a heterodimer of ring finger proteins as catalytic center. This RING-RING dimer associates with Chromobox protein (CBX) and Polyhomeotic homolog (PHC) to form the complex (de Potter et al. 2023). In plants, direct homologs have only been identified for the catalytically active subunits of PRC1, but not for any of the other canonical components. Therefore, plants appear to only contain variant PRC1 and lack a full canonical PRC1 complex (Baile, Gómez-Zambrano, and Calonje 2022). These plant-specific complexes are made up of a H2A E3 monoubiquitin ligase module (E3 module) paired with a variety of accessory proteins (Figure 1, A). In *Arabidopsis thaliana* five different E3 module proteins have been identified. ARABIDOPSIS THALIANA RING 1A and 1B (RING1A/1B) are homologs to the RING1 protein found in animals (L. Xu and Shen 2008). Conversely, BMI1A, BMI1B, and BMI1C are homologs of BMI1, a different animal monoubiquitin ligase (Merini et al. 2017). The overall number of PRC1 accessory proteins identified in plants is lower than in animals. Among those LIKE-HETEROCHROMATIN PROTEIN 1 (LHP1) and EMBRYONIC FLOWER 1 (EMF1) stand out, as these had been originally described exclusively as parts of PRC1, but have since been implicated in PRC2 complexes as well (Yin et al. 2021; Bloomer et al. 2020; Derkacheva et al. 2013; Y. Zhou, Tergemina, et al. 2017). Other accessory proteins include the transcription factors VIVIPAROUS1/ABI3-LIKE 1 and 2 (VAL1/2), which target PRC1 to RY DNA motifs (CATGCA) (C. Yang et al. 2013; Suzuki, Wang, and McCarty 2007) and ALFIN1-LIKE (AL) proteins. AL proteins bind to the activating trimethylation of lysin 4 of histone 3 mark (H3K4me3), subsequently recruiting PRC1. This allows for modulation of gene expression (L. Peng et al. 2018). While initial research in animals suggested a hierarchy of repressive action, with PRC1 acting downstream of PRC2 (L. Wang et al. 2004), more recent studies indicate that PRC1 and PRC2 can both act independently and recruit each other (Blackledge et al. 2014; Kalb et al. 2014). Overall, it was found that, in plants, PRC1 mainly deposits H2AK121ub close to the transcription start site of genes (Kralemann et al. 2020; Y. Zhou, Romero-Campero, et al. 2017). Unlike PRC2, which deposits unmistakenly repressive marks, the H2AK121ub mark deposited by PRC1 seems to be more expression moderating than repressing (Kralemann et al. 2020). Sites that harbor both PRC

marks were found to be more responsive to quick chromatin state changes than sites exclusively repressed by PRC2 (Yin et al. 2021).

PRC2

PRC2 is mainly responsible for the trimethylation of lysine 27 of histone 3 (H3K27me3), a chromatin mark strongly associated with repression of gene activity (Margueron and Reinberg 2011). In *A. thaliana*, this methylation is catalyzed by one of three paralogous histone methyltransferases: CURLY LEAF (CLF), SWINGER (SWN) or MEDEA (MEA). These enzymes work together with the nucleosome remodeler MULTICOPY SUPPRESSOR OF IRA 1 (MSI1). The nucleosome binding is established by FERTILIZATION-INDEPENDENT ENDOSPERM (FIE). Lastly, the interactions of these core components are facilitated through one of three WD40 proteins: EMBRYONIC FLOWER 2 (EMF2), VERNALIZATION 2 (VRN2) or FERTILIZATION-INDEPENDENT SEED 2 (FIS2) (Reviewed by Mozgova and Hennig (2015) and Godwin and Farrona (2022)). Although the core of PRC2 consists of only four components, the number of paralogs present enables a multitude of different combinations (Figure 1, B). In recent years it has become clear that specific combinations of these components (PRC2 cores), govern different developmental processes (Hinsch et al. 2021; Mozgova, Köhler, and Hennig 2015; Chanvivattana et al. 2004). In addition to these core subunits, a large number of accessory proteins have been identified (Baile, Gómez-Zambrano, and Calonje 2022). Whether these preferentially interact with specific PRC2 cores is largely unknown. As laid out in the previous section, LHP1 and EMF1 were both first described as PRC1 accessories but are now considered to be primarily accessories of PRC2.

The H3K27me3 mark deposited by PRC2 is clearly associated with chromatin compaction and transcription silencing (X. Zhang et al. 2007; Y. Liu et al. 2018). Furthermore, as outlined in the previous chapter, PRC2 can both recruit and be recruited by PRC1, further establishing PcG-mediated gene repression. Despite this, the heterochromatin established by H3K27me3 is considered facultative, as temporal and/or spatial activation of PRC2-controlled genes is common throughout plant development (Charron et al. 2009).

Considering the importance of PRC2 in plant development and its role in establishing facultative heterochromatin, it comes as no surprise that the factors determining PRC2 targeting are multitude (Xiao et al. 2017; Baile et al. 2021; Richter et al. 2019; Y. Wang et al. 2014; Y. Zhou et al. 2018). One such factor is *lncRNAs,* which play a role in PRC2 recruitment (Costa and Dean 2019), including in the recruitment of LHP1. LHP1, in turn, targets PRC2 to sites exhibiting so-called R-loops (Ariel et al. 2020). Alongside *lncRNAs*, targeting of the PRC2 complex is most often mediated by **T**ranscription **F**actors (TFs), since none of the four core components of PRC2 contain DNA-binding domains (Kassis and Brown 2013). To date, multiple different TFs have been

implicated in the recruitment of PRC2 (Baile et al. 2021). Interestingly, the PRC2 recruiting TF VAL1 has also been implicated in the recruitment of PRC1, as well as **H**istone **D**e**a**cetylases (HDAs) (Qüesta et al. 2016).

Among the TFs that have been shown to recruit PRC2 to target loci, TELOMERE REPEAT BINDING FACTOR (TRB) 1-3 stand out. Firstly, while many PRC2-recruiting TFs do not co-purify with the core components of the complex, TRB1 and TRB2 were found to directly interact with CLF and SWN (Krause 2019; Bloomer et al. 2020). Secondly, TRBs do not contain ERF-associated Amphiphilic Repression (EAR)-domains. The EAR-domain is a common motif found in almost all other PRC2 recruiters (Baile et al. 2021). The absence of TRB1-3 leads to strong developmental effects, resembling the most severe viable PRC2 knockout mutant, *clf swn* (Zhou et al. 2018). Recently, the TRB paralogs TRB4 and TRB5 were also described as interactors of CLF and SWN (Amiard et al. 2024). The role of TRBs in PRC2 recruitment is described in more detail in "1.3.2 Involvement of TRBs in Epigenetic Gene Regulation".

Another interesting PRC2 interactor is EMF1. Similarly to LHP1, it had been associated with PRC1 first but appears to be an important interactor of PRC2 (Bloomer et al. 2020). Not only does it interact directly with the histone methylation readers EARLY BOLTING IN SHORT DAYS (EBS) and SHORT LIFE (SHL) (Krause and Turck 2018; Z. Yang et al. 2018; Li et al. 2018), but also with histone demethylases INCURVATA 11 (ICU11) and JUMONJI 14 (JMJ14) (Bloomer et al. 2020; Y. Wang et al. 2014). This could indicate that EMF1 plays a pivotal role in the transition from active to repressive chromatin states.

1.1.1 PEAT-Complex

Another important epigenetic regulatory complex is the so-called PEAT complex. The complex is named after its core components which consists of members of four distinct protein families (Figure 1, C): **P**WWP-DOMAIN INTERACTORs OF POLYCOMB (PWWPs), **E**NHANCER OF POLYCOMB RELATED PROTEINs (EPCRs), **A**T-RICH INTERACTIVE DOMAIN PROTEINs (ARIDs), and **T**RBs (Wilsker et al. 2002; Tan et al. 2018). Among the TRBs, TRB1 and TRB2 were described as mutually exclusive core components of the PEAT complex (Tan et al. 2018), while TRB3 has not been described as a component of PEAT.

Initially, the PEAT complex had been described as both activating and repressing through histone acetylation / de-ubiquitination and histone de-acetylation, respectively (Tsuzuki and Wierzbicki 2018; Tan et al. 2018). More recent studies, however, focus more on its activating effect and have put the role of PEAT in histone de-acetylation into question (Zheng et al. 2023).

Within the PEAT complex, PWWPs are responsible for detecting pre-existing chromatin modifications (Qin and Min 2014), in particular the absence of phosphorylation of serine 28 of histone H3 (H3S28P) (Hohenstatt et al. 2018). Furthermore, recent protein interaction studies have concluded that PWWPs are likely the "center" of PEAT complexes, acting as a scaffold around which the other components aggregate (Zheng et al. 2023; Tan et al. 2018). EPCRs mainly act as recruiters for acetyltransferases, while ARIDs are likely involved in binding of DNA and subsequent chromatin remodeling (Zheng et al. 2023). Similarly, TRBs are probably fulfilling their eponymous role of binding telomeric repeats, targeting the complex towards telo-box motifs (Zheng et al. 2023; Tan et al. 2018). The role of TRBs as TFs and their target DNA motif are described in detail in chapter "1.2 TELOMERE REPEAT BINDING FACTORs (TRBs)".

Like TRBs, the other three core components of the PEAT complex are found in *A. thaliana* not as a single protein, but as multiple paralogs with varying degrees of redundancy (Tan et al. 2018; Mikulski et al. 2019). This plasticity of core components likely contributes to the seemingly contradictory observation that PEATs control both activation and repression in a site-dependent manner.

As part of the PEAT complex, TRBs also contribute to the recruitment of histone modifying enzymes. In particular, the interactions between TRB2/3 and the histone deacetylase HDT4, and the interactions between TRB2 and HISTONE DEACETYLASE 6 (HDA6) have been studied in detail (Lee and Cho 2016). It should, however, be noted that although TRB3 can interact with HDT4, it has not been identified as a part of any known PEAT complex (Tan et al. 2018; Zheng et al. 2023). Conversely, TRB1 and TRB2 have been shown to interact with the MYST family acetyltransferases HAM1/2. This means that TRB2 is the only family member currently known to interact with both histone deacetylases (HDT4 and HDA6) and acetyltransferases (HAM1/2) (Tan et al. 2018; Zheng et al. 2023). TRB1, on the other hand, was found to interact with UBIQUITIN-SPECIFIC PROTEASE 5 (UBP5), although this interaction appears to be facilitated through PWWPs instead of a direct interaction (Zheng et al. 2023). The same study argues that a previously reported interaction of PWWPs with core components of PRC2 (Hohenstatt et al. 2018) can also be traced to a shared binding of UBP5 instead of direct interaction.

In the current working model for PEAT-controlled gene activation, TRB1/2 occupy the role of DNA-binding partners together with ARID2/3/4. In this model, PEAT complexes act primarily as on-switches for establishment of active chromatin through simultaneous HAM1/2-mediated histone acetylation and UBP5-mediated H2A deubiquitylation (Zheng et al. 2023) (Figure 1, C). The exact nature of PEAT-mediated repression is less established but likely includes the activity of HDA6 (Tan et al. 2018).

1.1.2 NuA4-Complex

As the name implies, the primary function of the **Nu**cleosome **A**cetyltransferase of H**4** (NuA4) complex is the acetylation of histone H4 (Espinosa-Cores et al. 2020). The catalytic core of the NuA4 complex found in *A. thaliana* is made up of HAM1/2 (Latrasse et al. 2008). Both enzymes are able acetylate lysine 5 of histone H4, thus depositing the H4K5ac mark (Earley et al. 2007). Consistent with findings in animals and yeast, HAM1 (and presumably HAM2) is also able to acetylate histone H2A and H2A.Z (Bieluszewski et al. 2022).

The multiprotein complex that makes up NuA4 is categorized into four subunits, some of which are able to perform functions independently from the rest. The Piccolo-NuA4 subunit (Figure 1, D) contains the acetyltransferases HAM1/2 and is itself sufficient to perform non-targeted chromatin acetylation in animals, yeast, and plants (Chittuluru et al. 2011; Bieluszewski et al. 2022). In addition to HAM1/2, this subcomplex requires ENHANCER OF POLYCOMB-LIKE 1 A or B (EPL1A/B) (Tan et al. 2018). Based on their homolog in animals and yeast, EPL1A/B likely facilitate interaction with nucleosomes (Chittuluru et al. 2011). INHIBITOR OF GROWTH 1 and 2 (ING1/2) can recognize H3K4me3 and help with positioning the complex (W. Y. Lee et al. 2009; Barrero-Gil et al. 2025). The precise function of the last subcomplex component, ESA1-ASSOCIATED FACTOR 6 (EAF6) has not been elucidated (Espinosa-Cores et al. 2020).

Another subunit that was found to function independently from the others is "**T**rimer **I**ndependent of **N**uA4 involved in **T**ranscription **I**nteractions with **N**ucleosomes" (TINTIN). This subcomplex is made up of MORF RELATED GENE 1 and 2 (MRG1/2), and ESA1-ASSOCIATED FACTOR 7 (EAF7). MRG1 and 2 are chromodomain-carrying histone readers that recognize both H3K4me3 and the trimethylation of lysine 36 of histone 3 (H3K36me3) (M. Peng et al. 2018). The exact role of EAF7 in the plant TINTIN complex has not been elucidated (Espinosa-Cores et al. 2020). It has, however, been implicated in the abscisic acid (ABA) signaling pathway, as a target of SNF1-RELATED PROTEIN KINASE 2 (SnRK2) (Umezawa et al. 2013).

The other two subunits are the assembly platform, which is made up of two structural proteins, as well as the module of proteins that are shared between NuA4 and the **SW**I2/SNF2-**R**elated **1** chromatin remodeling complex (SWR1). Of the proteins assigned to the assembly platform, TRA1A/B are considered to be mostly responsible for the interactions of NuA4 with transcription factors (Knutson and Hahn 2011; Espinosa-Cores et al. 2020) (Figure 1, D).

NuA4 represents one of the most conserved epigenetic regulatory complexes in eukaryotes (X. Xu and He 2025). Similarly to PRC2, NuA4 components are often found in multiple paralogs. This leads to an overall higher diversity of NuA4 components in plants than in animals and yeast

(Espinosa-Cores et al. 2020). Another conserved feature of NuA4 complexes is their high degree of shared components. In yeast, four of the 13 core components of NuA4 are shared with the SWR1 complex, which itself is responsible for the replacement of histone H2A by H2A.Z (Gerhold and Gasser 2014). Similarly, in yeast, Tra1 is shared with the **S**pt-**A**da-**G**cn5 **A**cetyltransferase (SAGA) complex. The SAGA complex also represents a histone acetyltransferase and deubiquitination complex (Helmlinger and Tora 2017). The overlap between NuA4 and SWR1 appears to be conserved in plants (Luo et al. 2020; Crevillén et al. 2019). Furthermore, the inclusion of TRA1A/B in the SAGA complex has also been shown in plants (Wu et al. 2021).

This large number of shared components between NuA4 and other regulatory complexes provides a barrier to traditional genetic screening techniques. The phenotypical effects observed in mutants of NuA4 components cannot easily be linked to the functions of NuA4. Nevertheless, recent research has provided strong evidence that NuA4 is particularly important in the regulation of photosynthesis and plastid development (J.-X. Zhou et al. 2022; Barrero-Gil et al. 2022). In addition to its role as epigenetic regulatory complex, NuA4 also takes part in DNA damage response, although this function has been less thoroughly studied in plants. (Campi et al. 2012).

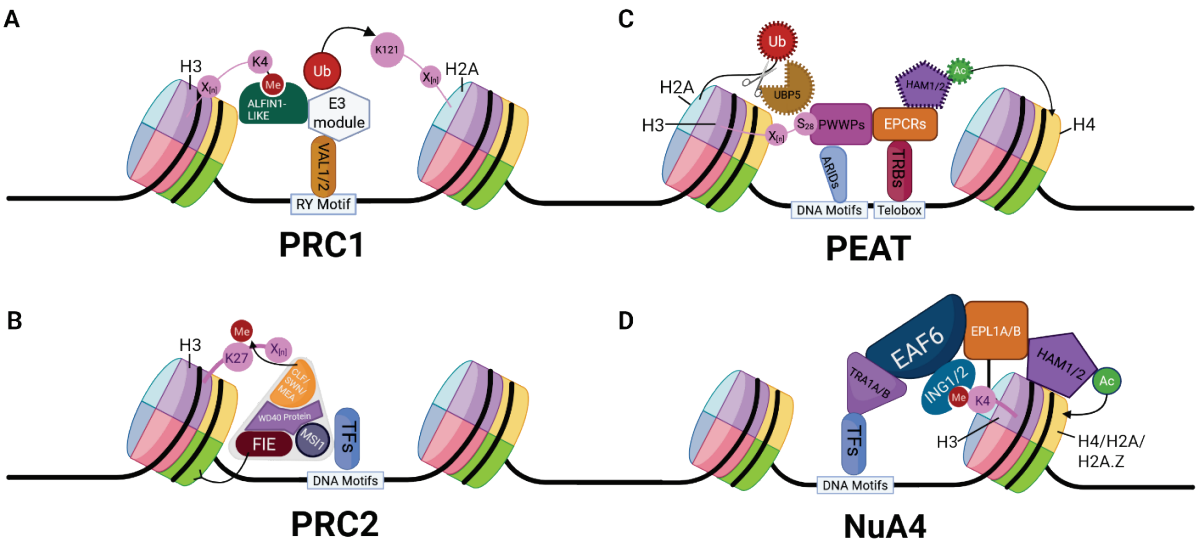

Figure 1, Schematic representation of four epigenetic regulatory complexes. ***A****, PRC1.* ***B****, PRC2. Subsequent depictions summarize the components depicted in the grey outline into a single multi-colored shape.* ***C****, PEAT. Proteins that are not accepted core components of PEAT are depicted with dashed outlines.* ***D****, Piccolo-NuA4 together with TRA1A/B (part of the assembly platform) and TFs. All complexes are depicted as nested between two nucleosomes. Triangle-headed arrows represent deposition of a mark. Scissors indicate removal of a mark. Y-headed arrows depict general interaction with the nucleosome. Relevant histones are labeled and their tales depicted in pink. Marks: Ub, monoubiquitination; Me, (tri-)methylation; Ac, acetylation.*

1.2 TELOMERE REPEAT BINDING FACTORs (TRBs)

The focus of this work lays on TELOMERE REPEAT BINDING FACTORs (TRBs), a group of plant-specific myb-domain containing transcription factors (Hofr et al. 2009). In *A. thaliana* five

TRB paralogs form two clades of three and two paralogs, respectively (Amiard et al. 2024; Kusová et al. 2023), Figure 2, A). Clade one, containing TRB1, TRB2, and TRB3, has been the primary focus of most of the investigations regarding the roles of TRBs (Tan et al. 2018; Zheng et al. 2023; Y. Zhou et al. 2018; Ming Wang et al. 2023b; Y. Zhou et al. 2016; Q. Wang et al. 2025). In recent years clade 2, consisting of TRB4 and TRB5, has also been more closely studied (X. Wang et al. 2025; Amiard et al. 2024; Kusová et al. 2023). Generally, TRBs are notable for their remarkable redundancy within the clades (Y. Zhou et al. 2018; Amiard et al. 2024), as well as their roles in telomere protection and epigenetic gene regulation (P. P. Schrumpfová et al. 2014; Amiard et al. 2024; Y. Zhou et al. 2018; Tan et al. 2018).

Phylogenetically, TRB4 and 5 were found to be closer related to a more ancestral TRB lineage (Figure 2, C). This lineage can be found in Streptophyte algae, Lycophyta and Bryophyta (Kusová et al. 2023). The definite evolutionary origin of TRB proteins, however, could not yet be fully determined (Kusová et al. 2025).

1.2.1 Molecular structure of TRBs

All five TRBs found in *A. thaliana* were first described as members of a novel protein family by Marian et al. (2003). TFs in this family, named **S**ingle **M**yb **H**istone (SMH), consist of three core domains (Figure 2, B): the eponymous N-terminal myb-domain, followed by a histone 1/5-like (H1/5-like) domain, and a C-terminal coiled-coil domain (Marian et al. 2003).

Among these, the myb-domain is responsible for the DNA binding ability of the protein. The domain consists of three imperfect tandem repeats of around 50 bp length which form three characteristic helices. The third of these determines the sequence-specific DNA binding ability of the domain (Ogata et al. 1992; W. K. Lee et al. 2012; Marian et al. 2003). It binds to double-stranded telomeric repeat sequences with slight sequence variations accounting for differences of telomere sequences found in different species (Bilaud et al. 1996; E. Y. Yu et al. 2000; Mozgová et al. 2008). In *A. thaliana* and many other plants, this sequence consists of $[CCCTAAA]_n$ repeats (Richards and Ausubel 1988; Adams et al. 2001). Although TRBs generally share little sequence similarities with proteins of similar function in animals and yeasts (Marian et al. 2003), the myb-domain offers an exception to this. The myb-domain, acting as sequence specific DNA-binding site, constitutes a conserved motif across multicellular life (Rosinski and Atchley 1998). Therefore, it is the domain of TRBs that is most similar to other telomere binding proteins in yeast and animals (Kusová et al. 2023; W. K. Lee et al. 2012). The strong conservation of the myb-domain even allows for plant specific SMH proteins to bind to the human telomere sequence $[TTAGGG]_n$ (Yun et al. 2014; W. K. Lee et al. 2012; Mozgová et al. 2008).

The histone H1/5-like domain appears to be mostly responsible for TRB-TRB interactions and non-sequence-specific DNA binding (P. P. Schrumpfová et al. 2008; Mozgová et al. 2008). It consists of the globular domain of linker histone H5, which is homologous to histone H1 (Ramakrishnan et al. 1993). Furthermore, due to its similarity with linker histones, this domain also contributes to general TRB binding to linker DNA (Bednar et al. 2017; Mozgová et al. 2008).

The final domain found in TRB proteins is the C-terminal coiled-coil domain. Its name derives from the characteristic structure of two or more α-helices wound into coils (Lupas and Gruber 2005). While the histone H1/5-like domain has been primarily implicated in TRB-TRB interactions, the coiled-coil domain was found to be required for the ability of TRB3, but not TRB1, to interact with CLF or SWN (Y. Zhou et al. 2018). Because of this observation, it has been proposed that the coiled-coil domain is involved in many of the protein-protein interactions that TRBs are engaged in (Kusová et al. 2023; Dvorácková et al. 2010). As such, the coiled-coil domain is the most divergent of the three domains and, in *A. thaliana*, each of the two TRB clades is defined by a distinct coiled-coil domain (Amiard et al. 2024) (Figure 2, B). Nevertheless, it has been predicted that the three-dimensional structures of these divergent coiled-coil domains exhibit only minor differences (Kusová et al. 2023).

Shortly after they were first described, the ability of TRB1 to form multimers (both homo- and heterodimers with TRB2 and TRB3) was discovered (Kuchar and Fajkus 2004). In subsequent years, this ability to form multimers has been studied in more detail and it has now become clear that TRB1-3 can form homo- and heterodimers, as well as higher order multimers, among each other (P. Schrumpfová et al. 2004; Mozgová et al. 2008; Hofr et al. 2009). These multimers depend in large part on protein-protein interactions facilitated by the histone H1/5-like domain (P. P. Schrumpfová et al. 2008). Mobility shift electrophoresis indicates that TRB4 and TRB5 are also likely to multimerize, with bimolecular fluorescence complementation (BiFC) analysis suggesting both homo- and heterodimeric interactions with other TRBs (Kusová et al. 2023). This propensity to form multimers is further supported by similar findings for the ancestral TRBs in moss (Kusová et al. 2025). Lastly, all five TRB paralogs have been found in the *A. thaliana* phospho-proteom (Arico et al. 2021). Although TRB4 has only been implicated *in silico* predictions of phosphorylation sites, the other four paralogs were experimentally determined to be phosphorylated *in vivo* (D. Wang et al. 2020; Durek et al. 2010; Yao et al. 2014).

1.2.2 Cellular Localization

The subcellular localization of all TRB paralogs has not been fully elucidated. Literature agrees that clade I TRBs (TRB1, TRB2, TRB3) preferentially localize to the nucleus, particularly enriching

in the nucleolus (Amiard et al. 2024; Kusová et al. 2023, 2025; Dvorácková et al. 2010; P. P. Schrumpfová et al. 2014; Y. Zhou et al. 2018). Overexpression of TRBs under the control of the Cauliflower Mosaic Virus 35S promoter (p35S) indicates that this localization is driven primarily by the histone-like domain, with the myb domain contributing. In contrast, the coiled-coil domain on its own is not sufficient to trigger nuclear localization (Dvorácková et al. 2010). The localization patterns of TRB4 and TRB5, on the other hand, appear to be more complicated. Initial investigations using transient expression in *Nicotiana benthamiana* found TRB4 and TRB5 to be more often localized to the cytoplasm, with TRB5 being almost exclusively found outside the nucleus (Kusová et al. 2023). More recently, however, immunofluorescence staining of GFP-fused TRB4 and TRB5 under the control of the *HMGA2* promoter has revealed subcellular localization patterns much more in line with the established nuclear and nucleolar distribution of clade I TRBs (Amiard et al. 2024).

1.2.3 Genomic Distribution

While the genomic distribution of all TRB paralogs has not been fully investigated, chromatin immunoprecipitation followed by sequencing (ChIP-Seq) analysis has been performed for all but TRB5 (Amiard et al. 2024; Teano et al. 2023; Ming Wang et al. 2023b; P. P. Schrumpfová et al. 2016; Y. Zhou et al. 2016; Q. Wang et al. 2025). These experiments give valuable insight into the distribution of different TRBs throughout most of the genome. Due to the limitations of sequencing-based methods, telomeres are not easily accessible to traditional ChIP-Seq analysis (Vaquero-Sedas, Luo, and Vega-Palas 2012). TRBs have, nevertheless, been found to bind to telomeres through different methods. Dvorácková et al. (2010) used GFP-tagged TRB1 in conjunction with fluorescence in situ hybridization (FISH) to show that TRB1 co-localizes with telomeres. Later studies used similar methods to show that TRB1 co-localizes with PROTECTION OF TELOMERES 1 (POT1b). This interaction was shown both at *A. thaliana* telomeres, as well as probe-labeled telomeric repeats P. P. Schrumpfová et al. (2014). More recently, a CRISPR-based live-cell imaging method was used to further confirm this finding (Dreissig et al. 2017). The ancestral TRB paralogs PpTRB1, PpTRB2, and PpTRB3, found in the moss *Physcomitrella patens* were also shown to co-localize with telomere sequences when transiently expressed in *N. benthamiana* (Kusová et al. 2025). Previous localization studies have primarily focused on TRB1. The remaining clade I TRBs (TRB2 and TRB3) have been less studied regarding their telomere localization. While it was found that both interact with TELOMERASE REVERSE TRANSCRIPTASE (TERT) (P. P. Schrumpfová et al. 2014), TERT itself has been found to localize to areas outside the telomeres as well (Zachová et al. 2013).

Although the telomeric repeats needed for TRB binding are primarily found at the telomeres, short stretches of repeats, named “telo-box” motifs, can also be observed outside of the telomeres. Larger stretches of these repeats are often referred to as Interstitial Telomeric Repeats (ITR) (Regad et al. 1994). These are likely the result of genomic rearrangements, such as chromosome fusions, that lead to the incorporation of telomere sequences (Uchida et al. 2002). Shorter repeats of telo-boxes (often spanning only a single repeat), on the other hand, can be found throughout the genome. They occur disproportionally at the 5’ UTR of genes (Gaspin et al. 2010), where they can act as cis-regulatory elements (Xiao et al. 2017). These short repeats were shown to also be bound by TRBs (P. P. Schrumpfová et al. 2016; Y. Zhou et al. 2016, 2018; Mozgová et al. 2008). It has been proposed that all five *A. thaliana* TRBs are capable of binding to single telo-boxes (Kusová et al. 2023).

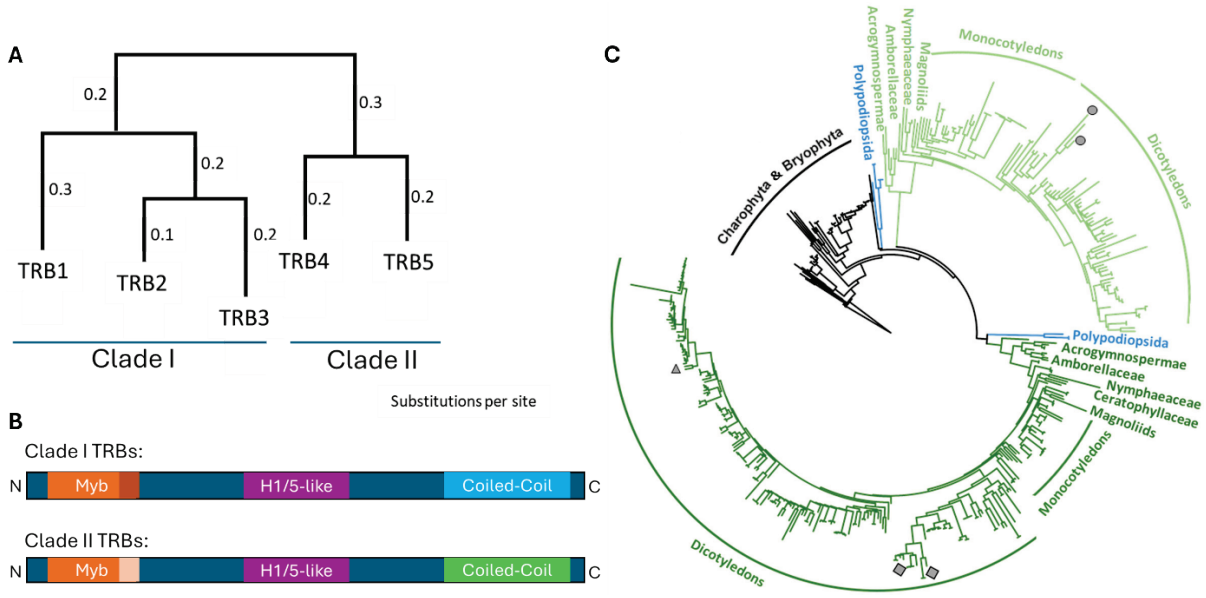

Figure 2, Overview of the molecular structure and phylogenetic origins of TRBs. ***A****, Unrooted phylogenetic tree of the five TRB paralogs found in* A. thaliana. ***B****, Overview of the three main domains found in both clades of TRBs. Different colors indicate sequences that are conserved within each clade but not between clades. Adapted from Amiard et al. (2024).* ***C****, Phylogenetic tree of TRBs in Spermatophyta. Light and dark green branches indicate the two clades. The* A. thaliana *paralogs are indicated by shapes: Triangle: TRB1, Square: TRB2 and TRB3, Circle: TRB4 and TRB5. Modified from Kusová et al. (2025). Original published under CC BY 4.0 License (https://creativecommons.org/licenses/by/4.0/)*

1.3 Functions of TRBs

Despite their paralog diversity and spread throughout the clade of terrestrial plants, the functions of TRBs remain relatively constant. Their eponymous function of binding telomere repeats and related role as part of the telomere protection machinery is conserved throughout all investigated members of the TRB protein family (Kusová et al. 2025, 2023; Zellinger and Riha 2007). Similarly,

their importance for correct plant development has been described in mosses, as well as seed plants (Kusová et al. 2025; Y. Zhou et al. 2016).

1.3.1 Involvement of TRBs in Telomere Protection

All organisms with linear genomes face a set of problems arising from these linear DNA molecules. Firstly, the differentiation between unwanted double strand breaks and the end of their chromosomes is vital for the maintenance of genomic integrity. Additionally, the nature of DNA replication leads to a shortening of linear DNA molecules with each replication cycle, the so-called end-replication-problem (Soudet et al. 2014). Telomere interacting proteins play a crucial part in the mitigation of these problems. In animals, a specific set of telomere-interacting proteins, named the shelterin complex, is responsible for the protection of telomere ends (de Lange 2005). Although some homologs of shelterin components have been identified in plants (Shakirov et al. 2005; Karamysheva et al. 2004), a fully assembled shelterin complex has not been described. Additionally, some homologs identified in plants appear to be more diverse in plants than in animals. In vertebrates the shelterin complex contains two telomeric repeat binding proteins that bind double-stranded DNA (TRF1 and TRF2) (de Lange 2005). These are myb-domain proteins exhibiting a C-terminal myb-domain (Broccoli et al. 1997). In *A. thaliana,* 10 homologs, named TRF-LIKE 1-10 (TRFL1-10) have been described (Karamysheva et al. 2004). In addition, the five TRB proteins also fulfill a similar role (Figure 3, A), despite their myb-domain being N- instead of C-terminal. As part of that role, TRBs interact with other homologs of shelterin components, such as Pot1b (P. P. Schrumpfová et al. 2008) and TERT (P. P. Schrumpfová et al. 2014). Interestingly, although all telomeres are made up of telomeric repeats, overlap of dCAS9-tagged telomere sequences and TRB1-GFP revealed that TRB1 is not always found at all telomeres simultaneously. (Dreissig et al. 2017). Similar observations where previously made using FISH (Dvorácková et al. 2010). This was initially attributed to an inability of TRB1 to bind to a subsection of telomeres. Up to 50% of *A. thaliana* telomeres are so-called blunt-ended telomeres, meaning they miss the single stranded G-overhang required for TRB binding (Kazda et al. 2012). More recent findings, on the other hand, indicate that the absence of TRB1 at a subset of telomeres might also be related to histone H1-mediated exclusion of TRB1 (see "1.3.3 Other roles of TRBs").

The overall effect of TRB mutations on telomere length has been discussed more controversially. Some studies claim to have found significant shortening of telomere length in *trb1* mutants, albeit only after several generations (Schrumpfová et al. 2014). Similarly, observations of relative telomere length and TRB expression levels have found that in oriental plane (*Platanus orientalis*) all three clade I TRBs correlate positively to relative telomere length (Y. Zhang, Yu, and Zhang 2025). Subsequent studies could only detect similar shortening in *trb123* triple mutants (Y. Zhou

et al. 2018). TRB2 knockouts, in contrast, were described as causing gradual telomere elongation over generations (Tan et al. 2018; W. K. Lee and Cho 2016). Mutations of TRB4 and TRB5 appear to not affect telomere length, even when both clade II TRBs are mutated (Amiard et al. 2024).

Another, less prominently discussed, role of TRBs in telomere length maintenance is their involvement in the recruitment of the epigenetic regulatory machinery responsible for protecting the telomere (Lee and Cho 2016). This is made evident by the high prevalence of H3K27me3 at the telomeres, the repressive mark associated with TRB-mediated PRC2 recruitment (Schubert 2019).

1.3.2 Involvement of TRBs in Epigenetic Gene Regulation

Among the multitude of known epigenetic modifications, addition of covalently bound marks to the tails of histones is the most diverse type, both in number of known modifications and their effects on chromatin state and gene regulation (Bannister and Kouzarides 2011). TRBs play a major role in both the establishment and removal of these marks through recruitment and active participation in regulatory complexes. TRBs have been found to be core components of the PEAT complex, in addition to being implicated in the recruitment of Polycomb-group (PcG) complexes (Y. Zhou et al. 2016; Tan et al. 2018; Amiard et al. 2024).

As stated in “1.2.3 Genomic Distribution” above, TRBs can bind to telo-boxes acting as cis-regulatory elements. They can act either as simple transcription factors and/or as the DNA-binding elements of more elaborate regulatory complexes. Besides TRBs multiple other TFs with telo-box-binding activity have been identified (Xiao et al. 2017), further increasing the complexity of TRB-related genetic screenings.

The role TRBs play in the recruitment of PcG complexes was first described in 2016. Mutations of LHP1, the H3K27me3-binding component of PRC1, are enhanced by mutations of either TRB1 or TRB3 (Y. Zhou et al. 2016). The same study also found that loss-of-function mutants of TRB1 can affect gene expression at different genes in different directions, noting a seemingly unpredictable effect of TRB1 on gene expression. Subsequently, PRC2 was also implicated in TRB-mediated gene regulation (Y. Zhou et al. 2018). In the case of PRC2, both clade I and clade II TRBs are able to directly interact with PRC2 (Figure 3, B - Top). Clade I TRBs can trigger PRC2-mediated H3K27me3 through the interaction with CLF and SWN, the core catalytic subunits of PRC2 (Y. Zhou et al. 2018). Although clade II TRBs were also found to interact with CLF and SWN, they appear to act as transcriptional activators of a subset of PRC2-target genes. Furthermore, TRB4 was found to preferentially associate with genes that are transcriptionally active and marked by H3K4me3 (Amiard et al. 2024). Taken together, it appears that clade I and clade II TRBs work

together to fine-tune PRC2-mediated gene repression, particularly at key flowering time regulating genes.

PcG complexes are not the only epigenetic regulatory complexes that TRBs are associated with. As detailed in "1.1.1 PEAT-Complex", TRB1 and TRB2 were described as core components of the PEAT complex (Figure 3, B – Bottom). In this histone deacetylation complex, TRBs assume the role of sequence specific DNA binding component, together with ARIDs (Tsuzuki and Wierzbicki 2018; Tan et al. 2018).

Lastly, a recent study suggests that TRBs can also take part in two additional complexes centered around histone demethylation. The first one associates TRBs with the histone demethylase JMJ14 and its associated NAC domain containing TFs NAC50/52. This complex leads to the removal of H3K4me3 and thus acts as de-activator of gene expression (Ming Wang et al. 2023b). It has also been proposed that ICU11, another de-activating demethylase, putatively targeting H3K36me3, takes part in the same complex (Q. Wang et al. 2025). The second demethylation-associated complex contains TRBs with ICU11 but without JMJ14. Instead, the two interact with three, previously undescribed, proteins named HELIX-TURN-HELIX 1-3 (HTH1-3) (Q. Wang et al. 2025).

Considering all these studies, it becomes clear that TRBs play a central role within epigenetic gene regulation. At minimum, they are involved in: Deposition of H3K27me3 (Y. Zhou et al. 2018), H4K5ac (Tan et al. 2018), and H2A-ubiquitination (Y. Zhou et al. 2016), as well as the removal of H3K4me3 (Ming Wang et al. 2023b), H2A-ubiquitination (Zheng et al. 2023), and possibly H3K36me3 (Q. Wang et al. 2025).

1.3.3 Other roles of TRBs

Besides their role in telomere protection and epigenetic gene regulation, TRBs have been ascribed multiple other roles. While none have been studied as closely, these functions can give valuable insight into the way TRBs behave outside of their narrow role as TFs or telomere protection proteins.

Despite the strong affinity of TRBs to telo-box DNA motifs, Teano et al. (2023) reported a notable lack of TRB1 binding to telo-boxes found at histone H1 deposition sites. They conclude that linker histone H1 can prevent TRB1 invasion into compacted chromatin (Figure 3, C). This is in part attributed to the H1-domain found in TRBs, which acts in direct competition to histone H1 (Teano et al. 2023).

Additionally, as with many gene regulatory mechanisms, liquid-liquid phase separation (LLPS) has recently been implicated in the regulatory role of TRBs. The TRB1 homolog in rice, TRBF2, was

found to exhibit LLPS inducing properties with PRC2 component CLF both *in vivo* and *in vitro* (Xuan et al. 2022).

Lastly, prior to the discovery of the involvement of TRBs in PRC2 and PEAT, the presence of telo-boxes was shown to specifically enhance the activating effect of site II DNA motifs (Trémousaygue et al. 2003). Whether this is a distinct function of TRBs or is caused through their participation in regulatory complexes has not been investigated (Figure 3, D).

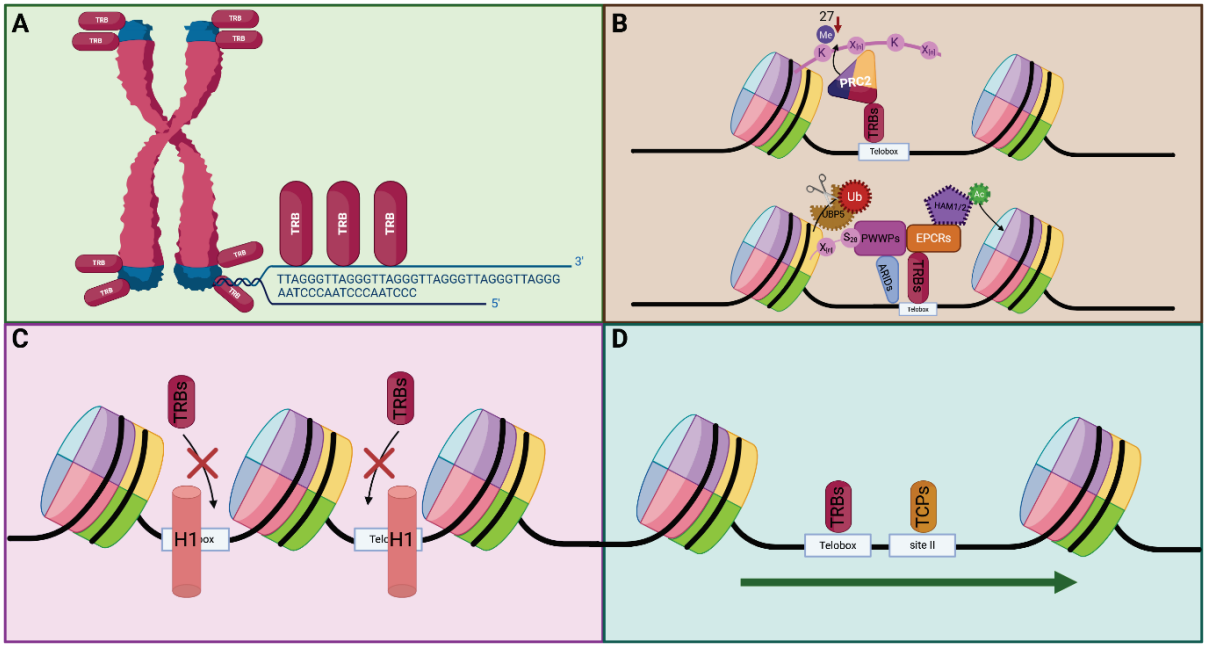

Figure 3, Overview of the known functions of TRBs. ***A****, TRBs bind telomeric sequences and are part of the telomere protection machinery.* ***B****, TRBs take part in a variety of epigenetic regulatory complexes. Top: TRBs can directly recruit PRC2 to telo-boxes. Bottom: TRBs are core components of the PEAT complex.* ***C****, TRBs and linker histone H1 are competing at certain sites and H1 can "mask" teloboxes making them inaccessible to TRBs.* ***D****, TRBs binding to telo-boxes enhance the activating effect of site II sites through an unknown mechanism.*

1.4 Previous Research

The premise of this thesis relies in large part on the work performed by Krause (2019) and Zündorf (2022). Krause (2019) showed that TRB2 and TRB3 can recruit PRC2 alongside TRB1 and generated ChIP-Seq data of TRB2 and TRB3. Alongside the data we published earlier (Y. Zhou et al. 2016), this allowed me to fully analyze the genomic binding behavior of all clade I TRBs. Her thesis, furthermore, showed that TRB2 and TRB3 are more closely associated with PRC2, while TRB1 appears to have significantly more binding sites in the wild-type (WT) Col-0 genome. The observation of this divergence between the paralogs is further bolstered by unpublished phenotypical observations generated by our group. We observed that the effect on flowering time that clade I *trb* mutations cause is not the same for all paralog combinations. This indicates that the paralogs are not completely redundant and that their loss-of-function flowering time phenotype is dependent on temperature and photoperiod.

Zündorf (2022) provided further evidence of the divergent roles of clade I TRBs. Through immunoprecipitation coupled with mass spectrometry (IP-MS) she unveiled the protein-protein interaction network of TRB1 and TRB3. A more detailed analysis of her work is found in section 3 “Publication: TRB-mediated epigenetic gene regulation is controlled by distinct regulatory complexes utilizing specialized TRB paralogs”. She additionally identified three UNSTRUCTURED TRB INTERACTORS (UTIs) that are reliably detected in TRB interaction studies but had not been functionally characterized.

1.5 Aim of the Dissertation

Given the previously observed TRB interaction network in combination with their ability to influence gene regulation in both activating and repressive manner, this dissertation aims to elucidate some of the underlying epigenetic regulatory complexes on a genomic level. The primary focus lies in investigating the factors determining the roles of TRBs as either activating or repressive transcription factors. To this end, the unequal redundancy seen in genetic screenings of TRB1,2, and 3 is considered and further investigated on a molecular level as a potential contributor to TRBs bivalent nature of gene regulation. Lastly, the potential of additional, thus far undescribed, epigenetic regulatory complexes with TRB involvement is explored. Overall, this dissertation seeks to enhance our understanding of the role of TRBs in gene regulation, and by which factors this role is determined.

2 Results

2.1 Previous Research Suggests the Existence of an ICU11-containing TRB-complex

In 2023, two groups working on TRB-mediated epigenetic gene regulation uncovered sub-complexes of PRC2 and PEAT, respectively. Both subcomplexes involve a bi-functional regulatory state switch. In the case of PRC2, Ming Wang et al. (2023b) showed that the PRC2-TRB complex first described by Y. Zhou et al. (2018) can work together with the histone demethylase JMJ14 to remove the activating H3K4me3 histone mark (Figure 4,B Top). This occurs simultaneously to the PRC2-mediated deposition of the repressive H3K27me3 mark, therefore conveying both de-activation and repression through the same complex. Conversely, Zheng et al. (2023) showed that the PEAT complex can recruit the ubiquitin protease UBP5 together with the histone acetyltransferases HAM1/2 (Figure 4,B Middle). This leads to simultaneous removal of the repressive H2A-mono-ubiquitination and deposition of the activating H4K5 acetylation. Through this, the same complex mediates de-repression and activation.

The discoveries of these two bi-functional complexes prompted me to re-evaluate the IP-MS data generated in our group Zündorf (2022). My goal was to test if our data supports the complexes proposed by Zheng et al. (2023) and Ming Wang et al. (2023a). Additionally, I was looking for other potential "bi-functional" complexes that could be deduced from the interactions we observed. First, I reduced the TRB interaction network to proteins known to take part in epigenetic gene regulation (primarily in context of PRC2 and PEAT). I furthermore grouped PcG proteins into a single category and collapsed protein functions found as multiple paralogs into single nodes. The resulting simplified interaction network was used to display both bi-functional complexes published in 2023 (Figure 4, A). Examination of the remaining nodes revealed a pattern similar to the PRC2-TRB-JMJ14 complex. In this putative complex the demethylase ICU11 interacts with both PRC2 and the TRBs. Since ICU11 likely catalyzes the removal of the activating H3K36me3 mark (Mateo-Bonmatí et al. 2018), this would constitute a bi-functional complex similar to PRC2-TRB-JMJ14. Although the interaction data also showed a direct interaction between ICU11 and NAC50/52, TFs that have long been associated with JMJ14 (Ning et al. 2015). Because of this, I decided to include the undescribed UTI proteins identified by Zündorf (2022) as the structural and/or secondary TF for this complex. The three UTI paralogs interacted with all other components of this proposed complex. The putative PRC2-TRB-ICU11 complex would therefore include: TRBs as DNA binding component, PRC2 as methyltransferase for the repressive H3K27me3 mark,

ICU11 as demethylase of the activating H3K36me3 mark, and UTIs as a structural component and/or secondary DNA binder (Figure 4, B).

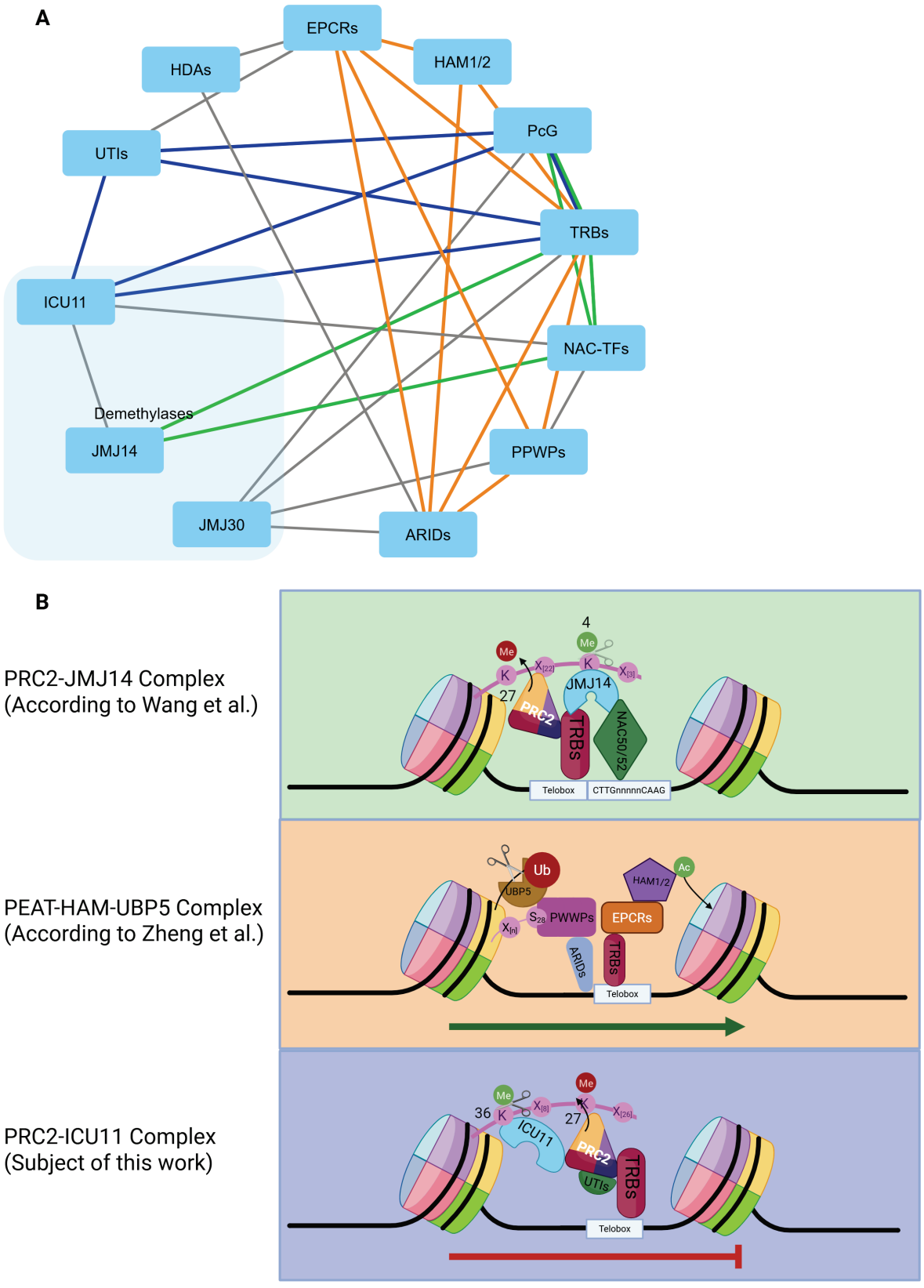

Figure 4, Previously published bi-functional regulatory complexes involving TRBs as well as the proposed ICU11 containing complex. ***A****, Interaction network of a selection of TRB-interacting proteins produced using IP-MS data*

generated by Zündorf (2022). The three complexes relevant for this work are highlighted with colored edges. Green: PCR2-JMJ14 complex as established by Ming Wang et al. (2023a). Orange: PEAT-HAM-UBP5 complex as established by Zheng et al. (2023). Blue: Proposed PRC2-ICU11 complex. Edge colors correspond to background colors in B. ***B****, Model representations of the three complexes highlighted in A. It should be noted that UBP5 in the PEAT-HAM-UBP5 complex was the only component not detected as TRB interactor in the IP-MS. Arrows indicate deposition of a histone mark, scissors depict removal. The histone tail in the PRC2-containing models represents the N-terminal tail of histone 3. Histone marks: Me, (tri)-methylation; Ub, mono-ubiquitination; Ac, acetylation. Marks depicted in red are generally assumed to be transcription activating, marks in green are generally assumed to be repressive.*

2.2 Genetic Interaction of Components of the Putative PRC2-ICU11-TRB Complex

The possible connections between ICU11, TRBs, and UTIs were assessed through reverse genetics. Single-, double-, and triple-mutants of TRBs were already available in our lab as T-DNA insertion (*trb1-2 and trb3-2*) and CRISPR loss-of-function mutants (*trb2-3*). Throughout this work, *trb1*, *trb2*, and *trb3* refer to these alleles unless stated otherwise. In order to generate combinatory mutants, I opted to use CRISPR-Cas9 to mutate *UTI1* in *trb* double mutant combinations. The *trb1-2 trb2-3 trb3-2 (trb1 trb2 trb3)* triple mutants were not included in this screen, because of their severe developmental phenotype. Two single guide DNAs (sgDNAs) targeting exon 2 of *UTI1* (Figure 5, A) were previously designed and tested in our lab. The sgDNAs were subsequently incorporated into shuttle vectors according to the modular CRISPR-Cas9 expression system developed by Stuttmann et al. (2021). The shuttle vectors were then used in a GoldenGate cloning reaction to assemble the Cas9 expression vector pDGE347. Besides an intron-optimized version of Cas9, this vector carries multiple selection markers, two for bacteria (spectinomycin and chloramphenicol) and phosphinothricin (BASTA) resistance for plants. Additional selection in plants is enabled through a fluorescent seed-coat marker (Figure 5, B). After selecting transformed seeds based on fluorescence, the plants were grown on soil and PCR amplification of the target locus was used to screen for large deletions or insertions. PCR products that appeared to be mutated were subsequently sequenced to validate a full disruption of the target locus.

Using this method, I generated multiple independent alleles for each of these genotypes: *uti1* in Col-0, *uti1 trb1 trb3*, and *uti1 trb2 trb3* (See Supplementary Table 2). While all ten alleles incorporated a frameshift, seven alleles showed edits only at the target site of sgUTI1-2. Since these frameshifts are located at the end of exon 2, they might not result in a fully disrupted protein function. To investigate whether all alleles constitute a full loss-of-function mutation, I compared *uti1-11* with *uti1-12* and *uti1-13*. Although all three alleles were generated in the *trb2 trb3* background, *uti1-11* was only edited at the sgUTI1-2 site, while *uti1-12* and *uti1-13* were edited at both sites. This comparison revealed that there is no significant difference between these alleles

(Figure 5, C), suggesting that a single frameshift at the sgUTI1-2 site is sufficient to disrupt protein function.

Two initial experiments were performed, comparing all alleles of *uti1* in Col-0 together with the *trb1 trb3* background in long day conditions (16 h light). These revealed significantly later flowering of *uti1* in Col-0, paired with a non-significant trend for early flowering for both the *trb1 trb3* double mutant and the combination *uti1 trb1 trb3* (Figure 5*,* D). The reproducibility of these findings across both experiments was, however, poor. This led to large variance and subsequent low statistical power.

Previous research from our group had uncovered that *TRB* double mutants exhibit early flowering time phenotypes primarily in conditions that generally slow down development (unpublished work from the group). Phenotypes of *uti1* mutants were therefore determined in low temperature (13 °C) and equinox photoperiod (12 h light).

These subsequent experiments additionally included *uti1* alleles in the *trb2 trb3* double mutant. This enabled a direct comparison of the effect of *uti1* in both backgrounds (*trb2 trb3* and *trb2 trb3*) (Figure 5, E-F). The loss-of-function of *UTI1* does not significantly change the flowering time compared to WT plants in either low temperature or equinox conditions. At equinox, both *trb1 trb3* and *trb2 trb3* flower at the same time and earlier than WT. The additional disruption of *UTI1* in these mutants, however, revealed an unsuspected pattern. In the *trb1 trb3* background, mutating *UTI1* further expedites the flowering, leading to significantly earlier flowering compared to the double mutant with intact *UTI1*. In *trb2 trb3*, on the other hand, loss of *UTI1* has the contrary effect. The plants flower significantly later than the double *trb* mutant, restoring flowering time to WT levels.

While *trb1 trb3* and *trb2 trb3* did not exhibit significant differences in flowering time in equinox, a difference emerges in cold conditions. Although both mutants still flower early compared to WT, *trb1 trb3* also flowers earlier than *trb2 trb3* at 13 °C. In addition, the restoration of WT flowering time in *uti1 trb2 trb3* can also be observed in the cold, while the earlier flowering in *uti1 trb1 trb3* could not be reliably shown in cold conditions. These results indicate that UTI1 is involved in TRB-mediated flowering time control. The results also indicate that the effect of UTI1 appears to be dependent on the availability of different TRB paralogs. The loss of intact UTI1 can either delay flowering, when only TRB1 is available, or expedite it, when only TRB2 is available.

Overall, the reverse genetics approach unveiled that UTIs are very likely to be involved in TRB-mediated gene regulation. However, the variant nature of the effects of *uti1* mutations makes

it clear that the role of UTIs is more complex than originally anticipated, possibly involving different types of interactions between UTI1 and different TRB paralogs.

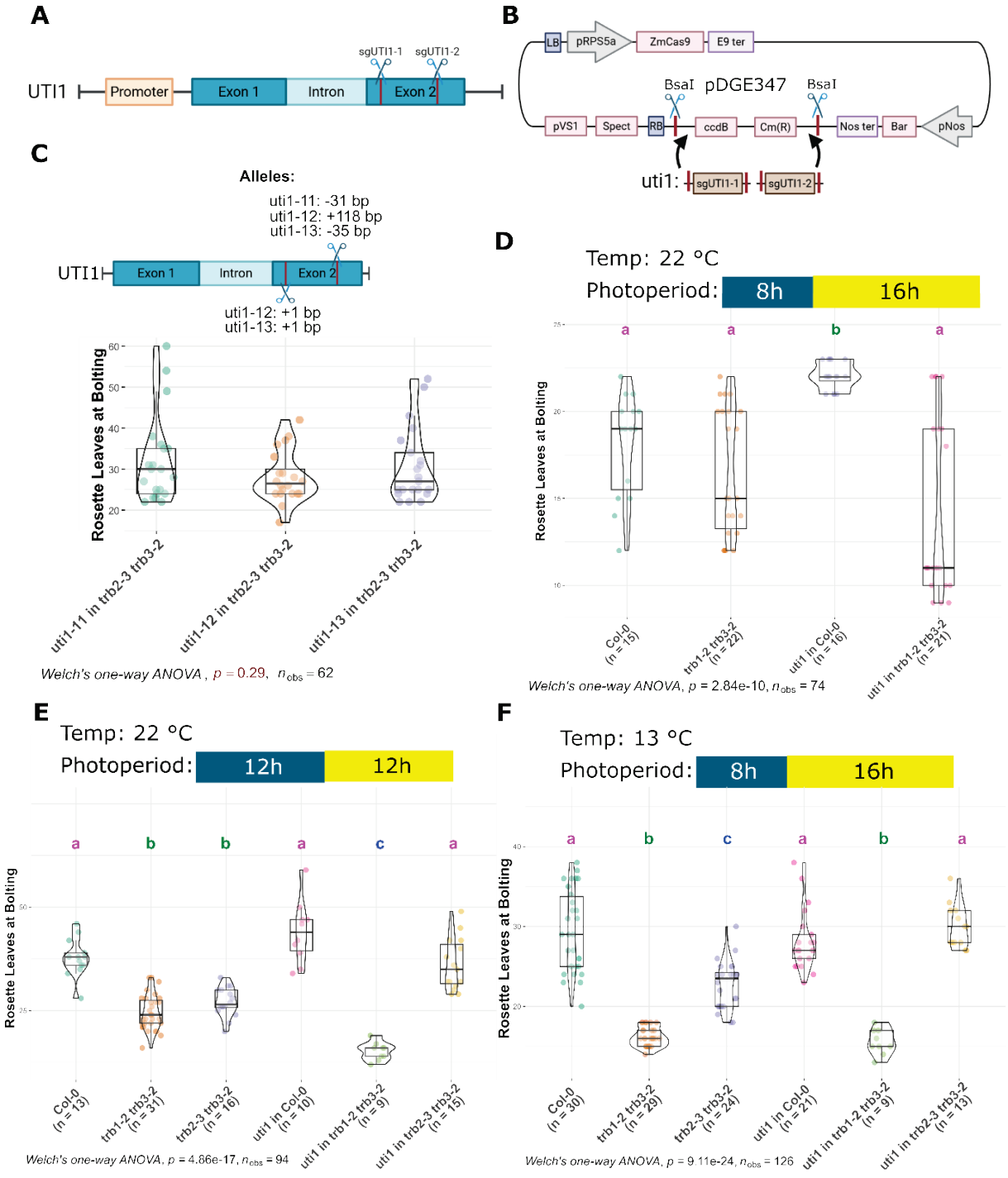

*Figure 5, Genetic interaction of components of the putative PRC2-ICU11-TRB complex. **A**, Schematic overview of the UTI1 gene targeted for knockout in the experiment. Locations of sgDNA binding sites are indicated by scissors. **B**, Schematic overview of the CRISPR expression vector pDGE347 used in the experiment. sgDNAs are incorporated through GoldenGate cloning utilizing Type IIS restriction enzyme BsaI. **C**, Flowering time of three alleles of uti1 edited in trb2 trb3. Grown at 22 °C with 12-hour light (MD). The concrete mutations are indicated on the schematic overview analogous to A. **D**, Flowering time of uti1 CRISPR loss-of-function alleles in 22 °C with 16-hour light (LD). **E**, Flowering time of uti1 CRISPR loss-of-function alleles in 22 °C with 12-hour light (MD). **F**, Flowering time of uti1 CRISPR loss-of-function alleles in 13 °C with 16-hour light (LD). For all flowering time data (C-F), Welch's one-way ANOVA was used to determine difference in means. Subsequently, a Games-Howell test with multiple comparison adjustments according*

to Holm (1979), was used to determine significant differences between samples. Groups of samples with non-significantly different means are depicted using colored letters.

2.3 Further Analysis of the Observed Phenotypes using Transcriptomics

Since *uti1* mutant alleles had opposing effects on flowering time in *trb1 trb3* and *trb2 trb3* for plants grown in equinox, I decided to investigate the transcriptome of both mutants. I chose to include *trb1 trb3* and *trb2 trb3* in both absence and presence of *uti1* mutant alleles in comparison to controls. In two independent RNA-Seq experiments, the transcriptomes of 14-day old seedlings growing under equinox photoperiod were determined one hour before the start of the night cycle (ZT11). The first experiment included Col-0 and *trb1 trb3,* both alone and in two combinations with *uti1*. Col-0 was combined with alleles *uti1-3* and *uti1-4,* while *trb1 trb3* was combined with *uti1-9* and *uti1-10*. The second experiment also included *uti1-4* and *trb1 trb3 uti1-9* but was amended by *trb2 trb3* and *uti1-11 trb2 trb3*. Principle component analysis of the combination of all samples of both experiments revealed a strong separation of samples by experiment (Figure 6,A). Both my flowering time data and previous RNA-Seq experiments in our group (data not shown) had already indicated that the phenotypical effects of *trb* double mutants are rather weak. A strong separation by experiment in the first principal component is, therefore, expected and not necessarily problematic. Observing the second and third principal component of the data supplies a more useful metric in this case (Figure 6,B). Among these two components, the genotypes involved in both experiments mostly cluster together, indicating sufficient quality to continue the analysis. To compensate for the strong inter-experiment variance, I opted to modify the design formula used in the R-package DESeq2 (Love, Huber, and Anders 2014) from ”~ genotype” to “~ experiment + genotype”, allowing it to take into account batch effects introduced in the two repetitions.

After differential expression analysis of all samples, I split the data into two sets: One comprised of all *uti1*, *trb1 trb3*, and *uti1 trb1 trb3* samples (Set: uti1trb13), and one made up of the same *uti1* samples, but paired with *trb2 trb3* and *uti1 trb2 trb3* (Set: uti1trb23). In both sets all alleles present in the same background genotype were pooled. This allowed for the analysis of the *uti1* mutation in each *trb* double mutant background without interference from the other. The number of differentially expressed genes (DEGs) for both sets, as well as their overlaps were similar (Figure 6, C-D).

Across the three mutant genotypes, set uti1trb13 yielded a total of 875 DEGs compared to WT, with 89 (10.2%) being shared between all three genotypes. Consistent with its weaker phenotype, *uti1* differentially expressed less genes than either *trb1 trb3* or *uti1 trb1 trb3* (239 vs. 559/420

DEGs). The combination mutant, *uti1 trb1 trb3* displayed more DEGs than the simple combination of *uti1* and *trb1 trb3* would suggest. In fact, 24.9% off all DEGs found in the set were exclusive to the combination mutant (Figure 6, C).

Most of the observations found in the uti1trb13 set hold true for uti1trb23 as well. Compared to WT, this set contained 830 DEGs, of which 38 (4.6%) were shared between the mutant genotypes. Like in the uti1trb13 set, the *trb2 trb3* mutants differentially expressed more genes than *uti1* (309 vs. 239 DEGs). The combination mutant *uti1 trb2 trb3* differentially expressed even more genes than *trb2 trb3* (498 vs. 309 DEGs), with 41.3% of DEGs being exclusive to *uti1 trb2 trb3*. This is interesting, since the early flowering time phenotype of the *uti1 trb2 trb3* combination mutant was less pronounced than the *trb2 trb3* mutant alone (Figure 6, D).

These results indicate that the expression changes in *trb* mutants that lack functional *uti1* are not merely an additive result of the combination of DEGs between the two disrupted protein functions. Instead, they appear to be an emergent property, likely caused by systemic changes in gene regulation. To understand which genes are affected by this, I focused on the 24.9% and 41.3% of DEGs that were exclusively differentially expressed in the combination mutants of set uti1trb13 and uti1trb23, respectively (Figure 6, E-F). Gene ontology (GO) enrichment analysis revealed that the two groups enriched distinct terms across all three aspects: Molecular Function (MF), Biological Process (BP), and Cellular Compartment (CC).

While *uti1 trb1 trb3* DEGs did not enrich any terms in the BP aspect, its enrichment of CC-Terms indicated a connection to photosynthesis. All six enriched CC terms were connected to plastids in general or the thylakoid in particular (Figure 6, E). On the other hand, the DEGs detected exclusively for *uti1 trb2 trb3* enriched terms related to the ribosome. These terms included the BP and MF terms “ribosome biogenesis” and “structural constituent of ribosome”, respectively. They were joined by the CC term “ribosome” as the most enriched terms (Figure 6, F). Additionally, both sets of enriched GO-terms overwhelmingly featured genes that were expressed at lower levels in their respective combination mutant compared to WT (Figure 6, E-F). For many of the terms (e.g., all CC-Terms in uti1trb23) all contained genes were lower expressed in the mutant. On one hand, these enrichments further support the hypothesis that TRBs form specific sub-complexes with various regulatory proteins, including UTIs. On the other hand, the hypothetical PRC2-ICU11-TRB complex is expected to be repressive. Its disruption would, therefore, lead to up- not downregulation. A more thorough investigation is necessary to assess whether the observed lack of downregulation can be attributed to downstream effects or if a different, activating, UTI-containing complex is responsible for the effect.

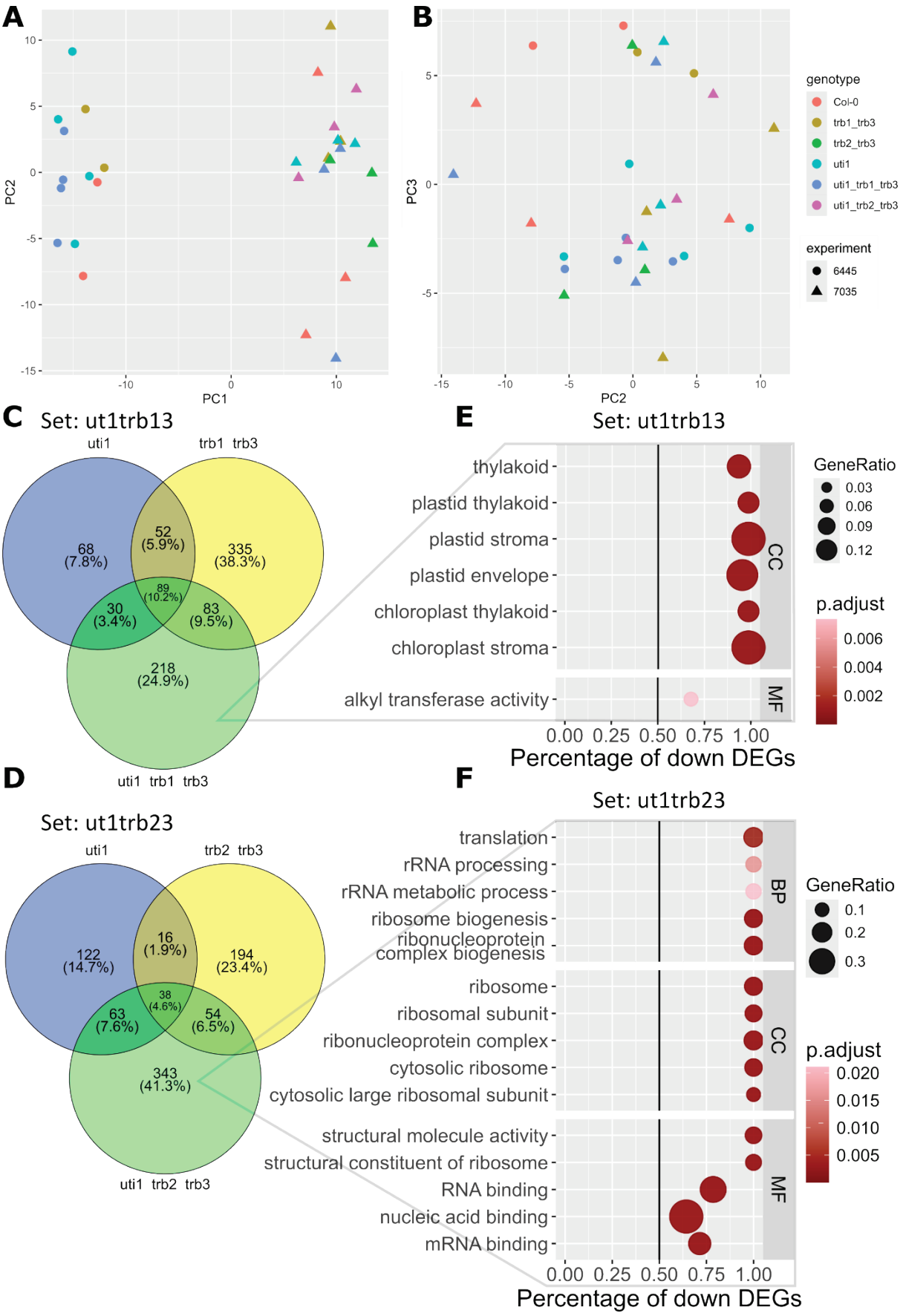

Figure 6, Transcriptome analysis of uti1 knockouts in trb double mutants. ***A****, Principal component analysis (PCA) of the first two principal components of RNA-Seq data derived from two experiments (6445 and 7035).* ***B****, PCA of the second and third principal components of the same dataset as A.* ***C****, Venn diagram depicting the overlap of genes differentially*

expressed compared to WT for uti1 in Col-0, trb1 trb3 and the combination mutant uti1 trb1 trb3. ***D****, Venn diagram depicting the overlap of genes differentially expressed compared to WT for uti1 in Col-0, trb2 trb3 and the combination mutant uti1 trb2 trb3.* ***E****, Enriched gene ontology (GO) terms of all genes differentially expressed exclusively in uti1 trb1 trb3. Only the five most significantly enriched terms are displayed. BP, Biological Process; MF, Molecular Function; CC, Cellular Compartment. X-axis depicts the percentage of DEGs that are less expressed than in WT.* ***F****, Same as E, but for DEGs exclusively found in uti1 trb2 trb3.*

The large amount of DEGs exclusive to the combination mutants in combination with the unexpectedly strong directionality of the expression changes of GO-term-enriching-genes prompted me to take a closer look at the effects the *uti1* mutation can have on genes. Considering all genes that are differentially expressed in at least one of the genotypes compared to WT controls, a heatmap of their expression patterns was grouped into 7 distinct categories (Figure 7, A): Genes that showed the same response compared to WT, independent of which genotype was evaluated ("Similar Effect"). Genes in which the combination mutant followed the expression change exhibited in either the *trb* double mutant or *uti1* ("trb-dominant" or "uti1-dominant", respectively). Genes whose differential expression in the *trb* double mutant was enhanced or rescued when adding *uti1* ("Enhancing trb" or "Rescuing trb", respectively). And, lastly, genes whose differential expression was in the opposite direction to either the expression change in the *trb* double mutant ("Counteracting – Only trb"), or both *uti1* and the *trb* double mutant ("Counteracting – Both").

Comparing both sets, the distribution of these categories differed notably. The uti1trb13 set was dominated by genes for which expression changes in *trb1 trb3* were rescued in the presence of *uti1* (Figure 7, A - Left). In ut1trb23, on the other hand, more genes fell into the "Enhancing trb" category. Additionally, many genes in the ut1trb23 set were categorized as "trb-dominant" (Figure 7, A - Right). Although both sets contained all seven types of expression patterns, effects of *uti1* mutations counteracted the effects of *trb* mutants more often in uti1trb13. Both the proportion of "Rescuing trb" and "Counteracting – Only trb" were higher in this set. Meanwhile, genes contained in uti1trb23 were often either unaffected by the *uti1* mutation (trb-dominant) or exhibited enhanced effects in the combination mutant compared to *trb2 trb3* (Enhancing trb).

Overall, counteraction appeared with similar frequency in both sets (~33% of all DEGs). The distribution of the two sub-categories ("Counteracting – Only trb" and "Counteracting – Both"), also aligned with the previous findings. In uti1trb23 the expression of genes in *uti1 trb2 trb3* were more often counteracting the expression seen in both *uti1* and *trb2 trb3*. In uti1trb13, on the other hand, the expression of genes in *uti1 trb1 trb3* often only contradicted their expression in *trb1 trb3* (Figure 7, B).

These patterns are particularly interesting when viewed in conjunction with their previously established flowering phenotypes. Even though *uti1 trb1 trb3* enhanced the early flowering of *trb1*

trb3, the expression patterns found in the mutant more often counteracted the expression changes observed in *trb1 trb3*. The exact opposite effect was observed for *uti1 trb2 trb3*. Although expression changes were often enhanced by the presence of *uti1* in *trb2 trb3*, the flowering time phenotype of the combination mutant reverted to controls.

Since transcriptome and phenotypic effects seemed contradictory, I took a closer look at a set of genes that had previously been described as implicated in the regulation of flowering time. Bouché et al. (2016) published a list of 378 genes together with their effect on flowering time (positive/negative effect) in a database the termed FLOR-ID. I used this information to filter the list of DEGs obtained in the analysis and kept only genes that are included in FLOR-ID and were differentially expressed in any mutant compared to wildtype. This reduced list contained 21 DEGs in set uti1trb13 and 19 DEG in set uti1trb23. Using SuperExact test shows that both overlaps are significantly enriched against all expressed genes, indicating that genes contained in FLOR-ID are 1.8 and 1.7 times more likely than expected to also be differentially expressed in at least one mutant, respectively.

I added this information to the analysis to get a clearer picture of the flowering time regulatory landscape in the mutants (Figure 7, D). Most of the expression patterns seen for all DEGs could also be observed in this list. Comparing the distribution of expression patterns revealed that DEGs in uti1trb23 are more likely to be categorized as “counteracting” if they are found in FLOR-ID, compared to all DEGs in this set (~ 47% vs. ~33%).

Next, I determined the expected effect on flowering time of each DEG found in FLOR-ID, based on a simple decision matrix (Figure 7, C / Section 6.4.2 - Table 2): A DEG was categorized as “expediting”, if it was expressed at higher levels in the combination mutant and was reported as affecting flowering time positively in FLOR-ID. Alternatively, a DEG was also categorized as “expediting”, if it was expressed at lower levels in the combination mutant, but reported as affecting flowering time negatively in FLOR-ID. In contrast, DEGs that were expressed at lower levels in the combination mutant while being annotated as negatively affecting flowering time in FLOR-ID, were categorized as “delaying. The same category was assigned to DEGs that were expressed at higher levels, but annotated as positively affecting flowering time in FLOR-ID.

Using these rules, set uti1trb13 contained a total of 21 DEGs that have been implicated in flowering time regulation. Of those 21, 8 DEGs were assumed to expedite flowering in *uti1 trb1 trb3*, while a further 6 DEGs were assumed to be delaying. The remaining 7 DEGs do not have a clear direction, mostly because their expression levels are very close to WT (Figure 7, D - Left). Set uti1trb23 had a total of 19 DEGs with known impact on flowering time. Of these DEGs, 8 can be

assumed to be expediting, while 5 appear to be delaying in the *uti1 trb2 trb3* mutant. This mutant also contained 6 DEGs that did not have a clear effect (Figure 7, D - Right).

In either set, no single gene or group of genes immediately stood out as a likely cause of the early flowering. Focusing on genes that differed between the *trb* double mutants, and the combinatorial mutants was more illuminating. In the set uti1trb13, one of the strongest differences was found in *VARIANT IN METHYLATION 1 (VIM1)*, which is expressed at significantly lower levels in *uti1 trb1 trb3* compared to *trb1 trb3*. VIM1 is a methylcytosine-binding PHD domain protein that has been implicated in maintenance of chromatin structure during cell division (Woo et al. 2007). Notably, both overexpression lines of *VIM1* (S. Liu et al. 2007) and loss-of-function mutants delay flowering. The later, however, only in combination with loss-of-function of its paralogs *VARIANT IN METHYLATION 2* and 3 (*VIM2* and *VIM3*) (Shook and Richards 2014). *VIM2* was not differentially expressed in the *uti* mutants, while *VIM3* expression was significantly increased in *trb1 trb3* but reverted to WT levels in *uti1 trb1 trb3*. In the uti1trb23 set, *VIM1* was also significantly lower expressed in the combination mutant. In that set *VIM3* was higher expressed in the same mutant. Because of this, potential effects of *VIM1* on flowering time were likely negated by *VIM3*, since the paralogs are highly redundant (Woo, Dittmer, and Richards 2008).

Another gene with strong divergent response is *FPA,* which encodes an RNA-binding protein that plays a significant role in mRNA processing (Schomburg et al. 2001). FPA is required to maintain correct splicing, polyadenylation, transcription termination, as well as RNA-mediated chromatin silencing (Hornyik, Terzi, and Simpson 2010; Duc et al. 2013; Bäurle et al. 2007). Furthermore, through the downregulation of the floral repressor *FLOWERING LOCUS C (FLC)*, FPA is implicated in the autonomous flowering time pathway (Michaels and Amasino 2001). Expression of *FPA* was increased in *trb1 trb3* but decreased in *uti1 trb1 trb3*. Both effects were therefore not correlated with the observed effect on flowering.

In the set uti1trb23, strong differences in expression between *trb2 trb3* and *uti1 trb2 trb3* were found in more DEGs. The flowering time delaying factor *MADS AFFECTING FLOWERING 5* (*MAF5*), for example, was expressed more strongly in the combination mutant, while *FPA* switched from reduced expression in *trb2 trb3* to increased expression in *uti1 trb2 trb3*. *CALCIUM-DEPENDENT PROTEIN KINASE 6 (CPK6)* followed a similar pattern and is annotated as flowering time expediting. Another interesting effect can be observed for *FLOWERING LOCUS K HOMOLOGY DOMAIN (FLK)*. Like *FPA*, *FLK* encodes a RNA-binding protein that contributes to the repression of *FLC* through the autonomous pathway, therefore having a positive effect on flowering (Lim et al. 2004). Although *FLK* was significantly higher expressed in *uti1*, *trb1 trb3*, *trb2 trb3*, and *uti1 trb1 trb3*, its expression was slightly less than WT in *uti1 trb2 trb3*. Through this expression pattern, *FLK*

could contribute to the observed flowering time phenotype of *uti1 trb2 trb3*. *FLK* expression does, however, not adequately explain the flowering time of the other mutants.

Another protein targeting *FLC* is the histone methyl transferase *SET DOMAIN PROTEIN 25* (*SDG25*) (Berr et al. 2009; Tamada et al. 2009). Unlike *FPA* and *FLK*, *SDG25* has a negative effect on flowering through the activation of *FLC* (Berr et al. 2009; Tamada et al. 2009). *SDG25* is the only flowering time associated gene whose expression was significantly increased on all tested genotypes. Interestingly, this was not the case across all its splice variants. While variant AT5G42400.5 exhibited increased abundance in all genotypes, AT5G42400.3 was less expressed in *trb2 trb3*. Since all eight splice variants of *SDG25* share the same protein sequence and differ only in their 5' and 3' UTRs, its alternative splicing is primarily involved in gene regulation rather than protein diversification (Cheng et al. 2017). Since the RNA-Seq data was generated using short-read sequencing, the exact distribution of splice variants cannot be reliably determined. Because of this, the Salmon-based abundance estimates are only indications of overall expression changes. The strong response of *SDG25* throughout all genotypes was furthermore notable because of its enzymatic function (Tamada et al. 2009). As a H3K36 methyltransferase, SDG25 would be a direct antagonist of the proposed PRC2-TRB-ICU11 complex.

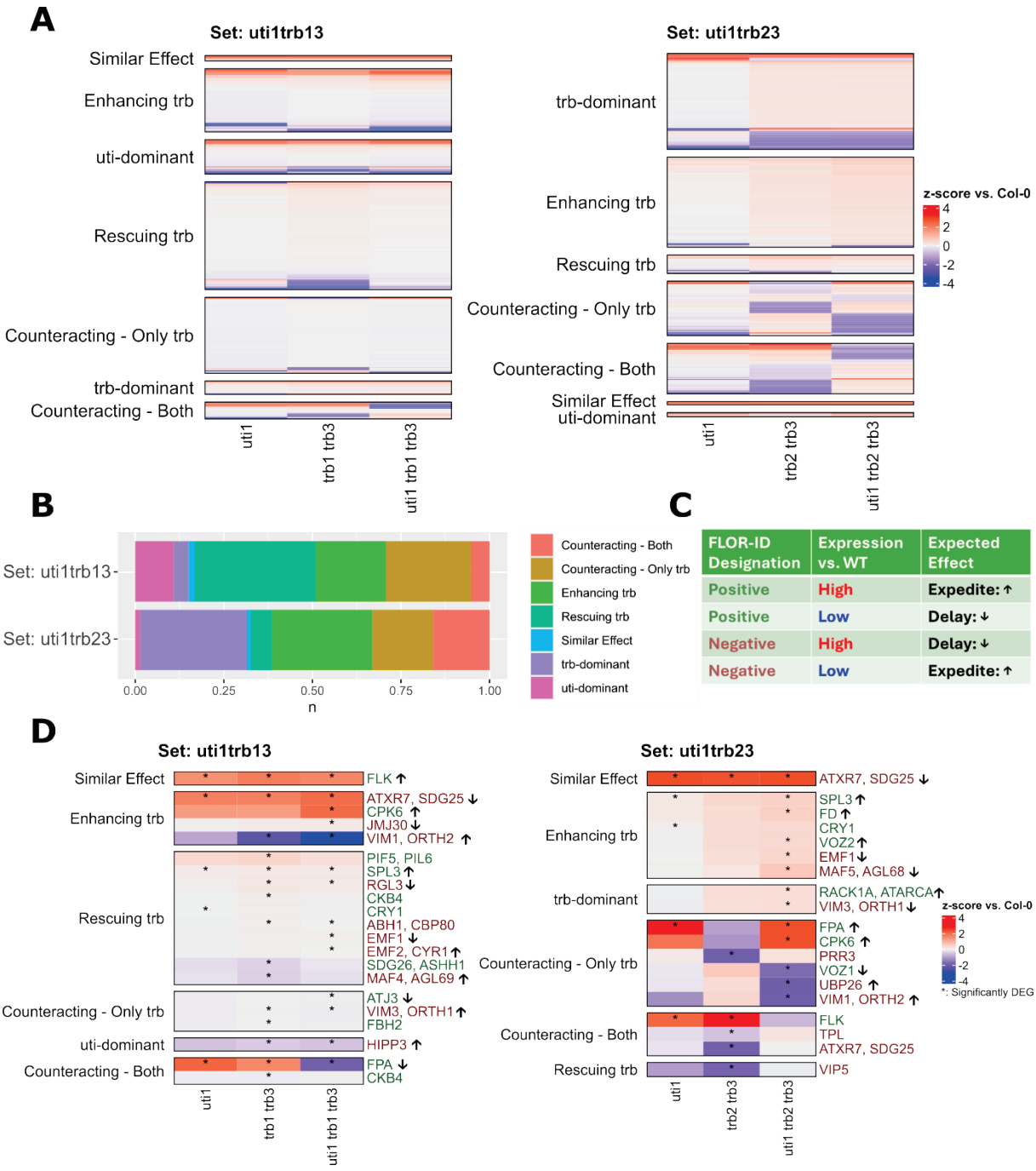

Figure 7, Analysis of the DEGs in uti knockouts. ***A****, Heatmaps of the z-Score of the expression relative to Col-0. Left: set uti1trb13 (uti1, trb1 trb3, and uti1 trb1 trb3). Right: set uti1trb23 (uti1, trb2 trb3, and uti1 trb2 trb3). Heatmaps include all genes with differential expression in at least one genotype. The genes are grouped by the effect that combining uti1 with the respective trb double mutant has (see Section 6.4.2).* ***B****, Bar plot depicting the distribution of the effects shown as groups in A for set uti1trb13 and set uti1trb23, respectively.* ***C****, Decision matrix displaying how the expected effect of each DEG on flowering time was determined.* ***D****, Same Heatmaps as A, but filtered for genes known to affect flowering time according to Bouché et al. (2016). Red gene names indicate genes with a negative effect, green genes names genes with positive effect according to FLOR-ID. The expected effect of each DEG is indicated by arrows: ↑, expedite flowering; ↓, delay flowering; no arrow, no clear effect. Genes found to be differentially expressed in a genotype are indicated with "*".*

Due to the complex nature of the flowering time gene regulatory network, I decided to take a more detailed look at the genes that impact flowering time in the context of their regulatory environment. To achieve this, I started by mapping expression data to WikiPathways pathway WP622 ("Long-day flowering time pathway"). Since many of the most significantly DEGs were not included in this pathway, I amended the analysis by adding most of the differentially expressed flowering time related genes. The precise roles of these genes were derived from (B. Liu et al. 2016; Shafiq, Berr, and Shen 2014; Radjacommare et al. 2023; Chahtane et al. 2023; Madrid, Chandler, and Coupland 2021; Hu et al. 2022). After building this expanded flowering time network, I decided to re-normalize the data to see the relevant expression patterns more clearly. Instead of comparing each sample to Col-0 expression levels, each genotype containing *uti1* was compared to its respective background line. The expression data examined in the network was therefore: *uti1* in Col-0 vs. Col-0, *uti1 trb1 trb3* vs. *trb1 trb3*, and *uti1 trb2 trb3* vs. *trb2 trb3* (Figure 8). Considering this flowering time regulatory network, it became obvious that almost all day-length associated key regulatory proteins were differentially affected by *uti1* mutations in any background. Especially the floral integrator *FLOWERING LOCUS T (FT)* and the transcriptional regulators *FRUITFULL (FUL)* and *LEAFY (LFY)* did not show any differences in expression in *uti1* containing mutants. The genes that exhibited the most counteracting behavior in Figure 7C, *FLK*, *FPA*, and *VIM1* also showed the strongest differential expression in this representation. *FPA* and *FLK* are both classified as flowering time expediting, due to their role as repressors of *FLC*. In this analysis, however, it appeared that this repression did not have a significant effect on the levels of *FLC*. On the contrary, *FLC* transcripts are increased in *uti1 trb2 trb3* compared to *trb2 trb3*. While this could explain the delayed flowering in *uti1 trb2 trb3*, the expected downstream effects of elevated levels of *FLC* (e.g., repression of *FT* expression) could not be detected. VIM1 is not a direct part of the regulatory network. In its role as a E3 ubiquitin ligase (Kim et al. 2014) it is likely involved in epigenetic gene regulation of many flowering time regulators. The decreased number of transcripts of *VIM1* in *uti1 trb2 trb3* could, therefore, be part of a systemic misregulation of many genes.

Taken together, the RNA-Seq results paint a picture of significant misregulation of flowering time genes in *trb* double mutants when combined with *uti1* loss-of-function alleles. Although *uti1* in Col-0 already led to expression changes, the combination with either *trb1 trb3* or *trb2 trb3* increased the amount of misregulated genes. While some transcriptome changes could be caused by the disruption of a putative TRB-UTI complex, a full picture of how TRBs and UTIs jointly control gene expression cannot be deduced from transcription data alone.

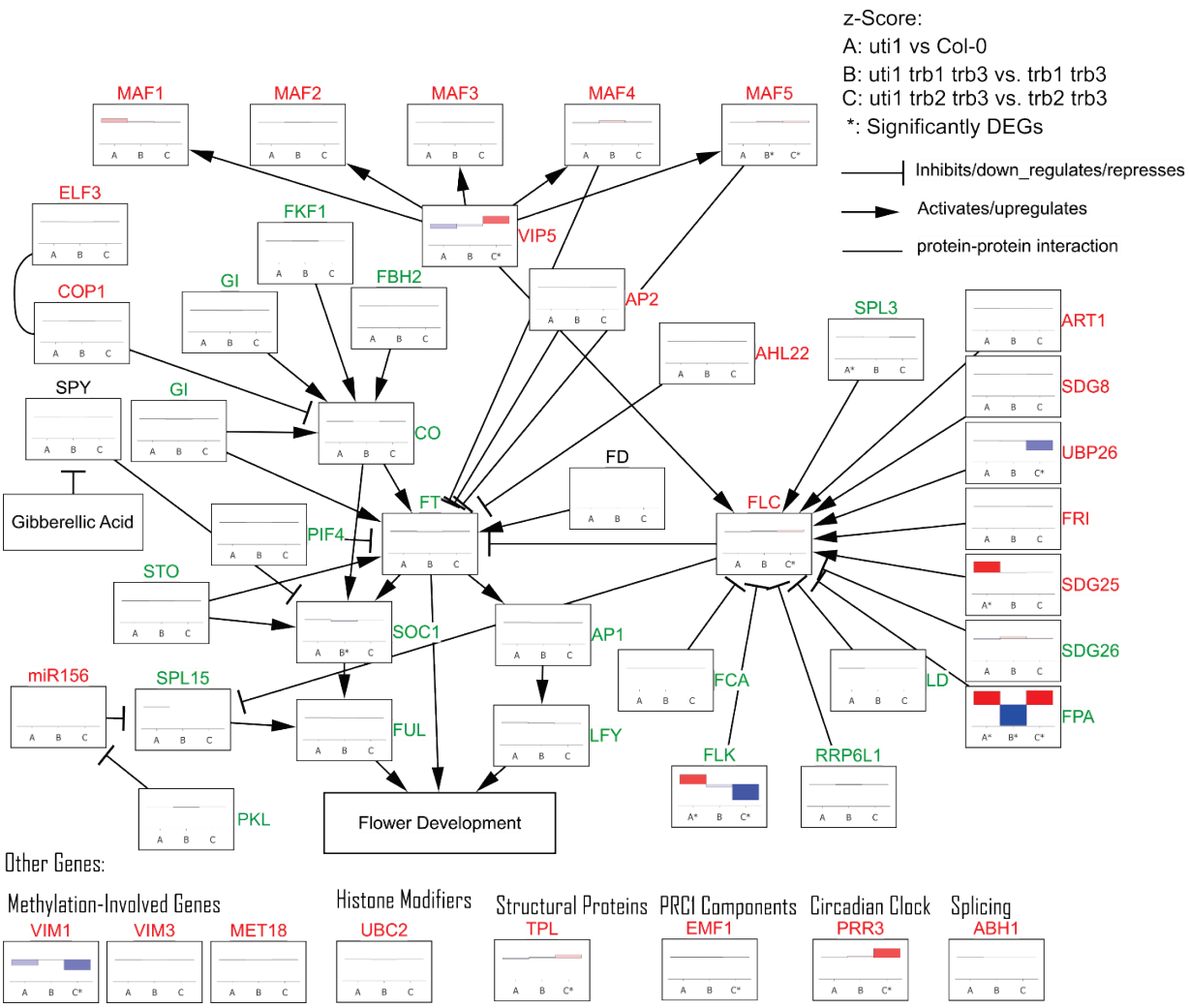

*Figure 8, Simplified flowering time gene regulatory network. Based on WikiPathway WP622 with expansions based on (Chahtane et al. 2023; Madrid, Chandler, and Coupland 2021; Shafiq, Berr, and Shen 2014). Nodes depict z-Score of relative expression level of: A, uti1 in Col-0 vs. Col-0; B, uti1 trb1 trb3 vs. trb1 trb3; C, uti1 trb2 trb3 vs. trb2 trb3. Significantly differentially expressed genes are depicted with *. Absence of bar graph indicates no transcript detection in sample.*

2.4 Using ChIP-Seq Datasets to Look for Signatures of the Putative ICU11 Complex

Since transcriptome analysis alone was not sufficient to find evidence of a PRC2-TRB-ICU11 complex, I opted to also investigate the distribution of ICU11 and histone modifications on a genomic level. I used original ChIP-Seq data for H3K36me3 and H3K27me3, each in Col-0 and *trb123* (*trb* triple mutant) that was generated in the group by Marije Vos. These sets were combined with published TRB ChIP-Seq data from our group (Krause 2019; Y. Zhou et al. 2016), as well as recently published ICU11 ChIP-Seq data from Xin-Jian He's group (Q. Wang et al. 2025).

The comparison of histone H3 modifications in Col-0 and the *trb* triple mutant revealed a strong overlap of peaks found in both sets (Figure 9, A). The H3K36me3 modification was found at slightly more sites in the *trb* triple mutant compared to Col-0 (440 sites more than Col-0). Nevertheless, the overlap between both genotypes was still substantial, with 7526 (82%) of the H3K36me3 sites being shared between *trb123* and Col-0. H3K27me3 ChIP-Seq presented very similar results, albeit with slightly smaller number of overlapping peaks. H3K27me3 was found at more sites in Col-0, resulting in 689 fewer peaks in the triple mutant. The overlap between Col-0 and *trb123* totaled 5211 (74.7% of the total Col-0 peaks). Therefore, both the overall number of peaks and their distribution appeared to be largely unaffected in TRB triple mutants for both histone marks.

If the removal of H3K36me3 was indeed controlled by a TRB-containing bi-functional complex, both histone marks would be mutually exclusive at TRB target sites. Additionally, this exclusivity would be negatively affected in the *trb* triple mutant. Analysis of the overlap of both histone marks in the two genotypes, however, only supported the first hypothesis. (Figure 9, B). In the WT, the overlap between H3K27me3 and H3K36me3 sites accounted for only 357 peaks (2.4% of total peaks). In *trb123*, the number of overlapping peaks stayed relatively stable with 303 peaks (2.1% of total peaks). This overlap occurred despite the increase in the number of H3K36me3 peaks and the decrease of H3K27me3 peaks. The relative amount of H3K36me3 peaks that overlapped H3K27me3 therefore decreased in *trb123* from 4.4% to 3.5%. Meanwhile, the reverse, peaks of H3K27me3 overlapping with H3K36me3, increased from 5.4% to 6%. Statistical evaluation of these findings through the SuperExactTest library (Minghui Wang, Zhao, and Zhang 2015) confirmed the significance of these findings. The overlaps of each histone mark between both genotypes were significant, while the overlaps between the marks were significantly lower than random. This indicates mutual exclusivity of H3K27me3 and H3K36me3 in both genotypes.

Analysis of the binding behavior of both histone marks across gene bodies revealed unexpected changes in H3K36me3 distribution (Figure 9, C). While H3K27me3 in *trb123* did not show large

changes in gene body occupancy compared to WT, regions upstream of the transcription start site (TSS) appeared to carry the mark slightly less frequently in the *trb* triple mutant. This is consistent with the published role of TRBs in recruitment of PRC2 to promoter regions (Y. Zhou et al. 2018). H3K36me3, on the other hand, did exhibit multiple significant changes in the absence of TRBs. In regions upstream of the TSS, the histone mark was found more frequently in the *trb* triple mutant. This is consistent with the putative TRB-mediated recruitment of ICU11 and subsequent histone mark removal in WT. In gene bodies, however, H3K36me3 was significantly increased in regions towards the center of the gene but declined sharply towards the transcription termination site (TTS). The TTS itself exhibited a similar differential binding to the TSS, but with even larger difference between WT and *trb123*. This "re-distribution" of H3K36me3 was not only detected in the metagene analysis. Evaluation of the ChIP-Seq signals in the Integrative Genomics Viewer (IGV) (Thorvaldsdóttir, Robinson, and Mesirov 2013) revealed that the pattern of increased H3K36me3 at TSS and TTS combined with a decrease in the gene body could be directly observed at numerous genes (Figure 9, D).

In the search for the putative PRC2-TRB-ICU11 complex, the overlap of ICU11 and TRBs is of particular interest, especially in combination with H3K36me3 (Figure 9, E). The overlap of TRB and ICU11 binding sites proved to be substantial. ICU11 shared 4914 (49.9%) of its 9838 binding sites with TRBs, while TRBs shared 61.8% of their 7951 collective binding sites with ICU11. Among those shared sites, 1874 (38.1%) exhibited H3K36me3 in either Col-0 or *trb123*. Overall, slightly more of the 4914 ICU11-TRB co-bound sites were marked by H3K36me3 exclusively in *trb123* than in Col-0 (283 vs. 181 sites). The significance of these overlaps was confirmed through SuperExactTest (Figure 9, G). The only non-significant overlaps were between ICU11 and H3K36me3 in either genotype. Furthermore, the sites of trimethylated H3K36 that were found in both sets did significantly overlap with ICU11. The by far largest overrepresentation of peaks can be found in the overlap of all four sets: Sites that are H3K36 methylated in both genotypes, as well as bound by ICU11 and at least one TRB, were found 8.1 times more often than random chance would suggest. Metagene plots of the H3K36me3 pattern at these genes revealed additional differences between sites bound by ICU11 and TRBs, and the remaining sites (Figure 9, F). The overall pattern of H3K36 trimethylation changes between Col-0 and *trb123* remained consistent (see Figure 9, D). By separating the genes into two sets: ICU11&TRB-bound and "other sites", significant differences between the sets emerged. While H3K36me3 in regions upstream of the TSS is increased in *trb123* in both sets, the ICU11&TRB-bound sites experience an even stronger increase in H3K36me3. The same effect was seen in Col-0. The previously observed gene body methylation changes did not seem to vary between the ICU11&TRB set and the "other sites". At

the TTS, however, another variation could be observed: ICU11&TRB sites exhibited less H3K36me3 compared to the “other sites” set, a reverse of the effect seen at the TSS.

In their totality, the results of this ChIP-Seq analysis suggest a strong association of ICU11 with TRBs. Both the overlaps of TRB and ICU11 binding sites, and the strong effect of *trb123* on the distribution of H3K36me3 provide evidence of this connection. While it seems that genes generally do not lose or gain H3K36me3, the observed shift could be evidence of ICU11-mediated H3K36me3 removal and the lack thereof in *trb* triple mutants, particularly in promoter regions.

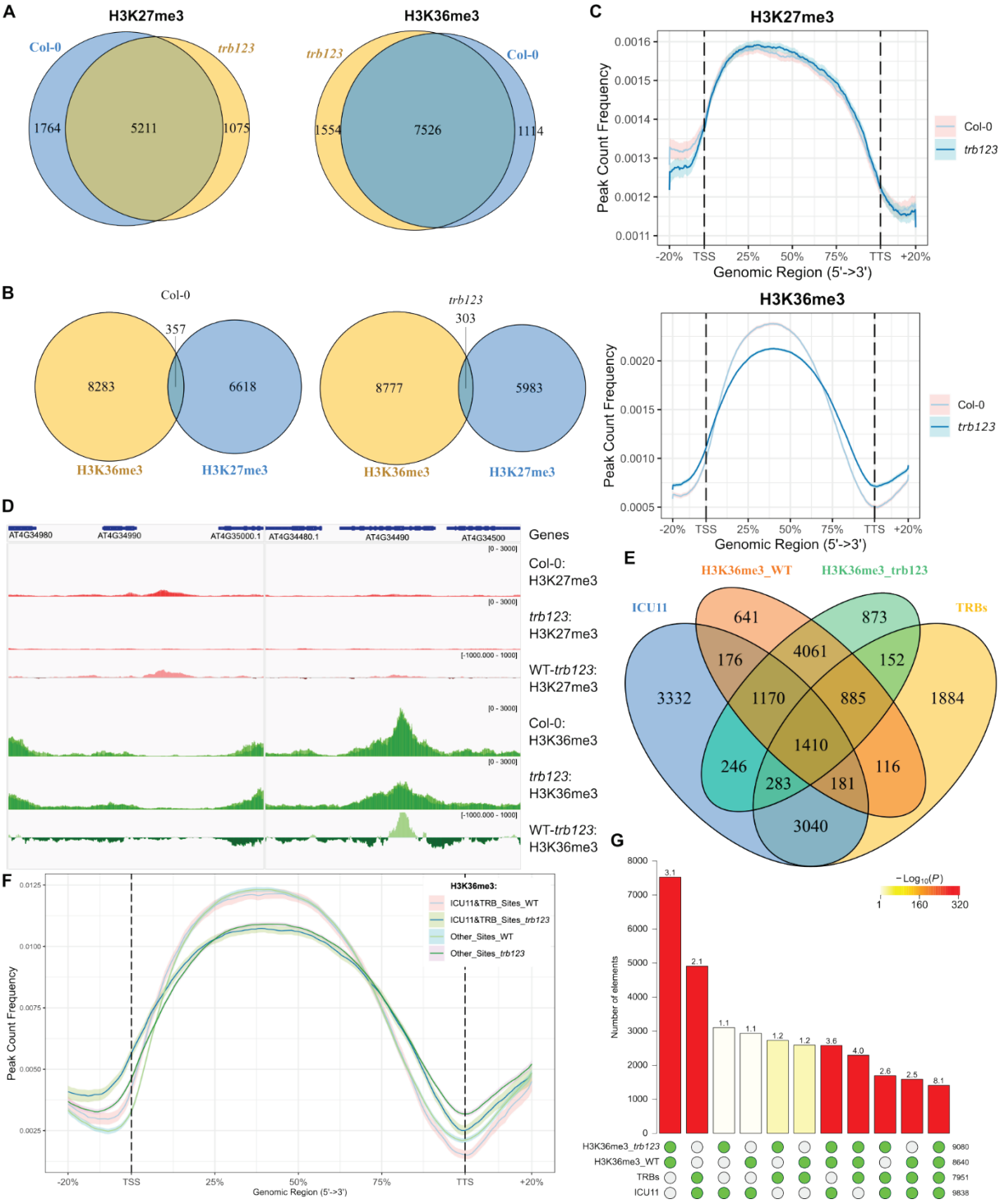

Figure 9, Analysis of H3K27 and H3K36 tri-methylation ChIP-Seq in Col-0 and trb123. ***A****, Overlap of peaks derived from ChIP-Seq against H3K27me3 (left) and H3K36me3 (right). Each in Col-0 and trb123.* ***B****, Overlap of peaks derived from ChIP-Seq against H3K36me3 and H3K27me3 in Col-0 (left) and trb123 (right).* ***C****, Metagene plots depicting the peak count frequency of H3K27me3 in Col-0 and trb123 (left) or H3K36me3 in Col-0 and trb123 (right). Plot covers gene body +- 20% bp upstream and downstream. Shaded area indicates 95% confidence interval.* ***D****, Genomic tracks of two exemplary genes (AT4G34990 and AT4G34490) exhibiting histone modification changes in trb123 consistent with the patterns depicted in C. Two replicates of ChIP-Seq tracks are overlayed in each lane. The third and sixth displayed track depict the difference between the tracks for Col-0 and trb123.* ***E,*** *Overlap of ChIP-Seq peaks against TRBs (sum of peaks derived from TRB1, TRB2, and TRB3 ChIP-Seq), ICU11, and H3K36me3 in Col-0 and trb123.* ***F****, Metagene plot depicting the peak count frequency of H3K36me3 in Col-0 and trb123. Subset by either genes co-bound by ICU11 and TRBs or by all other genes. Plot covers gene body +- 20% bp upstream and downstream. Shaded area indicates 95% confidence interval.* ***G****, SuperExactTest results of the four categories of peaks displayed in A and B (H3K27me3 and H3K36me3 in Col-0 and trb123). Number of overlapping genes displayed against each combination of two sets. The numbers on top of the bars display the fold enrichment of the set overlap compared to expected overlap. Colour displays significance:*

red, significant enrichment of overlap. White, significant depletion (determined by separate MSET function). The values right of the set overlap information depict the number of genes included in the set.

The genome-wide analysis revealed that H3K36me3 undergoes intra-gene rearrangements in *trb123*. This approach, however, is limited by the binary classification of genes as targets of histone modification. To better account for more subtle rearrangements, I opted to further analyze the ChIP-Seq data using the DiffBind package (Rory Stark 2017). This allows for differential binding analysis beyond the simple present/absent binary. The resulting lists of differentially bound sites (DBS) that either gain or lose histone marks in *trb123* was used for subsequent analysis. Based on the previously established mutual exclusivity of H3K27me3 and H3K36me3, I determined how many sites "switch" from one mark to the other (Figure 10, A). Surprisingly, neither the switch from H3K27me3 to H3K36me3 nor the reverse are common. Only 0.8% of differentially modified sites exhibit the switch to H3K36me3, while the reverse is found at 1.2% of sites. Using SuperExactTest to analyze the overlap of all four categories of DBS supports these findings and provides further evidence of the mutual exclusivity of both marks (Figure 10, B). The number of sites that gain H3K36me3 at the expense of losing H3K27me3 is about equal to what a fully random distribution would provide. The inverse pattern is even less common, reaching only 0.4 times the number of sites that a random distribution would suggest. Generally, H3K27me3 behaves in a much more "binary" manner than H3K36me3, either being present or absent at sites. H3K36me3, on the other hand, displays a more pronounced spectrum of enrichment. Sampling multiple genes that "switch" histone marks revealed that their H3K27me3 levels were often more intermediary, breaking from this "binary" pattern (Figure 10, C). This indicated that the simultaneous loss of one mark by gaining the other could be an artefact of bulk tissue sequencing, with only a subset of tissues exhibiting the full loss or gain of histone marks.

To investigate whether these "switch" sites are connected to the putative PRC2-TRB-UTI complex, I performed a similar analysis to Figure 9,E. After annotating the peaks to genes, I compared the list of genes to those that are targeted by ICU11 or one of the three TRBs. This analysis revealed that more genes that lost H3K27me3 in favor of H3K36me3 were targets of both ICU11 and TRBs than either ICU11 or TRBs alone (14 versus 4 and 5 respectively). In fact, the majority (53.8%) of all genes in this category were also TRB and ICU11 targets. Genes that underwent the inverse switch displayed a similar, albeit less extreme, pattern. Although only 24% of genes that lost H3K36me while gaining H3K27me3 were bound by ICU11 and TRBs, this number was still higher than the 5.5% similar genes that were bound only by TRBs but not ICU11. Overall, the small number of affected genes severely diminished the statistical power of the SuperExactTest used to analyze the significance of these findings (Figure 10, E). Nevertheless, overrepresentation of sites that gain H3K36me3 while losing H3K27me3 in *trb123* could be detected. When co-occurring with

either TRBs (3.3 times more common than expected) or TRBs and ICU11 (8.2 times more common than expected), these intersections proved to be statistically significant.

Next, I investigated the 14 genes that were found in the intersection of TRB binding sites, ICU11 binding sites, and sites that gained H3K36me3 while losing H3K27me3. Among these genes, both ribosomal genes (e.g., *NUCLEOLIN LIKE 2 (ATNUC-L2)*) and genes affecting chromatin modification (e.g., *EMF1*) were enriched. *EMF1*, a known PcG component, was not only among these 14 genes (Figure 10, G), but was also detected as a DEG in the transcriptome of *uti1 trb1 trb3* and *uti1 trb2 trb3*, but not any of the *trb* double mutants or *uti1* (Figure 7, C). Because of this discovery, I decided to use the SuperExactTest to determine whether the intersection of genes that switch histone marks with flowering time affecting genes was statistically significant. I chose to test against both, all flowering time affecting genes and the subset of genes that were also differentially expressed in either *uti1 trb1 trb3* or *uti1 trb2 trb3*. Despite the low number of samples in the analysis, multiple intersections were found to be significant (Figure 10, H). This indicates that genes that are associated with flowering were significantly more likely to undergo either type of "histone mark switch" in *trb123*, particularly those genes that are also differentially expressed in the *uti1 trb1 trb3* or *uti1 trb2 trb3* mutants.

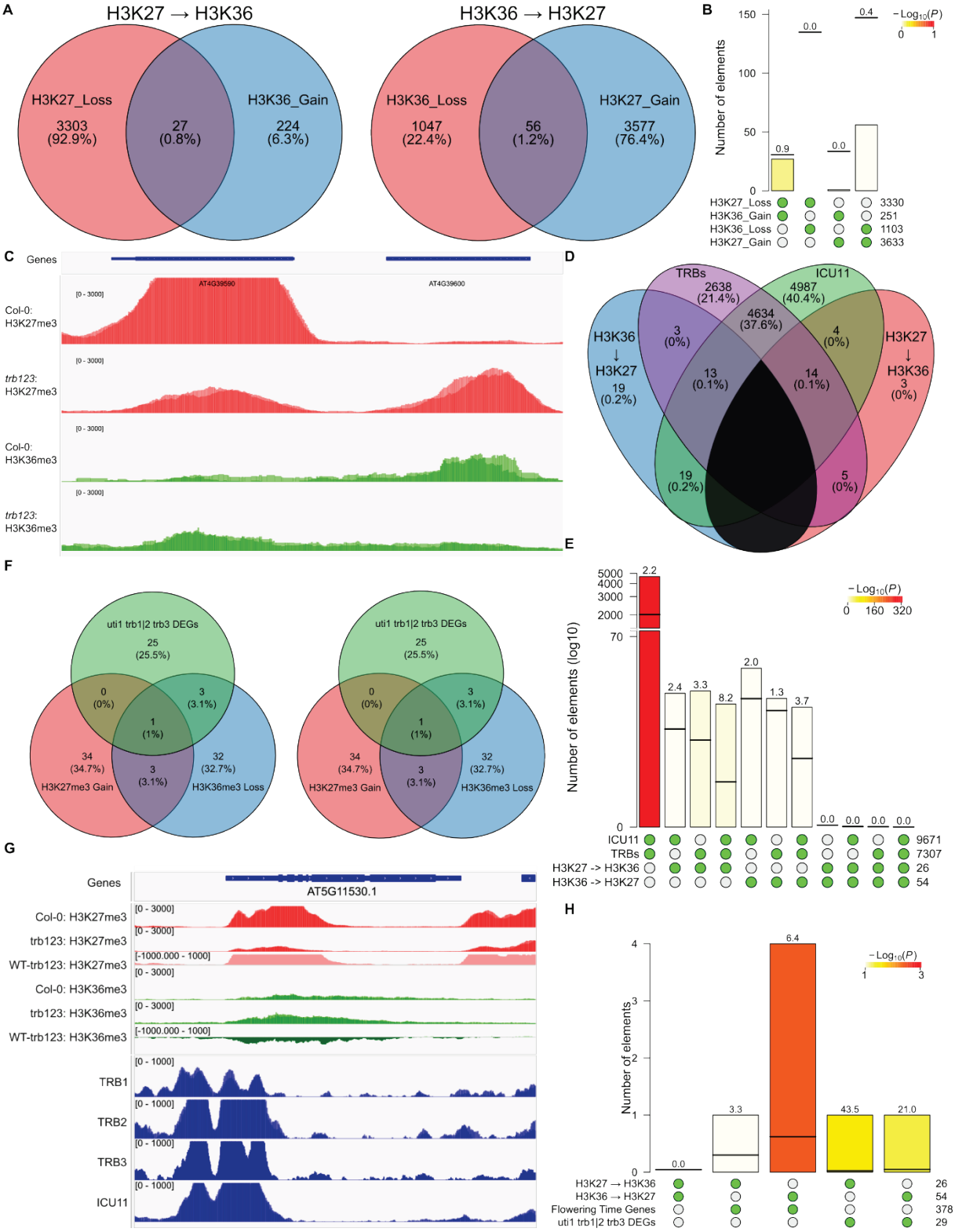

Figure 10, Analysis of differentially modified sites in Col-0 and trb123. ***A****, Overlaps of sites with differential histone modifications in trb123. H3K27 → H3K36 (Left): Overlaps of sites that lose H3K27me3 with sites that gain H3K36me3. H3K36 → H3K27 (Right): Overlaps of sites that lose H3K36me3 with sites that gain H3K27me3.* ***B****, SuperExactTest results of any combination containing two of the four categories of peaks displayed in A (sites gaining or losing either H3K27me3 or H3K36me3). The numbers on top of the bars display the fold enrichment of the set overlap compared to expected overlap. Expected overlap is depicted as horizontal bar. The values right of the set overlap information depict the number of peaks included in the set.* ***C****, Genomic tracks of two exemplary genes (AT4G39590 and AT4G39600) exhibiting histone modification changes in trb123 consistent with the overlapping sections of A. Two replicates of ChIP-Seq tracks are overlayed in each lane.* ***D****, Overlap of ChIP-Seq peaks against TRBs (sum of peaks derived from TRB1, TRB2, and*

TRB3 ChIP-Seq) and ICU11 with sites that either lose H3K36me3 while gaining H3K27me3 in trb123 (H3K36 ↓ H3K27) or lose H3K27me3 while gaining H3K36me3 in trb123 (H3K27 ↓ H3K36). Since both histone-change patterns are mutually exclusive, their overlapping area is shaded black. ***E****, SuperExactTest results of any combination of the four categories of peaks displayed in D. The numbers on top of the bars display the fold enrichment of the set overlap compared to expected overlap. Expected overlap is depicted as horizontal bar. The values right of the set overlap information depict the number of peaks included in the set.* ***F****, Sites that, in trb123, lose H3K36me3 and/or gain H3K27me3 (left) or vice versa (right) overlapped with the flowering time affecting genes that were differentially expressed in uti1 trb1 trb3 or uti1 trb2 trb3.* ***G****, Genomic tracks of EMF1 (AT5G11530), exhibiting histone modification changes and protein binding consistent with the intersection of all sets of A. Two replicates of ChIP-Seq tracks are overlayed in each lane, except TRB3. The third and sixth displayed track depict the difference between the tracks for Col-0 and trb123.* ***H****, SuperExactTest results of any combination containing two of four categories. H3K27 → H3K36: Intersection of genes that lose H3K27me3 with genes that gain H3K36me3 in trb123. H3K36 → H3K27: Intersection of genes that lose H3K36me3 with genes that gain H3K27me3 in trb123. Flowering Time Genes: All genes implicated as flowering time regulating by Bouché et al. (2016). uti1 trb1|2 trb3 DEGs: Intersection of flowering time regulating DEGs found in uti1 trb1 trb3 and uti1 trb2 trb3. The numbers on top of the bars display the fold enrichment of the set overlap compared to expected overlap. Expected overlap is depicted as horizontal bar. The values right of the set overlap information depict the number of peaks included in the set.*

2.5 The Complexity of the Regulatory Landscape Surrounding TRBs Necessitates a More Integrated Approach

The previous approaches made it clear that the regulatory landscape surrounding TRBs is even more complex than initially anticipated. The pivotal role TRBs play in epigenetic gene regulation and plant development make it exceedingly complicated to use traditional reverse genetics approaches. Each disruption to TRBs and the complexes they are involved in can result in a multitude of systemic changes. This is likely caused by misregulation of multiple, sometimes opposing, regulatory complexes. The high degree of redundancy found in TRBs further complicates these interactions. This is exemplified by the observation that *uti1* alleles can have different effects based on which *TRB* allele is present. It has therefore become clear that further research into the role of TRBs requires a better understanding of how and where they interact with regulatory complexes. In addition, the role TRB paralogs play in the formation of different regulatory complexes is crucial information necessary for further inquiries into TRB-mediated gene regulation.

3 Publication: TRB-mediated epigenetic gene regulation is controlled by distinct regulatory complexes utilizing specialized TRB paralogs

3.1 Significance for this Dissertation

This manuscript provides substantial evidence of both the participation of TRBs in epigenetic regulatory complexes on a genomic level, and the specialization of TRB paralogs. This contributes greatly to the aim of this dissertation by providing solid understanding of the mutual exclusive character of TRB-mediated epigenetic regulation and the molecular basis of the unequal redundancy of the three TRB paralogs. Additionally, this manuscript proposes the existence of at least two more TRB-associated epigenetic regulatory complexes, albeit not in connection with ICU11 or UTIs.

3.2 Author's Contribution

All sections of the manuscript directly pertaining to the comparison of ChIP-Seq datasets were performed by the author, apart from the original ChIP-Seq and RNA-Seq experiments.

This includes obtaining and analyzing the previously published ChIP-Seq datasets, the bioinformatic comparison of complex binding sites, the DNA motif enrichment analysis, and the determination of GO-Term enrichment.

In detail, figure 2, panel A of figure 4, figure 5, and figure 6 were generated by the author along with all accompanying text. Furthermore, the author provided the text of the conclusion of the manuscript. The manuscript is currently under review at PLOS Genetics.

3.3 Full Manuscript

Epigenetic gene regulation is controlled by distinct regulatory complexes utilizing specialized paralogs of TELOMERE REPEAT BINDING FACTORS

Maik Mendler[1#], Kristin Krause[12#], Simone Zündorf[1], Prathamesh Sannak[1], Petra Tänzler[1], Sara Stolze[1], Hirofumi Nakagami[1] and Franziska Turck[1&]

[1]*Max Planck Institute for Plant Breeding Research, Carl von Linné Weg 10, 50829 Köln*

[2]*Illumina Solutions Center, Berlin, Germany*

[&] Author for correspondence: turck@mpipz.mpg.de

[#]: contributed equally

bioRxiv preprint DOI: https://doi.org/10.1101/2025.11.10.687574

Posted: November 11, 2025, Version 1

Abstract

Epigenetic regulators shape chromatin landscapes, allowing cells to express distinct gene sets depending on cell-type, developmental stage or environmental cues. These regulatory complexes rely on interactions with sequence-specific DNA binding proteins, such as the small family of TELOMERE REPEAT BINDING FACTORS (TRBs). TRBs are components of chromatin regulatory complexes with opposing functions, such as the epigenetic repressors Polycomb Repressive Complex 2 (PRC2) and a JMJ14/NAC complex that respectively add and removes the repressive H3K27me3 and positive H3K4me3 modification, but also with the plant-specific PEAT complex that is linked to histone acetylation and gene activation.

We dissected the partial redundancy between TRB1, TRB2 and TRB3 in target gene selection and interaction with different chromatin regulatory complexes. High redundancy of TRBs is suggested by major phenotypic changes that are only observed *trb* triple mutants; however, we found different target site preference between TRB1-3 and preferred partnership with chromatin complexes. Furthermore, TRB paralogs interacted with the NuA4 histone acetylation complex, both together with and in absence of PEAT. Among the three paralogs, TRB1 had more unique binding sites and correlated stronger with PEAT and NuA4 functions. In contrast, TRB2 and TRB3 were more dependent on the presence of *bona fide* telo-box motifs and were more likely to be found at PRC2 associated sites. Overall, we provide insight into the diverse roles of TRBs in epigenetic gene regulation and how their diversification contributes to their apparent redundancy, as well as their observed activating and repressing effects on gene expression.

Background

In *Arabidopsis thaliana*, telo-box motifs are widely found at gene regulatory elements; furthermore, they are native to the telomeres at chromosomal ends, where they occur as direct repeats (TTTAGGG × n; n = 2 to 1000+) and associate with several telomere repeat binding proteins, including TELOMERE REPEAT BINDING FACTOR (TRB) 1-5 [1–3]. TRB proteins belong to the Single myb histone (Smh) family and contain an N-terminal myb, a H1/H5-linker and a C-terminal coiled-coil domain [4]. The direct interaction of TRBs with telomere repeats is mediated by their N-terminal myb-domain, which belongs to the telobox class of myb-domains that is shared among telomere repeat binding proteins in all eukaryotes [5, 6]. TRBs directly interact with the telomerase subunit TERT and are thought to be part of the plant shelterin complex which aids the telomerase in solving the end-replication problem and protects telomere ends from being falsely recognized as DNA double strand breaks [1, 7]. The H1/H5-linker histone domain is involved in the formation of TRB multimers at telomere ends. For TRB1, it was shown that binding to interstitial telomeric repeats, which are relics of chromosomal fusions specific to *A. thaliana*, is prevented by the presence of linker histone H1, indicating that while the H1/H5 domain may contribute to target binding, it cannot outcompete the canonical linker histone [8]. The C-terminal coiled-coil domain is thought to mediate the interaction with other proteins [5, 9]. Telo-box motifs were first linked to promoter regions of highly expressed genes of the translation machinery [3]. Genome-wide binding analysis of TRB1 confirmed the link to genes encoding for the translational apparatus [9, 10].

TRB1 is an integral component of the plant-specific PWWP-ENHANCER OF POLYCOMB-LIKE-ARID-TRB (PEAT) complex, which is predominantly involved in gene activation [11, 12]. PEAT activates target genes through a dual approach that involves histone acetylation and deubiquitination of mono-ubiquitinated H2A (H2AKub1) [11]. Histone acetylation is facilitated through HISTONE ACETYLASE RELATED TO MYST (HAM) 1 and 2 which links PEAT to the Nucleosomal Acetyltransferase of histone H4 (NuA4) complex, which co-purifies with PEAT components [11]. Co-purification of UBIQUITIN SPECIFIC PROTEASE 5 (UBP5) and PEAT positions PEAT as a direct antagonist of the epigenetic repressor Polycomb Repressive Complex (PRC) 1, which sets the H2AKub1 mark [13].

Mutated alleles of *TRB1* and *TRB3* were identified as genetic enhancers of mutations in *LIKE-HETEROCHROMATIN PROTEIN 1* (*LHP1*) and *CURLY LEAF* (*CLF*). LHP1 and CLF act as accessory and integral part of PRC2, respectively [9, 14] and LHP1 also interacts with PRC1 components that catalyze H2AKub1 [15]. PRC2 establishes the covalent modification tri-methylation of histone H3 at lysine 27 (H3K27me3) at thousands of loci, resulting in transcriptional repression of target

genes (reviewed by [16, 17]). TRBs can recruit PRC2 to telo-box motifs via their direct interactions with the PRC2 components CLF/SWN, which is essential for stable H3K27me3 coverage and epigenetic repression of a subset of these genes [14]. While TRB1 binding sites were under-represented within H3K27me3 marked regions, telo-box motifs were overrepresented, in particular at regions that show reduced H3K27me3 in *clf* mutants [18]. Telo-box motifs were also enriched in regions bound by the PRC2 components FERTILISATION INDEPENDENT ENDSPERM (FIE), SWINGER (SWN) and CLF [19–21]. Finally, TRB1-3 are also part of a transcription repressive complex composed of the histone de-methylase JUMONJI (JMJ14), NAC50 and NAC52 (names after the founding family members No Apical Meristem (NAM1), ARABIDOPSIS TRANSCRIPTION FACTOR (ATAF1/2), CUP SHAPED COTYLEDONE (CUC2)) [22, 23].

The association of telo-box motifs and TRBs with repressed as well as highly expressed genes and with repressive as well as activating chromatin complexes raises the question of how the functional context is established and to which extent TRBs are specialized in their molecular function. Phenotypic analysis confirmed the high redundancy between TRB1-3, as strong phenotypic changes were only observed in triple mutants. In contrast, comparison of genome-wide binding revealed many sites exclusively bound by TRB1 that were more likely associated with PEAT/NuA4 or NuA4. In contrast, binding sites preferred by TRB2 and TRB3 over TRB1 were the most highly associated with PRC2-mediated gene repression.

Results

Transcriptomic changes in *trb* double and triple mutants indicate a limited partial redundancy between paralogs

As we and others have previously reported, plants homozygous for two mutated alleles of *TRB1*, *TRB2* or *TRB3* are indistinguishable from wild-type controls grown under standard conditions, but a deletion of the third allele has a catastrophic effect on plant development [14, 23]. To evaluate the extent of genetic redundancy, we grew plants that still segregated one functional *TRB* allele (*prope triple*) together with all double mutant combinations and Col-0 controls in standard growth conditions (LD, 16h light/8h dark, 21°C). Triple *trb123* mutants were strongly dwarfed and usually died before their *prope triple* or double homozygous siblings flowered (Manuscript Figure 1A). While *prope triple* mutants that segregated functional alleles of *TRB1* and *TRB3* flowered as controls, plants carrying only one functional allele of *TRB2* flowered significantly earlier indicating that the latter is a slightly weaker paralog with respect to a role in flowering time regulation (Manuscript Figure 1B).

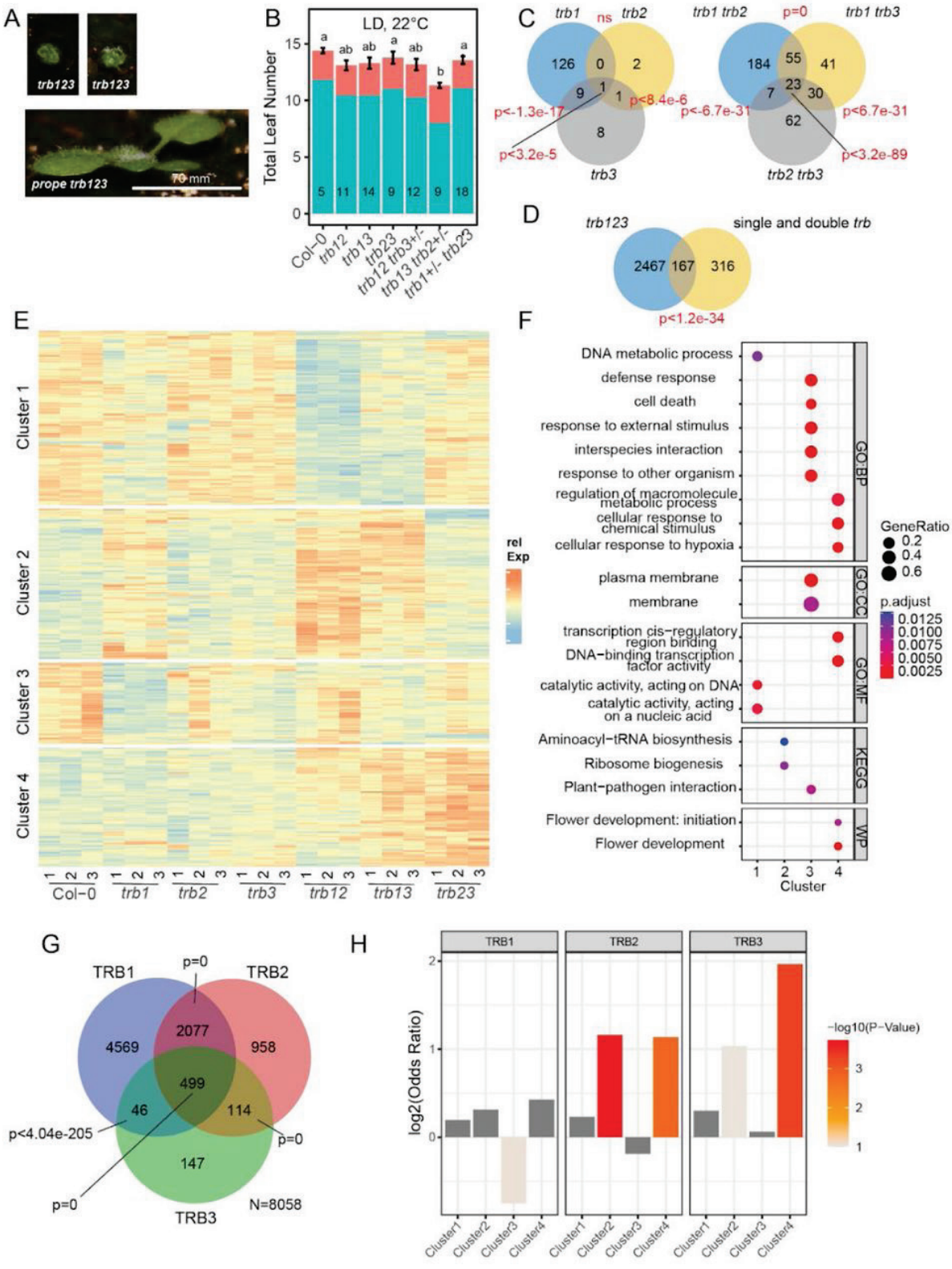

Manuscript Figure 1. Limited partial redundancy of TRB1-3. ***A)*** *Phenotypes of trb123 triple mutants and siblings with one functional TRB allele. Common scale bar indicated.* ***B)*** *Flowering time of double trb mutant and prope triple mutants scored as total leaves on main shoot (rosette leaves: green, cauline leaves: red). Plants were grown at 22°C in long days (16h light/8h dark) in culture chambers. Significant differences determined by ANOVA, letters indicate HSD groups at p<0.01. Replicates (5 < n < 18) are indicated within bars. Error bars show standard error of the mean.* ***C)*** *Venn diagrams showing the number of differentially expressed genes (DEGs) in single trb (left) and double trb mutants (right) compared to Col-0.* ***D)*** *as C) comparing DEGs in triple trb123 mutants against all DEGs in C). Significance of overlap in C) and D) determined by SuperExact test using all expressed genes as background.* ***E)*** *Heatmap of clusters of all DEGs as in C). Clustering was performed after Variance Stabilization Transformation (VST) of read count data and normalization by the*

mean for each gene. ***F)*** *Gene-Onthology (GO) and pathway enrichment analysis for clusters shown in E). Significance was tested against the background of all expressed genes. Relative enrichment of GO terms for Biological processes (GO:BP), cellular compartment (GO:CC), molecular function (GO:MF) and KEGG metabolic pathways and wikipathways (WP) are indicated by bubble sizes, statistical significance by color codes.* ***G)*** *Venn diagram showing the number of genes associated with ChIP-seq peaks identified for TRB1, TRB2 and TRB3. Statistical test as in C using all annotated genes as background.* ***H)*** *Distribution of TRB1, TRB2 and TRB3 target genes among the transcriptional clusters shown in E). Bar plots show Odds ratio and −log10 pValues as determined by Fisher's Exact test are indicated as color code.*

Both, high redundancy and signs of unequal redundancy, were also observed at the level of transcriptome changes. Using above ground tissue of 14-day-old seedlings grown on soil in standard growth conditions (LD, 16h light/8h dark, 21°C), we found overall 483 differentially expressed genes (DEGs) in *trb* single and double mutants compared to Col-0 (Manuscript Figure 1C and Supplemental File 1). Of these DEGs, most were specific to *trb1* single and *trb1 trb2* double mutants, indicating that *TRB2* and *TRB3* cannot fully compensate for the loss of *TRB1*. Only around a third (35%) of the DEGs identified in single and double mutants were shared with *trb123*, which represent only 6% of the 2634 DEGs identified in these mutants (Manuscript Figure 1D). While a higher number of DEGs is expected from the strong phenotypic changes observed in *trb123*, the occurrence of genes specific to the milder mutants is more difficult to rationalize.

To gain more insight on the specific impact of *TRB* paralogs on the transcriptome, we performed partitioning around medoid (PAM)-clustering of all mis-regulated genes based on their relative expression profile. The number of clusters k=4 was empirically determined as best (Manuscript Figure 1E). Cluster 1 and 2 correlated with the loss of *TRB1* function, showing respectively decreased- and increased expression. GO-term enrichment analysis associated cluster 1 with functions in DNA damage and repair, while cluster 2 enriched GO-terms related to ribosome biogenesis (Manuscript Figure 1F, Supplemental File 1). Cluster 3 showed decreased expression in *trb1*, *trb3* and *trb13* double mutants and enriched GO-terms related to responses to biotic stress. Cluster 4 was mostly determined by the combination of *trb3* with either *trb1* or *trb2*, showing increased expression of genes in these double mutants. Cluster 4 enriched the wiki-pathway flowering initiation and flowering development (https://www.wikipathways.org/) based on the presence of the floral organ identity genes *AGAMOUS* (*AG*), *SEPELLATA* (*SEP*) *1* and *3*, the flowering time regulator *TEMPRANILLO 1* (*TEM1*) and the PcG component *EMBRYONIC FLOWER 1* (*EMF1*), which were previously identified as TRB-dependent targets of PRC2 [14] (Supplemental Figure 1).

Binding sites of TRB1-3 reveal distinct target site preferences

To better understand the redundant and specific roles of TRB paralogs, genome-wide binding profiles of all three were compared. TRB ChIP-seq libraries were prepared using chromatin from 14-day old seedlings stably expressing *TRB2* and *TRB3* carboxy-terminal fusions to *YELLOW FLUORESCENT PROTEIN* (*YFP*) under the control of their respective promoters (*TRB2-YFP* in Col-

0 background and *TRB3-YFP* in *trb3-2* background, [14]). TRB1-GFP ChIP-seq data were taken from Zhou *et al*. (2016). Enriched peaks were called against control ChIP-seq libraries prepared from Col-0 chromatin precipitated with the same anti-GFP antibody from two biological replicates using the Irreproducible Discovery Correction (IDR) framework at a cut-off of IDR ≤0.05 (Supplemental Figure 2,[24]). The analysis identified 7483, 3771, 845 peaks for TRB1, TRB2, TRB3 respectively (Supplemental Figure 3A and Supplemental File 2). The observed proportion of peaks for TRB paralogs is similar to those obtained in a recent study by Wang *et al*. 2023 (Supplemental Figure 3B). Visual inspection of gbrowse tracks showed that many sites unique to TRB1 showed clearly distinct peaks, while sites unique to defined as TRB2 or TRB3 frequently showed low enrichment (below the significance threshold) of the other TRBs (Supplemental Figure 3C). We annotated all TRB peaks to target genes to estimate whether transcriptional patterns detected in the double and triple mutants could be related to the binding of TRB paralogs (Manuscript Figure 1G, Supplemental File 3). Overall, DEGs were slightly more likely to be TRB target genes than expected by chance (Fisher's Test, $p< 0.017$, odds ratio 1.27). Next, we tested for specific TRB paralog enrichment between the four PAM-clusters. For TRB1, a direct effect on gene expression was suspected for transcriptional cluster 1 and 2 that show obvious changes in *trb1* and *trb1 trb2* mutants; however, a specific overrepresentation of TRB1 targets could not be confirmed for any of the clusters, while a mild underrepresentation was detected for cluster 3 (Fisher's test, $p<8.8\times10^{-2}$, Manuscript Figure 1H). In contrast, cluster 2 was overrepresented for TRB2 and TRB3 target genes (Fisher's test, $p< 1.8\times10^{-4}$ and 9.2×10^{-2}, respectively). While TRB2 was more significantly overrepresented in cluster 2, TRB3 was more significantly overrepresented in cluster 4 compared to TRB2 (4.8×10^{-4} and 1.5×10^{-3}, respectively). Taken together, despite a large redundancy, TRB1-3 show target site preference, which is reflected in the expression patterns of a small set of genes in double or, in the case of *trb1*, single mutants. Overall, a direct more specialized role of TRB2 and TRB3 in gene repression is supported by the overrepresentation of direct targets among clusters showing increased expression in double mutants.

TRB paralogs show preferred association with distinct chromatin regulatory complexes

To better understand the redundant and specific roles of TRB paralogs within the context of associated chromatin regulatory complexes, we compared the binding of TRB1-3 with available data for TRB-interacting protein complexes. Representative of the PEAT complex, genome-wide binding data were available for core-components EPCR1 and PWWP1 [12] and for UPB5, which removes the PRC1-associated mono-ubiquitination of H2A [13] and was recently proposed to be a PEAT component [11]. HAM1 and EPL1B are members of the NuA4-complex, the former but not the latter was also shown to interact with PEAT [11]. CLF and SWN are core components of the PRC2 complex [21]. The H3K4me3 de-methylase JMJ14 was shown to interact with TRB with a role

in balancing gene expression [23]. Since data were generated by different groups and analyzed through different bioinformatic pipelines, we classified peaks into decile bins based on the published significance scores for each protein. We divided the genome of *Arabidopsis thaliana* into 238296 bins of 500 bp length and considered proteins to co-localize if any part of their associated peaks was found in the same bin (Supplemental File 3). Pearson's correlation coefficient analysis identified four complex groups with strong correlations within the groups, corresponding to PEAT (EWPCR1, PWWP1, UBI5), NuA4 (HAM, EPL1B), TRBs-JMJ14 (TRB1, TRB2, TRB3, JMJ14) and PRC2 (CLF, SWN) (Manuscript Figure 2A). Obvious positive correlation was also observed between PEAT, NuA4, TRB1 and TRB2 and between TRB3 and PRC2. In contrast, JMJ14 showed negative correlation with PEAT and NuA4 and was rather neutral with respect to PRC2 binding sites, indicating that although JMJ14 and TRBs often bind targets together, they do not usually also bind at PEAT and NuA4 associated sites.

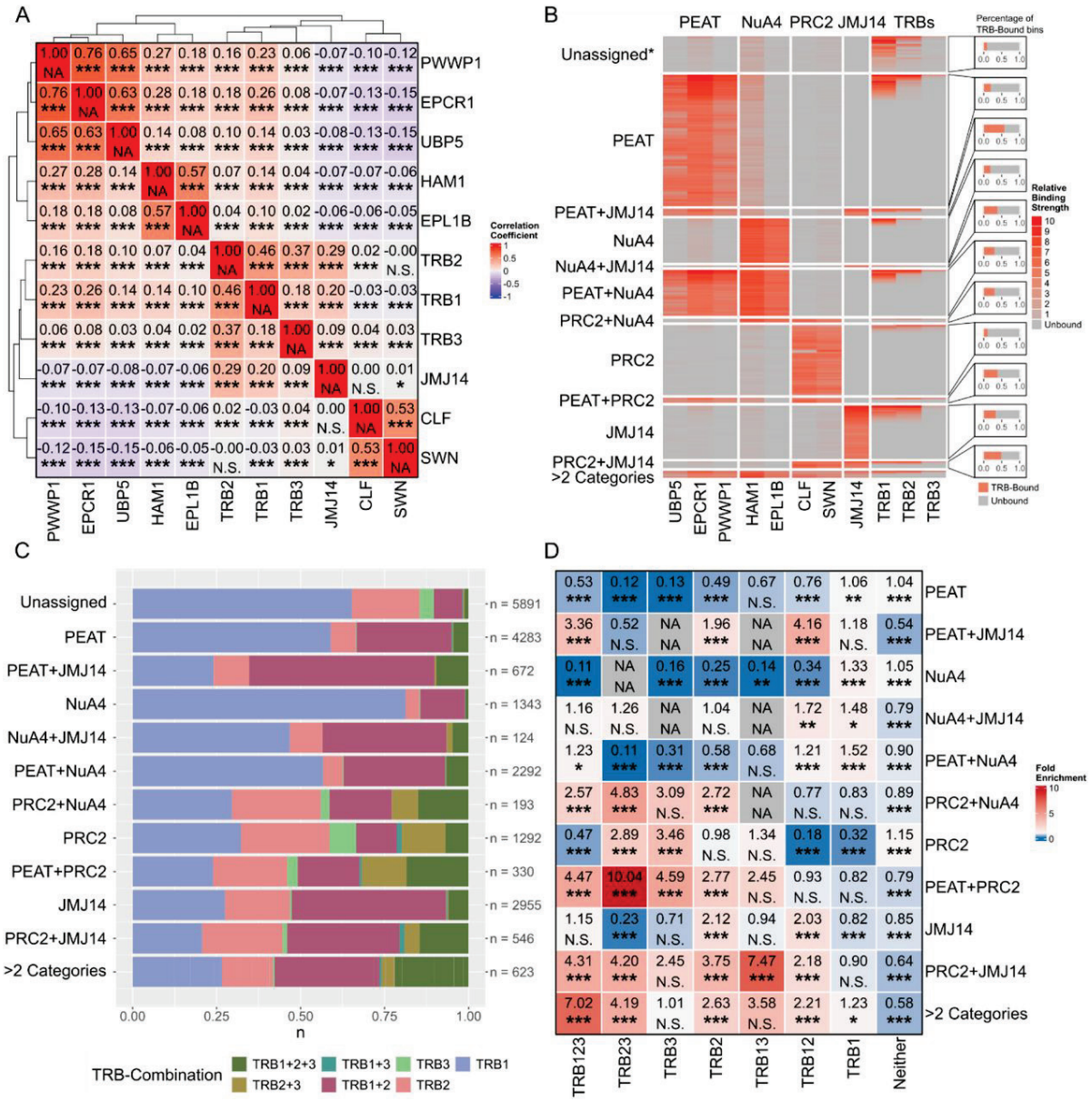

Manuscript Figure 2. Analysis of genomic binding locations of eleven epigenetic regulatory proteins. ***A);*** *Pairwise Pearson correlation matrix of ChIP-Seq peaks derived from eleven regulatory proteins and assigned to 500 bp genomic bins. Significance levels: ***, p<=0.0005, **, p<=0.005, p<=0.05, N.S., p>0.05.* ***B);*** *Left, Heatmap depicting the genomic bins bound by each of the ChIP-Seq sets used in A. Relative binding strength of each peak expressed through deciles. Columns depict proteins grouped by regulatory complex and rows depict bins assigned to complexes based on presence of at least two complex components. Bins assigned to more than two complexes were grouped into one category. *, 58676 bins which were neither assigned to complexes nor TRB-bound were excluded for the sake of readability. Right, Percentage of TRB-bound bins for each category.* ***C)*** *Distribution of TRBs in the TRB-bound bins of each category assigned in B.* ***D)*** *Pairwise exact test statistics as described by Wang et al. (2015) for bins assigned to complex categories and their corresponding TRB combinations. Significance levels: ***, p<=0.0001, **, p<=0.001, p<=0.01, N.S., p>0.01.*

A heatmap using the matrix of decile transformed binding sites across target categories underscored that TRBs rarely bind chromatin without any of the described partner complexes (Manuscript Figure 2B). The heatmap visualized the mostly exclusive, non-overlapping nature of complex categories except for PEAT and NuA4, which are equally likely to bind chromatin in

combination or alone. Next, we evaluated if TRB paralogs showed preference for specific partner complexes. Association of fully resolved TRB binding categories indicated a high proportion of PEAT and NuA4 sites that were exclusively bound by TRB1 (Manuscript Figure 2C). If JMJ14 was also associated with PEAT and/or NuA4, the proportion shifted to include more peaks co-bound by TRB1 and 2 or by all TRBs. The shift in distribution was significantly different from the expected based on a SuperExact Test of expected combinations (Manuscript Figure 2D) [25]. Presence of TRB2, in particular in combination with TRB1, was most significantly enriched for JMJ14 containing bins, irrespective of the presence or absence of other interacting complexes. In contrast, PRC2 was most overrepresented at peaks only bound by TRB3, followed by the combination of TRB3 and TRB2. At the rare sites where PRC2 co-bound with JMJ14 or with PEAT, the overrepresentation of TRB1/TRB3 and TRB2/TRB3 peaks became much higher.

Since TRB1 and TRB3 showed a strong propensity to associate respectively with PEAT/NuA4 and PRC2, we performed Immunoprecipitation Mass Spectrometry (IP-MS) to evaluate whether preferred complex associations could also be observed at the protein level. Plants expressing *TRB1* or *TRB3* to *YFP* fusions under the control of the *Cauliflower Mosaic Virus 35S* promoter (*35Sp*) were immunoprecipitated from nuclear extracts using a GFP-trap resin. Samples prepared from *35Sp-ENHANCED DISEASE SUSCEPTIBILITY 1 (EDS1)-YFP* transgenic lines were used as background control. Using biological triplicates, overall 1149 proteins were identified, of which 96 were significantly enriched in either TRB1 or TRB3 pull-downs or both (Supplemental File 4). Co-purified proteins included components of PEAT, NuA4, JMJ14 complexes and PRC2. Only 6 and 7 proteins were significantly enriched in TRB1 over TRB3 and TRB3 over TRB3, respectively (Manuscript Figure 3A). PEAT-components EPCR1 and EPCR2 showed significant preference to purify with TRB1 over TRB3 while other PEAT components showed a trend towards a higher enrichment for TRB1 (Manuscript Figure 3B). In contrast, the only NuA4 component that was enriched, TRA1A, was equally enriched by both TRBs (Manuscript Figure 3C). Equal purification was also observed for JMJ14 components, which showed only a slight bias towards TRB3 (Manuscript Figure 3D). EMF1 was the only PRC2 associated protein identified and it was exclusively enriched by TRB3 (Manuscript Figure 3E). Both, TRB1 and TRB3 co-enriched the transcription factor (TF) VIVIPAROUS1/ABI3-LIKE1;VP1/ABI3-LIKE 1 (VAL1), which can recruit PRC1 and PRC2 to target regions.

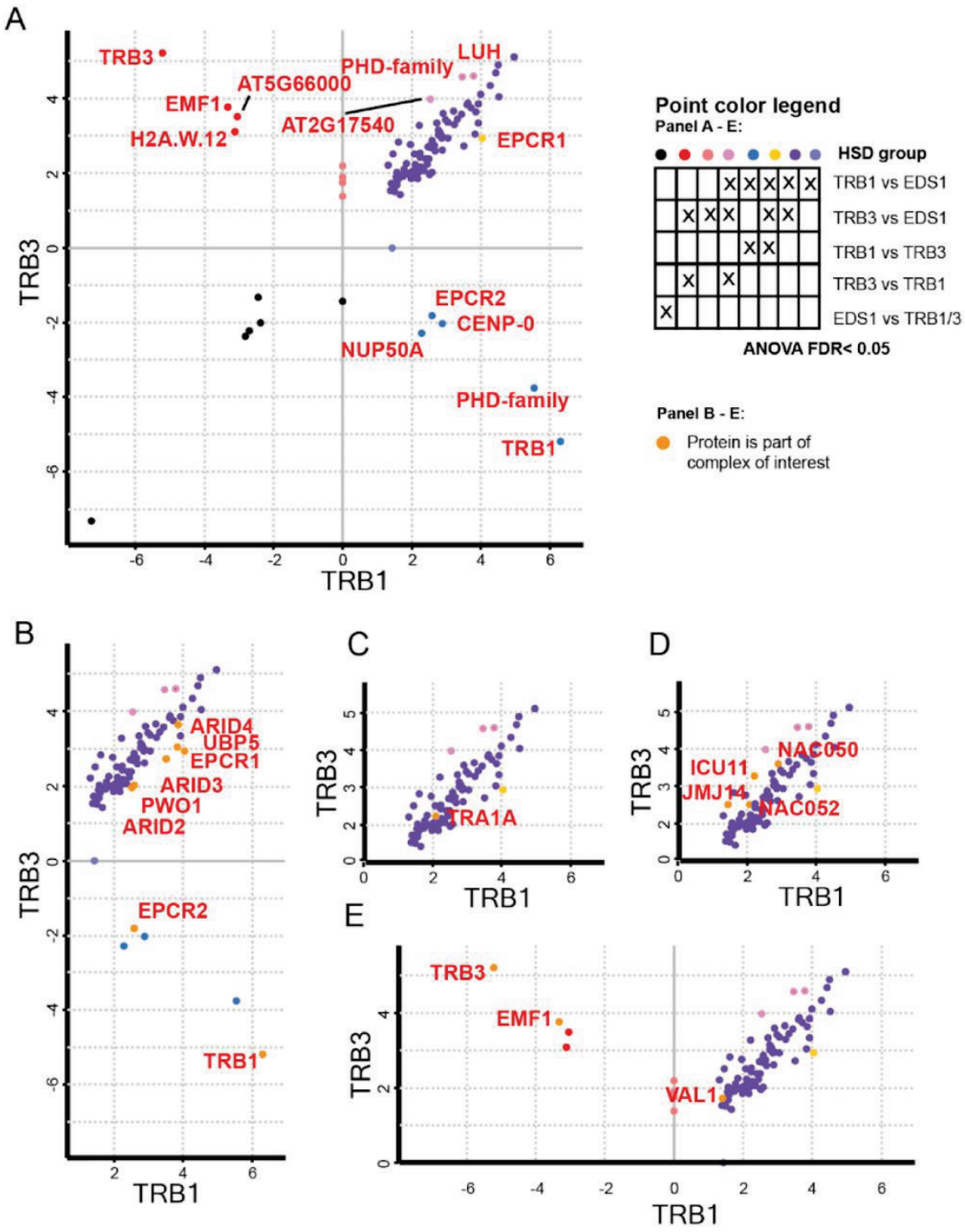

Manuscript Figure 3. TRB1 and TRB3 interactome. ***A)*** *Comparisons of IP-MS between TRB1 and TRB3 co-purifying proteins in nuclear extracts of 14-day-old seedlings. Axes show log2-fold enrichment data of log transformed LFQ data from TRB1-GFP vs EDS1-GFP and TRB3-GFP vs EDS1-GFP as indicated). Values with statistical significance (FDR < 0.05) enrichment or depletion as determined by ANOVA and HSD test are indicated. Significance groups indicated by colors as indicated in the legend. Gene symbols are indicated for genes that show significant difference between TRB3 and TRB1.* ***B)*** *Excerpt of A) showing PEAT complex components as indicated by color and gene symbol.* ***C)*** *excerpt of A) for NuA4 complex.* ***D)*** *excerpt of A) for JMJ14 complex.* ***E)*** *as in A for PRC complex.*

TRB1-3 peaks enrich distinct DNA motifs dependent on co-bound regulatory complexes

Analysis of DNA motif enrichment at TRB1-3 peaks classified by co-associated complexes provided further evidence of specialization among the three TRB paralogs. We used the XStreme

pipeline of the MEME-Suite to evaluate DNA motif enrichment at TRB1, 2 and 3 peaks as well as the peaks assigned to the different complex categories for each paralog (Manuscript Figure 4, Supplemental File 5). A comparison of enriched motifs of all TRB1-3 peaks regardless of complex association revealed that the main telo-box motifs bound by TRB1-3 are not identical. While all three paralogs enrich the canonical "AAACCCT" telo-box motif, TRB1 also significantly enriched the similar but distinct "CRACCTA" motif. While multiple secondary motifs were found for all three paralogs, it stands out that motifs associated with the basic/helix-loop-helix (bHLH) transcription factor family are only enriched in TRB1 ChIP-Seq peaks. Motifs related to TCP-TFs, on the other hand, only enriched in the peaks of TRB1 and TRB2.

A

Name	Motif	All TRB Peaks			TRB + PEAT			TRB + NuA4			TRB + PRC2			TRB + JMJ14			TRB Unassigned		
		TRB1	TRB2	TRB3	TRB1-PEAT	TRB2-PEAT	TRB3-PEAT	TRB1-NuA4	TRB2-NuA4	TRB3-NuA4	TRB1-PRC2	TRB2-PRC2	TRB3-PRC2	TRB1-JMJ14	TRB2-JMJ14	TRB3-JMJ14	TRB1-Unassigned	TRB2-Unassigned	TRB3-Unassigned
Telobox		1	1	1	1	1	1	64	1	N.E.	1	1	1	35	20	7	2	1	5
Telobox-like RMCCTA		N.E.	N.E.	N.E.	97	N.E.	N.E.	107	N.E.	N.E.	N.E.	N.E.	N.E.	69	89	N.E.	N.E.	N.E.	N.E.
Telobox-like CRACCTA		12	N.E.	N.E.	N.E.	N.E.	N.E.	13	9	N.E.	8	N.E.	N.E.	N.E.	N.E.	N.E.	1	N.E.	N.E.
BPC/GAGA		112	63	46	41	58	14	1	7	N.E.	27	12	11	114	110	82	32	72	2
NAC-Related		154	13	12	225	190	N.E.	125	N.E.	N.E.	18	83	N.E.	1	1	1	80	11	N.E.
SitelI-Motif		10	82	28	11	11	8	13	27	N.E.	N.E.	N.E.	N.E.	157	N.E.	N.E.	9	9	N.E.
AP2-EREBP-Related		33	68	81	22	36	15	92	6	N.E.	17	15	13	96	88	N.E.	49	32	8
GGAGGA		16	59	40	16	15	N.E.	19	17	N.E.	31	50	63	106	99	N.E.	23	15	N.E.
GATGAT		141	103	78	74	85	N.E.	48	N.E.	N.E.	47	17	21	97	124	76	56	106	N.E.
TCP-Related		308	447	N.E.	172	N.E.	N.E.	30	N.E.	N.E.	15	N.E.	N.E.	N.E.	N.E.	N.E.	105	N.E.	N.E.
bHLH-Related		240	N.E.	N.E.	N.E.	N.E.	N.E.	23	16	N.E.	N.E.	N.E.	N.E.	N.E.	N.E.	N.E.	123	N.E.	N.E.
ATATATATA		197	173	124	178	137	N.E.	N.E.	N.E.	N.E.	46	22	91	N.E.	98	N.E.	88	167	N.E.

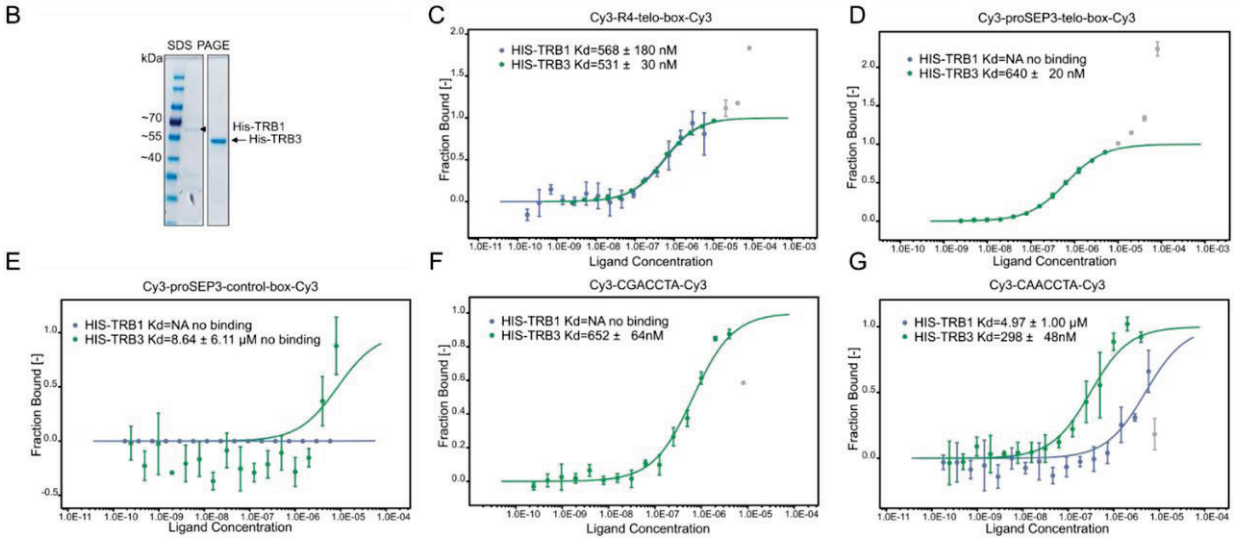

Manuscript Figure 4. Analysis of TRB bound and associated motifs. ***A)*** *DNA motifs enriched in ChIP-Seq peaks of TRB1, TRB2, and TRB3. Either all peaks, peaks assigned to gene regulatory complex binding sites or only peaks without complex assignment were used for the analysis as indicated in the header. Numbers indicate enrichment rank in the MEME-Suite results.* ***B)*** *Bacterial expressed HIS-TRB1 and HIS-TRB3 after affinity purification and SDS-PAGE.* ***C)*** *Fraction of Cy3-labelled double stranded 4x repeated telo-box probe bound by HIS-TRB1 and HIS-TRB3.* ***D)*** *as C) using Cy3 lablelled telo-box motif as found in the promoter of SEP3.* ***E)*** *as C) using a Cy3-labelled control region from the SEP3 promoter* ***F)*** *and* ***G)*** *as C using Cy3 labelled double stranded oligos containing the CGACCTA and CAACCTA motif, respectively.*

To identify motifs associating TRBs with one of the four regulatory complexes, we repeated the XStreme analysis pipeline using only TRB peaks from sites that were categorized as exclusive binding locations of PEAT, NuA4, PRC2, or JMJ14. This detailed analysis showed that TRB1 enriches a second telo-box-like motif ("RMCCTA") at sites not co-bound by PRC2. It furthermore indicates that the BPC-transcription-factor-related GAGA-box and NAC-TF associated motifs are universally enriched at all sites, independent of co-bound complex components. Other secondary motifs are specifically enriched in sites co-bound by certain regulatory complexes. This includes the siteII motif, which does not enrich at sites with PRC2 binding, ATATAT, which does not enrich at sites assigned to NuA4, and the contrasting bHLH-related motifs, which exclusively enrich at sites with NuA4 binding. Looking closer at the ranks associated with each enriched motif reveals interesting differences between sites with otherwise similar enrichment patterns. Most strikingly, peaks associated with sites of all three paralogs co-bound by JMJ14 show NAC-related TFs as their highest ranking motif, even surpassing the ranks of telo-box motifs.

These results indicate a substantial difference in DNA motifs found at sites where TRBs bind together with PEAT, NuA4, PRC2, or JMJ14 and could therefore indicate the role of different TFs in determining the targeting of epigenetic regulatory complexes.

TRB1 binding to non-canonical telo-box motifs is not explained by affinity to single motifs

Since differences in the telo-box related consensus motifs suggested that the DNA binding properties may differ between TRB1 and TRB2/3, we tested the affinity of TRB1 and TRB3 to single telobox and the two variants of the "CRACCTA" motifs by microscale thermophoresis (MST). MST determines dissociation constants between fluorescently labelled targets and unlabelled ligands by measuring changes in the velocity by which the fluorophore moves in or out of 1-6° K temperature gradients (Seidel et al. 2013).[26]. TRB1 and TRB3 were previously shown to bind probes containing four teloboxes (R4) that imitate telomeric repeats *in vitro* [27].

We could reproduce binding to R4 probes for bacterially expressed six histidine (HIS)-tagged TRB1 and TRB3 with binding affinities that were in the range of those previously reported (K_D=567± 180nM and K_D=531± 30nM for TRB1 and TRB3, respectively) (Manuscript Figure 4B and C). In contrast, only HIS-TRB3 interacted with an 28bp oligomer derived from the *SEP3* promoter containing a single telobox (K_D= 640 ± 19 nM) (Manuscript Figure 4D and E). Since the affinity of HIS-TRB3 towards the single telo-box motif was comparable to that of the R4 telobox repeat, a non-cooperative interaction mechanism between TRB3 and DNA is probable. Motif enrichment suggested that TRB1 may bind to single CRACCTA motifs; however, HIS-TRB1 did not bind to the CGACCTA variant and only with low affinity to the CAACCTA variant (K_D = 4.9 ± 1.0 µM) (Manuscript

Figure 4G and G). Unexpectedly, HIS-TRB3 bound CGACCTA with similar affinity as single teloboxes (CGACCTAA: K_D = 652 ± 64 nM) and CAACCTA slightly better (K_D = 298 ± 48 nM) (Manuscript Figure 4F and G).

In sum, TRB1 seems unable to bind single telo-box and CRAACTA motifs *in-vitro,* indicating that *in vivo* enrichment of these motifs by TRB1 may depend on the presence of accessory factors.

Genes bound by different regulatory complexes participate in distinct biological processes, dependent on co-bound TRBs

Next, we investigated whether the epigenetic regulatory complexes diverged not only in their binding sites and TRB paralog association, but whether their target genes were also involved in different biological processes. Through the annotatePeak function of the ChIPseeker library, peaks were annotated to the *A. thaliana* genome. This revealed that, while only 8.6% of the 500-bp bins were bound by TRBs, 29.4% of all annotated nuclear genes exhibited binding of at least one TRB.

We started by identifying the most enriched GO-terms for each complex, regardless of the TRB paralog they were associated with (Manuscript Figure 5 A and Supplemental File 6). Overall, it was possible to assign specific functions to each complex combination. Ribosome-related GO-terms were significantly enriched in genes assigned to PEAT with and without NuA4; however, the significance was higher for PEAT only genes, indicating a previously undescribed role of the PEAT complex in ribosomal regulation. PRC2 assigned genes enriched terms related to floral development. This is consistent with previously published functions of TRB-PRC2 complexes [14]. NuA4-assigned genes with and without PEAT overrepresented terms annotated to the circadian clock, an association that was previously detected for NuA4 [28]. The combination of JMJ14 and NuA4 target genes enriched GO-terms related to immune responses. Last, the five GO-terms with most enrichment in the unassigned set of genes were all related to oxygen response/hypoxia, indicating that our current understanding of TRB-related gene regulation is still incomplete.

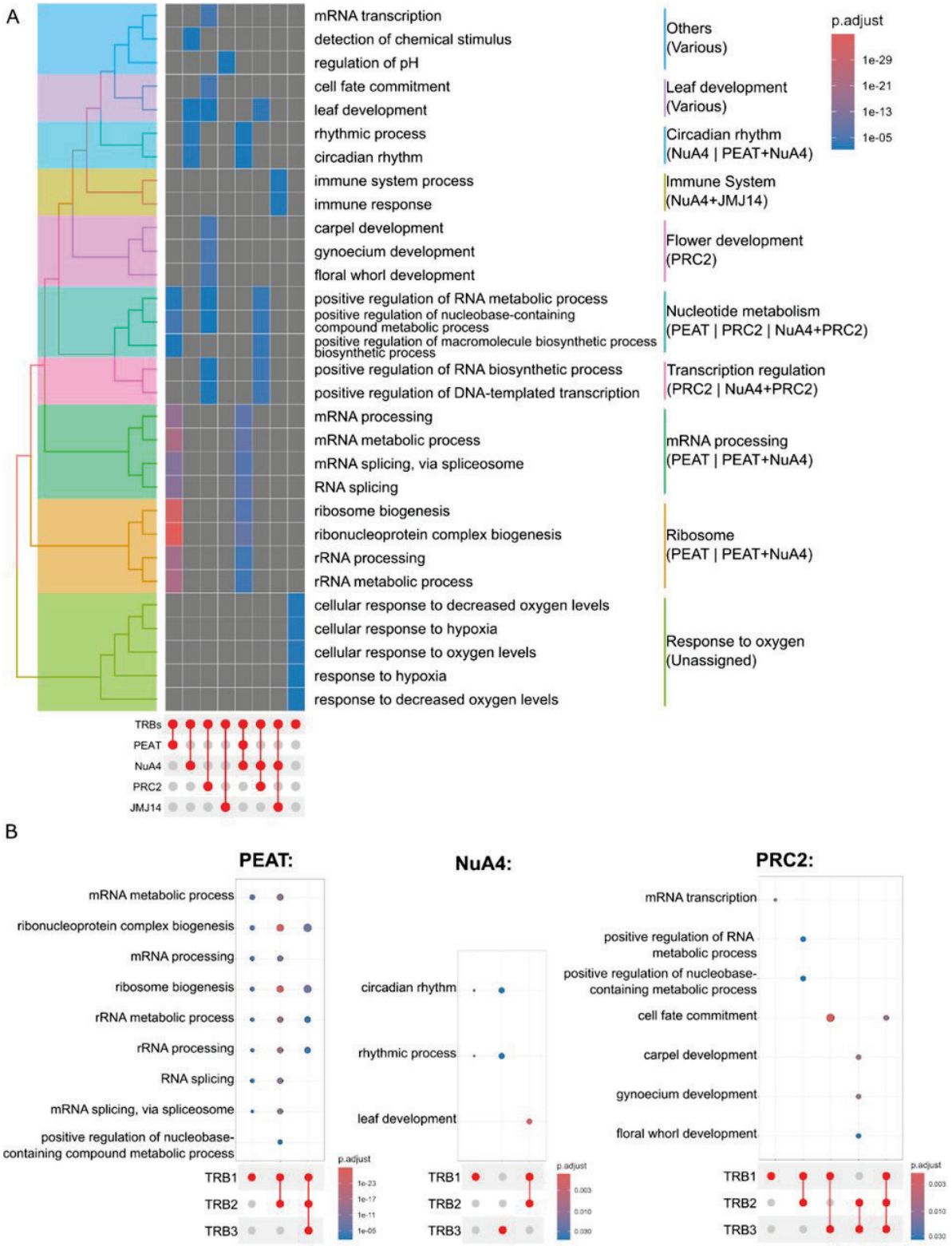

Manuscript Figure 5. Gene Ontology enrichment analysis. ***A)****, Enriched GO-Terms for genes assigned to either no complex (Unassigned), PEAT, NuA4, PRC2, JMJ14, or any of the four combinations of two complexes. Only the 5 most enriched GO-Terms of the "Biological Process" aspect are shown. Similar terms are summarized on the right.* ***B)*** *Enriched GO-Terms for the gene sets assigned to PEAT, NuA4, or PRC2, separated by co-bound TRB-paralog. The same terms as in A are shown.*

To expand this analysis and differentiate complexes based on their co-bound TRB paralog, we determined GO-term enrichment of all combinations. Overall, the GO-terms barely correlated

between genes assigned to the same complex, but bound by different TRB homolog combinations (Supplemental Figure 4). This functional split constitutes further evidence of the specialization between TRB paralogs, even within the same complex.

Since epigenetic regulatory complexes enriched different GO-terms, based on which TRB paralog combination they associated with, we took a closer look at the GO-terms enriched for genes assigned to PEAT, NuA4, and PRC2 (Manuscript Figure 5B). Comparing the TRB-paralog combinations, it became clear that the affinity of PEAT towards ribosomal and RNA-processing genes is driven largely by TRB1, as almost all possible TRB1-containing combinations enrich these terms. The role of NuA4 in the circadian clock appears to be coinciding with exclusively TRB1 or TRB3 bound genes. PRC2 target genes involved in floral development are only enriched in the genes that are also bound by TRB2 and TRB3.

Transcriptomic changes in *trb* mutants are partially explained by the assigned regulatory complexes

In order to validate the complex assignments and to improve our understanding of the effects of TRBs on gene expression, we tested whether specific complexes are over- or underrepresented in the sets of genes assigned to PAM-clusters identified for DEGs in single and double *trb* mutants (Figure 1E). The normalized average expression profile across all genes per cluster confirmed that clusters 1 and 2 exhibit an inverse pattern, with the loss of *TRB1* appearing as the driving factor behind the effects (Figure 6A). Genes in cluster 4 showed a progressive increase of expression, with mutations in *TRB2* and *TRB3* as strongest drivers. Based on these patterns, we hypothesized that cluster 1 contained genes primarily controlled by the activating PEAT complex, while cluster 3 genes were likely controlled by PRC2. Using the gene-to-complex assignments produced for the gene ontology analysis (Supplemental data 3), we intersected the PAM-clusters with complex combinations and performed multi-set interaction analysis according to [25] (Figure 6B). The test confirmed that cluster 1 exhibits a 2.2-fold enrichment of TRB-bound genes assigned to PEAT. Genes assigned to both PEAT and JMJ14, however, were significantly depleted in the same set (0.2-fold). Interestingly, cluster 2 exhibited an inverse enrichment, in line with its inverse expression profile. In this cluster, all combinations that include JMJ14 but not PRC2 were significantly enriched (between 1.8 and 3.2-fold enrichment). This suggests a so far undescribed role of PEAT and/or NuA4 in repressive gene regulation when found alongside JMJ14. Cluster 3 also shows a 2.9-fold enrichment of genes assigned to only JMJ14, but without a clear indication on how the expression profile can be explained. Lastly, cluster 4 is characterized by a 2.8-fold enrichment of PRC2-assigned genes with a simultaneous 0.3-fold depletion of PEAT-assigned genes, as expected based on its expression profile.

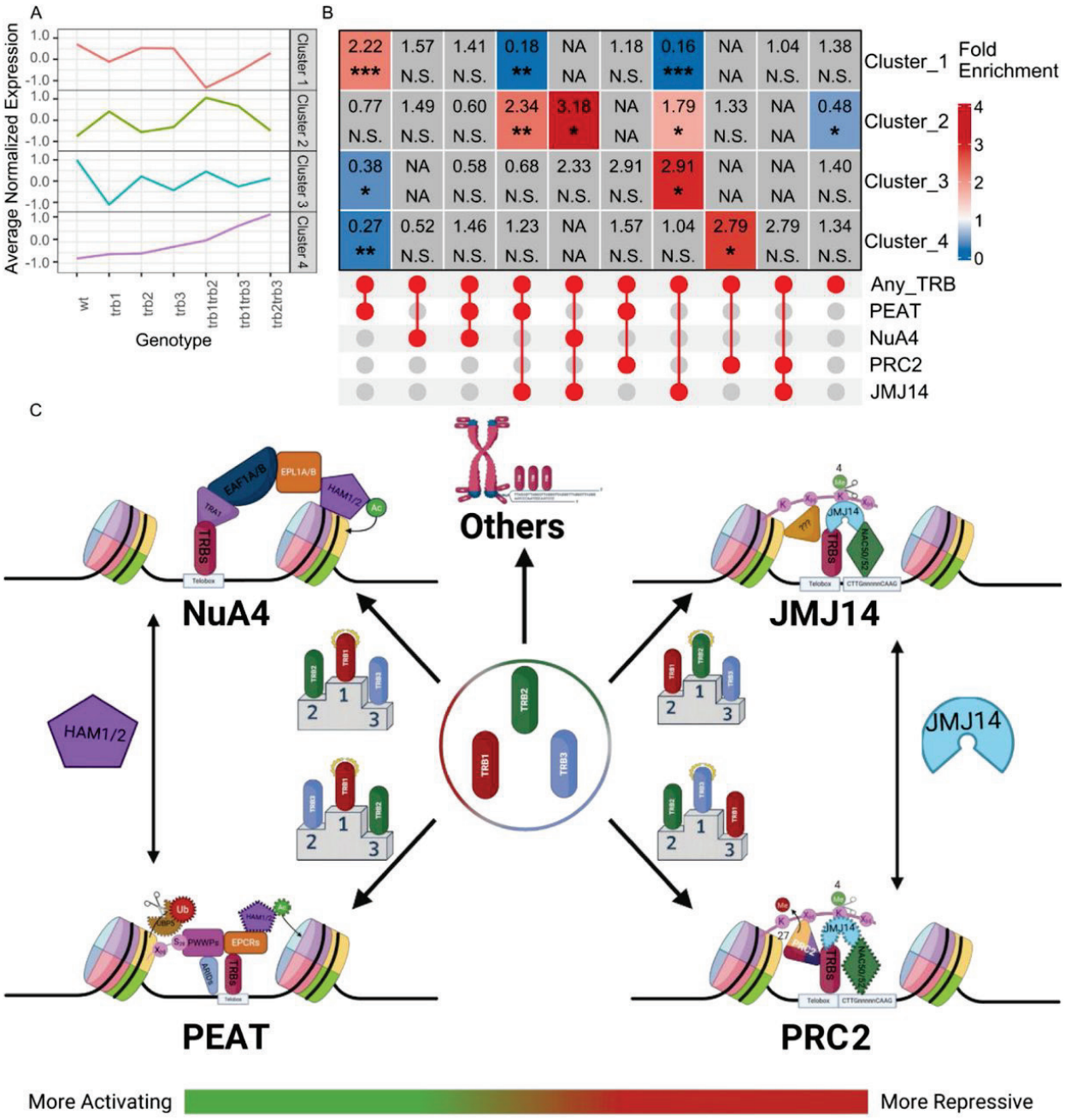

Manuscript Figure 6. TRB-mediated gene regulation in epigenetic context. ***A)*** *Average normalized expression of the transcription clusters displayed in Fig. 1E. Values of three replicates of each of genotypes were averaged.* ***B)*** *Pairwise Exact test statistics as described by Wang et al. (2015) for the same clusters as A intersected with the sets of genes annotated to either one, two, or none of the epigenetic regulatory complexes. Significance levels: ***, p<=0.0005, **, p<=0.005, p<=0.05, N.S., p>0.01.* ***C)*** *Model of TRB-mediated epigenetic gene regulation. Complex components which are not core to the TRB-containing complexes are indicated with dashed outlines. TRB-paralog specialization is conveyed via podiums. "???" indicates potential unknown complex participants. HAM1/2 and JMJ14 are shared between the complexes on the activating and repressive side, respectively.*

Discussion

TRBs associate with distinct epigenetic regulatory complexes in a primarily mutually exclusive manner

Since it was first discovered that TRBs can participate in multiple epigenetic regulatory complexes, it had been unclear whether TRB-bound genomic sites act as "landing sites" for

multiple complexes, or whether each site is associated with only a single complex. Our analysis of the ChIP-Seq-determined binding sites of eleven complex-forming proteins (including two novel TRB sets) serves as a useful tool to evaluate the overall binding behavior of TRBs. According to our analysis, it is likely that the majority of TRB-binding sites are associated with a single regulatory complex (Figure 2). The only exception seems to be PEAT and NuA4, which share a significant proportion of their binding sites, likely caused by the role of HAM1 in both complexes [12, 29]. It should, however, be noted that all the ChIP-Seq datasets included in this study are obtained from whole seedlings. It is therefore likely that temporal and/or tissue-specific binding differences are obscured in our analysis. In addition to mutual exclusivity, we also discovered that a large portion of the binding sites of the four complexes included in this study were not bound by any of the three TRB paralogs. In the case of PEAT, this is unexpected, since TRBs have been proposed as core components [12]. In part, this finding may be explained by differences in stringency thresholds defining binding sites in different bioinformatics pipelines.

Our analysis provides strong evidence of additional, thus far undescribed, TRB-containing complexes. First, the presence of a large contingency of TRB-JMJ14 co-binding sites in the absence of other complex components strongly indicates the presence of a JMJ14-mediated histone modification complex that acts independently of PRC2, while maintaining JMJ14 association with TRBs. NAC50/52, two strong TRB interactors with slight preference for TRB3 over TRB1, have already been shown to form regulatory complexes with JMJ14 [22]. Furthermore, the evidence clearly shows a split between PEAT and NuA4 bound TRB-sites, expanding on the previously observed role of TRBs in PEAT complexes which include the HAM1 component of NuA4 [11]. This serves as evidence of the presence of an additional NuA4-TRB complex targeting sites independent of PEAT. In addition to their genomic binding, evidence of these two proposed complexes can also be seen in the IP-MS data. TRA1, which had previously been described as the TF-binding domain of the NuA4 complex [29], is the NuA4 complex component with the strongest TRB1/3 binding score (Manuscript Figure 3). Last, a substantial number of target sites is associated with TRBs in absence of all other chromatin complex representatives. It is to be expected that other TRB partners will be identified to co-occur at these sites.

The three paralogs TRB1, 2 and 3 specialize in specific roles, without losing their redundancy

Although reverse genetics suggests almost complete redundancy between the three paralogs TRB1, 2, and 3, whether this redundancy is replicated on a molecular level had never been studied in detail. On the molecular level, TRBs exhibited an unexpectedly strong degree of specialization. In particular, a clear split between TRB1 and TRB2/3 could be detected throughout the analysis. First, transcriptome changes of single and double *trb* mutant combination identified two sets of

genes with opposing expression patterns that were predominantly associated with the loss of *trb1* (Manuscript Figure 1 and Manuscript Figure 6). A different set of genes was higher expressed when the *trb3* alles was combined with *trb2* or *trb1*. Furthermore, the association between TRB1 and activating complexes such as PEAT and NuA4 could be seen in the overrepresentation of TRB1 bound sites in the ChIP-Seq data of these complexes; furthermore, it is corroborated by GO-term analysis since terms enriched for TRB1 a more significantly overrepresented for TRB-PEAT and TRB-NuA4 target genes (Manuscript Figure 2 and 5). Conversely, the same data indicate that TRB2/3 associate more strongly with the repressive complex PRC2 and the proposed JMJ14-containing complex. The same trend can be observed in the IP-MS data comparing TRB1 and TRB3 co-purifying proteins since the only identified PRC2-associated protein, EMF1, was exclusive to TRB3 while PEAT-component EPCR1 was only co-purified with TRB1 (Manuscript Figure 3).

TRBs are low affinity transcription factors explaining their dependence on other interaction partners and motifs for target association

Although TRB proteins can bind telo-box and related motifs, their affinity towards tandemly repeated motifs was moderate at best and weak to non-binding in the case of single telo-box or related motifs (Manuscript Figure 4). Hypothetically, high affinity binding to telo-box motifs would strongly tether TRBs to telomeres, possibly preventing their binding to single motifs at genic regions. On the other hand, the weak affinity of TRBs to target sites *in vitro* suggests that TRBs require assistance to associate with genic target regions *in vivo*. TRBs feature a H1/H5-related domain that may increase the affinity to well-positioned telo-box motifs by interacting with core nucleosomes. Previous studies have shown that presence of the linker histone H1 competes with TRB1 binding to telomere-derived regions [8]. Alternatively, the association with chromatin complexes and other TFs may stabilize TRBs at single telo-box motifs.

While the analysis of DNA motifs could not fully explain likely (co)-recruiting motifs for different TRB-associated complexes, it provided further evidence of specialization. A few DNA motifs show differential enrichment between the regulatory complexes (e.g., the site II motif and bHLH related motifs) and ranks of the enriched motifs differ substantially between the complex target sites (Manuscript Figure 4). Most obviously, sites of TRB-JMJ14 binding enrich NAC-related motifs to a stronger degree than telo-box motifs. Several studies had already presented interaction data identifying a complex of NAC50/52 with TRBs and JMJ14 [22, 23], which was also confirmed in our study (Manuscript Figure 3). The predominant enrichment of NAC motifs indicates a TRB recruitment mechanism as part of the TRB-NAC-JMJ14 complex involving NAC's affinity to their cognate motifs.

In a second case, interaction between two closely linked motifs appears not to rely on a common complex. Earlier studies revealed that telo-box motifs in combination with site II motifs are able to act as transcriptional enhancers at ribosomal protein encoding genes [30]. Our analysis showed that TRB-PEAT bound genes enrich site II motifs and are associated with GO-terms associated with ribosomal functions (Manuscript Figure 2 and 4). In contrast, the site II motif binding TEOSINTE BRANCHED1/CYCLOIDEA/PROLIFERATING CELL FACTOR (TCP) family TFs were not enriched in our IP-MS data (Manuscript Figure 3).

Last, no singular motif was found that only enriches at sites co-occupied by PRC2 and TRBs. While GAGA-motifs, which are bound by TFs of the BPC family, were previously proposed a co-recruiters of PRC1 or PRC2 components [19, 31, 32], the corresponding motifs are also enriched at TRB-PEAT and TRB-NuA4 leaving the question of how PRC2-TRB sites are defined unanswered for now. BPC TFs were not enriched in our IP-MS dataset.

In summary, we observed an overall trend of TRB specialization, which can be best described as a preference for specific sites and complex partners (Manuscript Figure 6C). TRB1 appears to have a strong affinity with PEAT and NuA4, but is also present at many unrelated binding sites. By contrast, TRB3 and TRB2 are predominantly, though not exclusively, found at PRC2 and JMJ14 locations, respectively. These results are consistent with the remarkable redundancy observed at the phenotypic level. It is possible that TRBs are at the beginning of a process of functional specification. Alternatively, their partial functionalization could provide robustness to epigenetic gene regulation, particularly if changes in their relative abundance and activity are connected to environmental or developmental cues. Further studies are required to answer these questions.

Materials & Methods

Plant material and growth conditions

Plants were grown in greenhouse conditions or growth chambers as indicated under long day (LD) (16h light, 8h dark) photoperiod at 22°C ambient temperature. Plants were randomized within trays for phenotypic analyses. Plants for RNA-seq analysis were grown in growth chambers. Three biological replicates were grown in 1 week intervals in the same chamber, material was collected at ZT10 from 14-day-old seedlings. For ChIP-seq, plants were grown in tissue culture on GM plates in LD conditions at 21°C. Material from replicated plates was collected at ZT10 as biological replicates. The *trb1-2* (Salk_001540) and *trb3-2* (Salk_134641) alleles are previously described T-DNA insertion lines, *trb2-2* and *trb2-3* are CRISPR/Cas9 edited alleles as previously described except that the editing transgene was removed by segregation [14]. Double and triple mutants

were generated by crosses. Transgenic lines TRB2pro-TRB2-YFP and TRB3pro-TRB3-YFP were previously described [14].

Scoring of flowering time

Flowering time was scored as the number of leaves at the main shoot (rosette and cauline leaves). Statistical analysis was done by ANOVA with HSD grouping using the agricolae package in R. To distinguish segregating *prope* triple from double mutants, genotyping of individual plants was carried out on genomic DNA prepared using Biospring96 (Qiagen) using manufacturer's instructions. Alleles trb1-2 and trb3-2 were amplified using SALK_LBb1.3: ATTTTGCCGATTTCGGAAC in combination with SALK_001540_RP: ATGCCACCACAATAAATCTCG and SALK_13464_RP: ATGGTTCACGAGAAACCTGTG, respectively. To distinguish between trb2-3 and TRB2, two reactions were carried out for 28 cycles at 62°C annealing temperature dCAPS_TRB2_R: ATTGCCTCAAAGATGATCTTATCC in combination with 8-18-10-specifi: ACTTCCCCCGGAGGTTCTTG and 8-18-10-WT: ACTTCCCCCGGAGGTTCTG, respectively.

RNA preparation and RNA-seq

Total RNA was extracted from 3-4 14-d-old-seedlings with an RNeasy® Plant Mini kit (Qiagen) according to the manufacturer's instructions. To remove gDNA contamination, 10 µg of total RNA was DNase I treated, using the DNA-freeTM DNA Removal kit (InvitrogenTM), as described in the kit's instructions. RNA quality was assessed by Agarose Gel electrophoreses of an 200ng aliquot DNaseI treated RNA. The RNA samples were sent to BGI TECH SOLUTIONS (HONGKONG) for poly-A enrichment, library preparation and directional paired-end Nanoball sequencing on the DNBSEQ platform.

RNA-seq analysis

Paired end reads were mapped to the Arabidopsis thaliana TAIR10 reference genome indexed with the Araport11 genome annotation using STAR. Read counts were pooled for all splice variants as per gene counts. Sense strand gene counts were used for differential expression analysis with the R package DESeq2 using a threshold of padj < 0.05 to set differential expression of mutants vs Col-0. Venn diagrams and statistical testing of overlaps between samples used R packages ggvenn and SuperExactTest, respectively. Clustering of expression data and drawing of gene-normalized expression heatmaps were carried out using R package ComplexHeatmap using PAM-clustering.

ChIP and ChIP-seq library preparation

For all ChIP experiments, 2 g of 14-d-old seedlings were collected in 50 ml 1x PBS buffer (137 mM NaCl, 1.8 mM KH_2PO_4, 10.1 mM Na_2HPO_4, 2.7 mM KCl), fixed with 1 % formaldehyde under vacuum two times for 10 min after which the crosslinking reaction was quenched with 5 ml glycine (1 M) under vacuum for 5 min. Fixed plant material was collected in a sieve, washed with autoclaved water, and dried with paper towels before being snap frozen with liquid N_2. Frozen samples were ground at 7200 rpm three times for 30 s, using the Precellys Evolution Homogenizer in combination with a Cryolys Cooling Option (Bertin Instruments) in 7 ml reaction tubes with 3mm ceramic beads.

To extract nuclei, the ground samples were mixed with 30 ml NIB buffer (50 mM HEPES-NaOH (pH 7.4), 5 mM $MgCl_2$, 25 mM NaCl, 5 % sucrose, 30 % glycerine, 0.25 % Triton X 100, freshly add: 0.1 % β-mercaptoethanol, 0.1 % SIGMA proteinase inhibitor), vortexed, filtrated using Miracloth (Merk) and spun down at 4000 rpm and 4 °C for 10 min. The pellet was resuspended in 20 ml 1x Washing buffer (16.7 mM HEPES-NaOH (pH 7.4), 6.7 mM $MgCl_2$, 33.3 mM NaCl, 13.3 % sucrose, 13.3 % glycerine, 0.25 % Triton X 100, freshly add: 0.001 % β-mercaptoethanol, 0.001 % SIGMA proteinase inhibitor) and spun down at 4000 rpm and 4 °C for 10 min. Then, extracted nuclei were resuspended in TE-SDS (1 mM EDTA (pH 8.0), 10 mM Tris-HCl (pH 7.4), 0.25 % SDS) in a total volume of 600 µl, rotated at 4 °C and 12 rpm for 20 min, split in 2x 300 µl and sonicated with a Bioruptor Sonicator (Diagenode) that was attached to a Minichiller cooling system (huber) (Programme: red - 0.5 (on); green - 1 (off); 15 min, H) to produce DNA fragments of ~200-500 bp. Sonicated chromatin was separated from debris by centrifugation at 4 °C and maximum speed for 10 min. For ChIP-seq, 400 µl sonicated chromatin were mixed with 600 µl of IP dilution buffer (80 mM Tris-HCl (pH 7.4), 230 mM NaCl, 1.7 % NP40, 0.17 % DOC), 2 µl RNase I (10 mg/ml), 2 µl DTT (1M), and 2 µl SIGMA proteinase inhibitor. Afterwards, equal volumes of the sonicated chromatin mix were split into two different tubes, 5 µl of α-GFP (ab290, Abcam) were added to carry out IP. Samples were rotated at 4 °C, 12 rpm overnight in a bohemian wheel. After overnight incubation, unspecific precipitates were removed by centrifugation (4 °C, 20000g, 10 min) and the supernatant transferred to a tube containing 30 µl rProtein A Sepharose Fast Flow antibody purification resin (GE Healthcare) beads equilibrated in RIPA buffer (0.6x IP Dilution buffer, 0.1 % SDS). Samples were rotated at 12 rpm and 4 °C for 3 h. After centrifugation, 200 µl of the supernatant from control samples was reserved as input and kept on ice. Beads were washed with 1 ml RIPA for five times to remove the background. At the 5th time, the samples were transferred to fresh tubes with 800 µl RIPA and protein-DNA complexes were eluted from precipitated beads by mixing them two times with 160 µl glycine elution buffer at RT. IP samples were neutralised with 80 µl of Tris-HCl (1 M, pH 9.7). IP samples were de-crosslinked by adding 8 µl SDS (10 %) and 5 µl proteinase K (5 mg/ml). For input samples, only 5 µl proteinase K was added.

DNA was extracted twice with equal amounts of phenol/chloroform and precipitated with 1/10 volumes NaAC (3 M), 2.5 volumes EtOH (100 %), and 1 µl glycogen (10 mg/ml) at −20 ° for 3 h. Afterwards, the DNA was washed with 1 ml EtOH (70 %), dried, and resuspended in 14 µl H_2O.

For ChIP–seq library preparation, two independent immunoprecipitations for Col-0, TRB2pro-TRB2-YFP and TRB3pro-TRB3-YFP were processed. Libraries were prepared with Ovation Ultralow Library System (NuGEN) according to the manufacturer's instructions, using 71% (10 µl) of each ChIP as starting material. Before amplification DNA concentration was measured, using a Qbit 4 (ThermoFisher Scientific), to determine the appropriate number of PCR cycles needed for each sample (see manufacturer's manual). After amplification, DNA was run on a 2 % low-melt agarose gel and fragments between 200 and 500□bp length were purified using the MinElute Gel Extraction Kit (Qiagen) according to the manufacturer's instructions except that gel fragments were solved at RT and eluted in 15 µl EB buffer. An aliquot of each library was tested via qPCR before and after PCR amplification to confirm that libraries showed similar fold-change between control and target regions. Sequencing was performed as single-end 100-nt reads (ca 13 mio reads/sample) on the Illumina HiSeq3000 platform by the Max Planck Genome Centre Cologne.

ChIP-seq analysis

After sequencing, adapter sequences ≥ 12 bp were removed using Cutadapt [33]. Reads were aligned to the *A. thaliana* genome (TAIR10) with the Burrow-Wheeler Aligner (BWA) [34] and BAM-files created using SAMtools [35]. SAMtools was used to remove multi-mapping reads by filtering with MAPQ score < 10, which resulted in 8.8 to 12.2 million reads per sample. Unique BAM-files were indexed with SAMtools, normalised to Counts Per Million mapped reads (CPM), and converted to bigWig-files using bamCoverage of the deeptools2 suite [36] for visualization in the Integrated Genome Viewer (IGV). A blacklist of over- and under sampled regions was generated by scoring read coverage of input and Col-0 ChIP samples across 200bp windows using BEDtools [37]. Windows that were statistical outliers were determined using R and subsequently removed from the analysis. EPIC2 was used to determine enriched regions in two replicates against the pool of two Col-0 control IPs using pooled input samples as correction [38]. Replicates were compared using the Irreproducible Discovery Rate (IDR) framework [39]. Peak passing the threshold of 0.01 > IDR were merged using bedtools. Previously generated 35Sp-TRB1-YFP reads were included in the IDR analysis for better comparison [9].

Analysis of the binding behavior of various epigenetic regulatory complexes

Binding peaks of UBP5, EPRC1, PWWP1, HAM1, and EPL1B were sourced from [11], CLF and SWN from [21], and JMJ14 were obtained from [23]. To visualize the overlapping binding sites, the

TAIR10 genome of *A. thaliana* was tiled into 238296 bins of 500 bp length and all peaks of these eight datasets and TRB1,TRB2 and TRB3 were assigned to overlapping bins. As the datasets were derived using different ChIP-Seq pipelines, the “Score” column of each dataset was normalised into deciles. Preliminary analysis of the overlap of the ChIP-Seq sets was performed through pearson correlation using Hmisc [40].

To visualize the overlapping binding sites, the bins were assigned to distinct categories: Bins bound by at least two of the PEAT components, both NuA4 components, both PRC2 components, or JMJ14 were assigned to “PEAT”, “NuA4”, “PRC2”, or “JMJ14” respectively. In addition, each of the 12 possible combinations of multiple complex assignments were added along with a category for unassigned bins, bringing the total to 17 categories. Each bin was assigned to one of these categories. Statistical analysis was performed using the MSET function of the SuperExactTest package [25] for pairwise comparison of the overlap of the generated categories with TRB1,2,3-bound bins. Heatmaps were generated using the ComplexHeatmap [41] package.

Cis-motif enrichment analysis

DNA motifs enriched in peak-assigned bins were identified through the XSTREME pipeline of the MEME-suit [42] using standard settings except for *--meme-mod “anr”*, providing the DNA motifs identified by [43]. Motifs were declared as telobox-like, if the identified motif was closely related to the telobox, but did not fully capture the canonical *Arabidopsis* telomere repeat sequence of TTTAGGG. For each peak category, motifs were ranked based on their e-Value.

Gene Ontology enrichment analysis

The peaks of all ChIP-Seq sets used in this study were annotated to genes using “annotatePeak” of the “ChIPseeker” package [44, 45]. Since epigenetic regulatory complexes are not solely found at or near the TSS, the parameters “tssRegion” and “overlap” were set to “c(−2000, 2000)” and "all" respectively in order to correctly assign binding sites further away from the TSS. The resulting genes were assigned to epigenetic regulatory complexes in the same manner as the genomic bins. The different sets were subsequently used to calculate GO-Term enrichment using the “clusterProfiler” package [46].

Sample preparation for LC-MS/MS

Leaf tissue (7g) harvested from 5-week-old transgenic plants (*CaMV 35Sp-TRB1-GFP*, *CaMV 35Sp-TRB3-GFP*, *CaMV 35Sp-EDS1-GFP*) was cut with scissors into 0.5 - 1.0 cm pieces and disrupted on ice in 15 ml Precellys® tubes containing 5 ml extraction buffer (2 M hexylene glycol, 0.5 M PIPES-KOH pH7.0, 10 mM MgCl2, 5 mM beta-mercaptoethanol) and 13-15 sterilized metal

beads using a Precellys® 24 homogenizer (Bertin instruments) for three rounds set to 10 s at 7500 rpm. Samples were filtered through a single and then a double Miracloth (Merk) layer, adjusted to a volume of 45 ml. 10% Triton X-100 was added stepwise to a final concentration of 0.8%. While samples were incubated on ice, the Percoll® (Sigma-Aldrich) gradient was assembled by carefully underlying 6 ml of 30% Percoll® solution with 6 ml of 80% Percoll® in a centrifuge tube (Beckman Coulter #355631). In parallel, three 15 ml aliquots per sample were layered onto gradients and centrifuged (2,000 g, 4 °C, 30 min). The nuclei-enriched fractions (5ml) were collected from the interphase between the Percoll® layers using a 5-ml pipette and the combined aliquots diluted in 23 ml gradient buffer (0.09 M hexylene glycol, 0.09 mM PIPES-KOH pH7, 1.83 mM MgCl2, 0.92 mM β-mercaptoethanol, 0.18% Triton X-100). To gently pellet the nuclei, the samples cushioned on 6 ml 30% Percoll® solution were centrifuged at 2,000 g and 4°C for 10 min. The isolated nuclei were resuspended in 1 ml sample buffer (20 mM TrisHCl pH7.4, 2 mM MgCl2, 150 mM NaCl, 5% glycerol, 5 mM DTT, cOmplete™ protease inhibitor (Roche)) and transferred into fresh 1.5 ml Eppendorf tubes and once washed in sample buffer (cenrifugation 1,000 g at 4°C for 15 min) and resupended in a final volume of 600µl sample buffer. Samples were treated with 1 µl DNase I (10 u/µl) and 2 µl of RNase A (10 mg/ml) for 15 min at 37°C and subsequently sonicated in a Bioruptor (Diagenode) water bath connected to a Minichiller cooling system (Huber) (6x 15 s “on”/15 s “off” at high intensity). After removal of debris (centrifugation at 16,000 g and 4°C for 15 min), supernatants were transferred into clean 2 ml Protein LoBind® tubes (Eppendorf). The protein concentration was determined by Bradford assay (Bradford, 1976) and equal amounts (i.e., 1 mg) were used for subsequent affinity purification. Immunoprecipitation was carried out with 25 µl GFP-trap Agarose beads (gta-20; Chromotek) in 2 ml sample buffer with Triton X-100 (0.1%) and EDTA (2 mM) after incubation at 4°C for 2.5 h at constant rotation (12 rpm). The protein-bound GFP-trap beads were washed four times with 300 µL of wash buffer (20 mM Tris-HCl pH7.4, 150 mM NaCl, 2 mM EDTA).

Sample preparation and LC-MS/MS data acquisition

Proteins from GFP-trap enrichment were submitted to an on-bead digestion. In brief, dry beads were re-dissolved in 25 µL digestion buffer 1 (50 mM Tris, pH 7.5, 2M urea, 1mM DTT, 5 ng/µL trypsin) and incubated for 30 min at 30 °C in a Thermomixer with 400 rpm. Next, beads were pelleted, and the supernatant was transferred to a fresh tube. Digestion buffer 2 (50 mM Tris, pH 7.5, 2M urea, 5 mM CAA) was added to the beads; after mixing, the beads were pelleted, the supernatant was collected and combined with the previous one. The combined supernatants were then incubated o/n at 32 °C in a Thermomixer with 400 rpm; samples were protected from light during incubation. The digestion was stopped by adding 1 µL TFA and desalted with C18

Empore disk membranes according to the StageTip protocol [47]. Dried peptides were re-dissolved in 2% ACN, 0.1% TFA (10 µL) for analysis and measured without dilution. Samples were analyzed using an EASY-nLC 1200 (Thermo Fisher) coupled to a Q Exactive Plus mass spectrometer (Thermo Fisher). Peptides were separated on 16 cm frit-less silica emitters (New Objective, 75 µm inner diameter), packed in-house with reversed-phase ReproSil-Pur C18 AQ 1.9 µm resin (Dr. Maisch). Peptides were loaded on the column and eluted for 115 min using a segmented linear gradient of 5% to 95% solvent B (0 min : 5%B; 0-5 min -> 5%B; 5-65 min -> 20%B; 65-90 min ->35%B; 90-100 min -> 55%; 100-105 min ->95%, 105-115 min ->95%) (solvent A 0% ACN, 0.1% FA; solvent B 80% ACN, 0.1%FA) at a flow rate of 300 nL/min. Mass spectra were acquired in data-dependent acquisition mode with a TOP15 method. MS spectra were acquired in the Orbitrap analyzer with a mass range of 300–1750 m/z at a resolution of 70,000 FWHM and a target value of 3×10^6 ions. Precursors were selected with an isolation window of 1.3 m/z. HCD fragmentation was performed at a normalized collision energy of 25. MS/MS spectra were acquired with a target value of 10^5 ions at a resolution of 17,500 FWHM, a maximum injection time (max.) of 55 ms and a fixed first mass of m/z 100. Peptides with a charge of +1, greater than 6, or with unassigned charge state were excluded from fragmentation for MS^2, dynamic exclusion for 30s prevented repeated selection of precursors.

LC-MS/MS data analysis

Raw data were processed using MaxQuant software (version 1.6.3.4, http://www.maxquant.org/) [48] with label-free quantification (LFQ) and iBAQ enabled [49]. MS/MS spectra were searched by the Andromeda search engine against a combined database containing the sequences from *A. thaliana* (TAIR10_pep_20101214; ftp://ftp.arabidopsis.org/home/tair/Proteins/TAIR10_protein_lists/) and sequences of 248 common contaminant proteins and decoy sequences. Trypsin specificity was required and a maximum of two missed cleavages allowed. Minimal peptide length was set to seven amino acids. Carbamidomethylation of cysteine residues was set as fixed, oxidation of methionine and protein N-terminal acetylation as variable modifications. Peptide-spectrum-matches and proteins were retained if they were below a false discovery rate of 1%.

Statistical analysis of the MaxLFQ values was carried out using Perseus (version 1.5.8.5, http://www.maxquant.org/). Quantified proteins were filtered for reverse hits and hits “identified by site” and MaxLFQ values were log2 transformed. Missing values were imputed from a normal distribution (1.8 downshift, separately for each column). After grouping samples by condition, only proteins with three valid values in at least one condition were retained for subsequent

analysis. Statistically significant enrichment was performed by ANOVA followed by Honest True Difference (HSD) test for groups TRB1, TRB3, ESD1 with FDR<0.05.

Protein expression and purification

A single colony of *E. coli* SoluBL21™ (amsbio), carrying either *pET-28b-TRB1 or pET-28b-TRB3* was used to inoculate 5 ml preculture in LB-AMP (100 mg/ml ampicillin), and grown at 37 °C, 200 rpm overnight. The preculture was added to 1 l LB-AMP-medium and grown at 37 °C, 200 rpm until the OD_{600} was around 0.6 – 0.8. After addition of 1 mM IPTG the culture was transferred to 16 °C,200 rpm overnight. Bacterial cells were collected using a JLA 10.500 rotor (Beckman/centrifuge AvantiTM J-25) at 4000 rpm at 4 °C for 10 min. Afterwards, bacterial cells were resuspended in 40 ml ice-cold lysis buffer (50 mM $NaPO_4$, 300 mM NaCl, 10 mM imidazole, 0.1 M PMSF at pH 7.5) and disrupted using sonication (Ultrasonic-Desintegrator, Branson) (Programme: Strength: 6, Duty cycle: 40, 3x 2 min). The cell debris was removed using a JA 25.50 rotor (Beckman/centrifuge AvantiTM J-25) at 13000 rpm, 4 °C for 30 min. For affinity purification, 500 µl of Ni-NTA Agarose beads (Qiagen) were washed three times with 5 ml lysis buffer, collected at 800 g,4 °C for 1 min and added to the cell lysate. After incubation at 4 °C, 12 rpm for 2 h then beads were collected, transferred to a fresh 5 ml Eppendorf tube and washed five times with 5 ml washing buffer (50 mM $NaPO_4$, 300 mM NaCl, 20 mM imidazole, pH 7.5) at 4 °C, 12 rpm for 5 min. To elute proteins, the beads were incubated with 1.5 ml elution buffer (50 mM $NaPO_4$, 300 mM NaCl, 250 mM imidazole, pH 7.5) at 4 °C, 12 rpm for 2 h. After collecting the beads at 4 °C, 800 g for 1 min, the supernatant was collected and dialysed in 500 ml dialysis buffer (50 mM $NaPO_4$, 300 mM NaCl, pH 7.5) using Slide-A-Lyzer™ Dialysis Cassettes (10K MWCO, 3 mL, ThermoFisher Scientific) to remove the imidazole. Dialysed proteins were collected in Protein LoBind Tubes (Eppendorf) and kept at 4 °C. Protein quantity was determined by Bio-Rad Protein Assay according to manufacturer's instructions. To check protein integrity, 1 µg of protein was mixed 2x SDS-Loading buffer (126 mM Tris-HCl (pH 6.8), 20 % glycerol, 4 % SDS, 0.02 % bromophenol blue), incubated at 95 °C for 5 min, and run in 1x TGS buffer (Bio Rad) on a 1.5 mm, 12 % SDS-PAGE at 100 V for approximately 1.5 h. The SDS-PAGE was stained with Coomassie brilliant blue staining solution (1 g Coomassie Brilliant Blue (Bio-Rad), 500 ml MeOH, 100 ml glacial acetic acid, 400 ml H_2O) and de-stained with H_2O overnight.

Microscale thermophoresis (MST)

Forward and reverse 5'-Cy3-labelled oligonucleotides of 28 bp were ordered from SIGMA-ALDRICH. Sequences originating from the *SEP3* promoter region were Cy3-*proSEP3*-telobox-Cy3: TTTAAATGTTAGGGTTTTTTGTAGGATT and Cy3-*proSEP3*-NonInter-Cy3:

AAAAATATTTATATCACATCATTGTTAT). Two versions of the (C)RACCTA motif were Cy3-(C)AACCTAA-Cy3: CATCATGGCAACCTAAGGCTGGTACT AG and Cy3-(C)GACCTAA-Cy3: CATCATGGCGACCTAAGGCTGGTACTAG. A four-telobox-repeat (R4) oligomer Cy3-R4-telobox-Cy3: GGTTTAGGGTTTAGGGTTTAGGGTTTAG was published in [27]. Annealing was carried out in a heating block in dialysis buffer at a concentration of 10 µM sense and anti-sense oligonucleotides by first incubating at 95 °C for 15 min and subsequent slow cooling by switching off the heating block.

For all MST experiments, the Monolith NT.115 instrument (NanoTemper Technologies) and 1x dialysis buffer with Tween 20 (0.05 %) and BSA (1.25 mg/ml) were used. Oligomer fluorescence intensity, absorption, and bleaching was tested with the instrument's green channel *via* the *Pretest* feature included in the machine's MO.Control software (NanoTemper Technologies). Samples were prepared according to the suggested protocol included in the software. Oligomer concentration was adjusted to obtain ≥ 200 fluorescent counts at a laser power ≤ 80 %. These conditions were met at an oligomer concentration of 20 nM and an IR-laser power of 60 % for Cy3-*proSEP3*-telobox-Cy3 and Cy3-*proSEP3*-NonInter-Cy3 and of 80 % for Cy3-R4-telobox-Cy3, Cy3-(C)AACCTAA-Cy3, and Cy3-(C)GACCTAA-Cy3. Afterward, general TRB-telobox/telobox-like element interaction and suitability of different capillaries was tested *via* the Binding Check feature and samples were prepared as suggested by the software. For this purpose, the highest possible protein concentration was mixed with 20 nM of fluorescently labelled oligomers and incubated at RT and in the dark for 10 min. Afterward, the TRB-dsDNA mix was loaded onto Monolith NT.115 Premium Capillaries (NanoTemper Technologies) that prevented surface absorption, as TRB proteins tended to absorb to standard capillaries. Afterward, TRB-telobox/telobox-like element interaction was quantified by using the software's *Binding Affinity* feature. For this MST assay, a dilution series was prepared according to the software's instructions, using the beforehand determined laser powers and 20 nM of oligomer mixed with 8.5 µM to 260 pM of TRB protein. The TRB-DNA mix was incubated at RT in the dark for 10 min before being loaded onto Premium capillaries. Each measurement was repeated at least three times. Binding curves were analysed and K_D values were calculated with the MO.Affinity Analysis software (NanoTemper Technologies) according to the manufacturer's instructions.

Supporting information

Supplemental_Figures_and_Tables
[https://www.biorxiv.org/content/10.1101/2025.11.10.687574v1.supplementary-material]

Declarations

Availability of data and materials

The datasets supporting the conclusions of this article are available in the European Nucleotide Archive (ENA), under the project accession number PRJEB63124.

Competing interests

The authors declare that they have no competing interests

Funding

This work was supported by core funding from the Max Planck Society to all authors. FT also receives funding from the DFG through the Cluster of Excellence in Plant Sciences (CEPLAS, EXC 2048/1 Project ID: 390686111).

Authors' contributions

F.T., K.K., M.M. and S.Z. conceived the study. K.K., M.M., S.Z., P.T. conducted the experiments. S.S. and H.N. set-up and carried out MS-MS analysis. M.M, K.K., P.S. and F.T. analyzed the results. F.T., K.K. and M.M wrote the manuscript. All authors reviewed the manuscript.

Supplemental Information

Supplemental Figures

Supplemental Figure 1. Expression of flowering time pathway genes in *trb* mutants

Supplemental Figure 2. Bioinformatics pipeline for ChIP-seq analysis and ChIP-seq quality control

Supplemental Figure 3. Characterization of TRB1-3 ChIP-seq data

Supplemental Figure 4. Pearson's correlation matrix of enriched gene ontology (GO) terms across all combinations of TRBs and complex categories

Supplemental File 1: Details of RNAseq analysis

Tab sig_1_wt_inS: DEGs trb1-2 vs Col-0

Tab sig_2_wt_inS: DEGs trb2-2 vs Col-0

Tab sig_2_wt_inS: DEGs trb3-2 vs Col-0

Tab sig_12_wt_inS: DEGs trb1-2 trb2-3 vs Col-0

Tab sig_13_wt_inS: DEGs trb1-2 trb3-2 vs Col-0

Tab sig_23_wt_inS: DEGs trb2-3 trb3-2 vs Col-0

Tab vst countmatrix: vst countmatrix across all genotypes for all DEGs

Tab PAM countmatrix: row scaled countmatrix across all genotypes for all DEGs with PAMclusters indicated

Tab detected genes: all genes with acceptable read counts (total >50 across all samples) in RNAseq

Tab GO PAM: GO-term enrichment for DEGs per PAM cluster

Supplemental File 2: Details of ChIP-Seq analysis

Tab peaks_TRB1: Annotated ChIP-Seq Peaks of TRB1:YFP

Tab peaks_TRB2: Annotated ChIP-Seq Peaks of TRB2:YFP

Tab peaks_TRB3: Annotated ChIP-Seq Peaks of TRB3:YFP

Supplemental File 3: Details of genomic binding analysis

Tab bins: Table of 11 regulatory protein occupancy of 500 bp wide genomic Bins, assigned regulatory complexes, and combination of TRB paralogs

Tab genes: Table of 11 regulatory protein occupancy of genes, associated RNAseq Cluster, assigned regulatory complexes, and combination of TRB paralogs

Supplemental File 4: Details of IP-MS-MS analysis

Tab raw: MaxQuant result

Tab ANOVA_HSD_full: log2 transformed, filtered and imputed LFQ values, result of ANOVA and HSD annotated to all protein

Tab: Significant: All proteins part of significant HSD groups

Supplemental File 5: Details of DNA-Motif analysis

Supplemental_File_5.zip: FASTA sequences used as input for the XSTREME analysis of the MEME-Pipeline, as well as directories containing the outputs

Supplemental File 6: Details of GO-Term enrichment analysis

Tab All_GO_Terms: Table containing all enriched (p<=0.05) GO-terms, their associated complexes, and co-bound TRB-paralogs

Funder Information Declared

Deutsche Forschungsgemeinschaft, https://ror.org/018mejw64, CEPLAS, EXC 2048/1 Project ID: 390686111

References

1. *Kusová A, Steinbachová L, Přerovská T, Drábková LZ, Paleček J, Khan A, et al. Completing the TRB family: newly characterized members show ancient evolutionary origins and distinct localization, yet similar interactions. Plant Mol Biol. 2023;112:61–83.*
2. *Procházková Schrumpfová P, Fojtová M, Fajkus J. Telomeres in plants and humans: not so different, not so similar. Cells. 2019;8.*
3. *Gaspin C, Rami J-F, Lescure B. Distribution of short interstitial telomere motifs in two plant genomes: putative origin and function. BMC Plant Biol. 2010;10:283.*
4. *Kotliński M, Knizewski L, Muszewska A, Rutowicz K, Lirski M, Schmidt A, et al. Phylogeny-Based Systematization of Arabidopsis Proteins with Histone H1 Globular Domain. Plant Physiol. 2017;174:27–34.*
5. *Mozgová I, Schrumpfová PP, Hofr C, Fajkus J. Functional characterization of domains in AtTRB1, a putative telomere-binding protein in Arabidopsis thaliana. Phytochemistry. 2008;69:1814–9.*
6. *Bilaud T, Koering CE, Binet-Brasselet E, Ancelin K, Pollice A, Gasser SM, et al. The telobox, a Myb-related telomeric DNA binding motif found in proteins from yeast, plants and human. Nucleic Acids Res. 1996;24:1294–303.*
7. *Schrumpfová PP, Vychodilová I, Dvořáčková M, Majerská J, Dokládal L, Schořová S, et al. Telomere repeat binding proteins are functional components of Arabidopsis telomeres and interact with telomerase. Plant J. 2014;77:770–81.*
8. *Teano G, Concia L, Wolff L, Carron L, Biocanin I, Adamusová K, et al. Histone H1 protects telomeric repeats from H3K27me3 invasion in Arabidopsis. Cell Rep. 2023;42:112894.*
9. *Zhou Y, Hartwig B, James GV, Schneeberger K, Turck F. Complementary activities of TELOMERE REPEAT BINDING proteins and polycomb group complexes in transcriptional regulation of target genes. Plant Cell. 2016;28:87–101.*
10. *Schrumpfová PP, Vychodilová I, Hapala J, Schořová Š, Dvořáček V, Fajkus J. Telomere binding protein TRB1 is associated with promoters of translation machinery genes in vivo. Plant Mol Biol. 2016;90:189–206.*

11. *Zheng S-Y, Guan B-B, Yuan D-Y, Zhao Q-Q, Ge W, Tan L-M, et al. Dual roles of the Arabidopsis PEAT complex in histone H2A deubiquitination and H4K5 acetylation. Mol Plant. 2023;16:1847–65.*

12. *Tan L-M, Zhang C-J, Hou X-M, Shao C-R, Lu Y-J, Zhou J-X, et al. The PEAT protein complexes are required for histone deacetylation and heterochromatin silencing. EMBO J. 2018;37.*

13. *Godwin J, Govindasamy M, Nedounsejian K, March E, Halton R, Bourbousse C, et al. The UBP5 histone H2A deubiquitinase counteracts PRCs-mediated repression to regulate Arabidopsis development. Nat Commun. 2024;15:667.*

14. *Zhou Y, Wang Y, Krause K, Yang T, Dongus JA, Zhang Y, et al. Telobox motifs recruit CLF/SWN-PRC2 for H3K27me3 deposition via TRB factors in Arabidopsis. Nat Genet. 2018;50:638–44.*

15. *Bratzel F, López-Torrejón G, Koch M, Del Pozo JC, Calonje M. Keeping cell identity in Arabidopsis requires PRC1 RING-finger homologs that catalyze H2A monoubiquitination. Curr Biol. 2010;20:1853–9.*

16. *Mozgova I, Hennig L. The polycomb group protein regulatory network. Annu Rev Plant Biol. 2015;66:269–96.*

17. *Simon JA, Kingston RE. Occupying chromatin: Polycomb mechanisms for getting to genomic targets, stopping transcriptional traffic, and staying put. Mol Cell. 2013;49:808–24.*

18. *Wang H, Liu C, Cheng J, Liu J, Zhang L, He C, et al. Arabidopsis Flower and Embryo Developmental Genes are Repressed in Seedlings by Different Combinations of Polycomb Group Proteins in Association with Distinct Sets of Cis-regulatory Elements. PLoS Genet. 2016;12:e1005771.*

19. *Xiao J, Jin R, Yu X, Shen M, Wagner JD, Pai A, et al. Cis and trans determinants of epigenetic silencing by Polycomb repressive complex 2 in Arabidopsis. Nat Genet. 2017;49:1546–52.*

20. *Deng W, Buzas DM, Ying H, Robertson M, Taylor J, Peacock WJ, et al. Arabidopsis Polycomb Repressive Complex 2 binding sites contain putative GAGA factor binding motifs within coding regions of genes. BMC Genomics. 2013;14:593.*

21. *Shu J, Chen C, Thapa RK, Bian S, Nguyen V, Yu K, et al. Genome-wide occupancy of histone H3K27 methyltransferases CURLY LEAF and SWINGER in Arabidopsis seedlings. Plant Direct. 2019;3:e00100.*

22. *Ning Y-Q, Ma Z-Y, Huang H-W, Mo H, Zhao T, Li L, et al. Two novel NAC transcription factors regulate gene expression and flowering time by associating with the histone demethylase JMJ14. Nucleic Acids Res. 2015;43:1469–84.*

23. *Wang M, Zhong Z, Gallego-Bartolomé J, Feng S, Shih Y-H, Liu M, et al. Arabidopsis TRB proteins function in H3K4me3 demethylation by recruiting JMJ14. Nat Commun. 2023;14:1736.*

24. *Landt SG, Marinov GK, Kundaje A, Kheradpour P, Pauli F, Batzoglou S, et al. ChIP-seq guidelines and practices of the ENCODE and modENCODE consortia. Genome Res. 2012;22:1813–31.*

25. *Wang M, Zhao Y, Zhang B. Efficient Test and Visualization of Multi-Set Intersections. Sci Rep. 2015;5:16923.*

26. *Seidel SAI, Dijkman PM, Lea WA, van den Bogaart G, Jerabek-Willemsen M, Lazic A, et al. Microscale thermophoresis quantifies biomolecular interactions under previously challenging conditions. Methods. 2013;59:301–15.*

27. *Hofr C, Sultesová P, Zimmermann M, Mozgová I, Procházková Schrumpfová P, Wimmerová M, et al. Single-Myb-histone proteins from Arabidopsis thaliana: a quantitative study of telomere-binding specificity and kinetics. Biochem J. 2009;419:221–8, 2 p following 228.*

28. *Su Y, Wang S, Zhang F, Zheng H, Liu Y, Huang T, et al. Phosphorylation of Histone H2A at Serine 95: A Plant-Specific Mark Involved in Flowering Time Regulation and H2A.Z Deposition. Plant Cell. 2017;29:2197–213.*

29. *Espinosa-Cores L, Bouza-Morcillo L, Barrero-Gil J, Jiménez-Suárez V, Lázaro A, Piqueras R, et al. Insights into the function of the nua4 complex in plants. Front Plant Sci. 2020;11:125.*

30. *Trémousaygue D, Garnier L, Bardet C, Dabos P, Hervé C, Lescure B. Internal telomeric repeats and "TCP domain" protein-binding sites co-operate to regulate gene expression in Arabidopsis thaliana cycling cells. Plant J. 2003;33:957–66.*

31. *Hecker A, Brand LH, Peter S, Simoncello N, Kilian J, Harter K, et al. The Arabidopsis GAGA-Binding Factor BASIC PENTACYSTEINE6 Recruits the POLYCOMB-REPRESSIVE COMPLEX1 Component LIKE HETEROCHROMATIN PROTEIN1 to GAGA DNA Motifs. Plant Physiol. 2015;168:1013–24.*

32. *Petrella R, Caselli F, Roig-Villanova I, Vignati V, Chiara M, Ezquer I, et al. BPC transcription factors and a Polycomb Group protein confine the expression of the ovule identity gene SEEDSTICK in Arabidopsis. Plant J. 2020;102:582–99.*

33. *Martin M. Cutadapt removes adapter sequences from high-throughput sequencing reads. EMBnet j. 2011;17:10.*

34. *Li H, Durbin R. Fast and accurate short read alignment with Burrows-Wheeler transform. Bioinformatics. 2009;25:1754–60.*

35. *Li H, Handsaker B, Wysoker A, Fennell T, Ruan J, Homer N, et al. The Sequence Alignment/Map format and SAMtools. Bioinformatics. 2009;25:2078–9.*

36. *Ramírez F, Ryan DP, Grüning B, Bhardwaj V, Kilpert F, Richter AS, et al. deepTools2: a next generation web server for deep-sequencing data analysis. Nucleic Acids Res. 2016;44:W160–5.*

37. *Quinlan AR, Hall IM. BEDTools: a flexible suite of utilities for comparing genomic features. Bioinformatics. 2010;26:841–2.*

38. *Stovner EB, Sætrom P. epic2 efficiently finds diffuse domains in ChIP-seq data. Bioinformatics. 2019;35:4392–3.*

39. *Li Q, Brown JB, Huang H, Bickel PJ. Measuring reproducibility of high-throughput experiments. Ann Appl Stat. 2011;5:1752–79.*

40. *Harrell Jr FE. Hmisc: Harrell Miscellaneous. The R Foundation. 2024.*

41. *Gu Z, Eils R, Schlesner M. Complex heatmaps reveal patterns and correlations in multidimensional genomic data. Bioinformatics. 2016;32:2847–9.*

42. *Grant CE, Bailey TL. XSTREME: Comprehensive motif analysis of biological sequence datasets. bioRxiv. 2021.*

43. *O'Malley RC, Huang S-SC, Song L, Lewsey MG, Bartlett A, Nery JR, et al. Cistrome and epicistrome features shape the regulatory DNA landscape. Cell. 2016;165:1280–92.*

44. *Yu G, Wang L-G, He Q-Y. ChIPseeker: an R/Bioconductor package for ChIP peak annotation, comparison and visualization. Bioinformatics. 2015;31:2382–3.*

45. *Wang Q, Li M, Wu T, Zhan L, Li L, Chen M, et al. Exploring epigenomic datasets by chipseeker. Curr Protoc. 2022;2:e585.*

46. *Wu T, Hu E, Xu S, Chen M, Guo P, Dai Z, et al. clusterProfiler 4.0: A universal enrichment tool for interpreting omics data. Innovation (Camb). 2021;2:100141.*

47. *Rappsilber J, Ishihama Y, Mann M. Stop and go extraction tips for matrix-assisted laser desorption/ionization, nanoelectrospray, and LC/MS sample pretreatment in proteomics. Anal Chem. 2003;75:663–70.*

48. *Cox J, Mann M. MaxQuant enables high peptide identification rates, individualized p.p.b.-range mass accuracies and proteome-wide protein quantification. Nat Biotechnol. 2008;26:1367–72.*

49. *Tyanova S, Temu T, Cox J. The MaxQuant computational platform for mass spectrometry-based shotgun proteomics. Nat Protoc. 2016;11:2301–19.*

4 Further Results

4.1 Anti-GFP Nanobodies can Decrease the Amount of TRBs but are Unable to Phenocopy the *trb123* Mutant

Due to the complex nature of the role TRBs play in development, it is very difficult to pinpoint the exact time and place at which TRB-mediated gene regulation is vital for plant development. As can be seen in the phenotype of the *trb123* mutant, seed germination does not appear to be relying on TRBs, while the transition of embryo to vegetative growth is completely impeded under regular conditions in this mutant. In order to better understand TRB-controlled developmental processes, it is therefore paramount to establish ways to control the activity of TRBs in a spatial and temporal manner.

One promising approach is the anti-GFP nanobody based system established by Caussinus Kanca and Affolter (2011) and adapted for use in *A. thaliana* by Ma et al. (2019). The system relies on antibody fragments targeting GFP and other closely related fluorescence tags. This marks their target for degradation in the proteasome, leading to post-translational protein knockout. The production of the anti-GFP nanobody is under control of a dual promoter system. The first is a dexamethasone (DEX) inducible promoter, which requires an additional activator protein, which, in turn, can be expressed using any other promoter. Through this approach, both the time (through DEX induction) and place (through tissue-specific activator expression) can be controlled (Figure 11,A).

Since this system had never been used against TRBs, I started by evaluating the overall ability of the nanobodies to deplete TRB1 in *trb123 pTRB1-TRB1:YFP* plants. Since this line contains only the YFP-tagged TRB1, a full knockout of this protein throughout development should phenocopy the *trb123* mutant. To achieve this, the plants were transformed using a nanobody construct with ubiquitous activator expression through the p35S promoter, together with DEX induction throughout the entire lifecycle of the plants. A second construct included in the test involved a fusion of the nanobody with TFP1, a turquoise fluorescent protein that is not targeted by the anti-GFP nanobody. This construct was included as a control of correct induction of the nanobody.

While the plants did not phenocopy the *trb123* mutant (Figure 11, B), the depletion of TRBs was not without effect. Confocal microscopy revealed that the YFP signal in the root tips was depleted, but still visible. TFP1, on the other hand, was slightly increased after induction (Figure 11, C). Quantitative image analysis confirmed this observation, indicating a 50% decrease in YFP

fluorescence in root tips of plants treated with dexamethasone (Figure 11, D). Lastly, plants treated with the inducer flowered significantly earlier than plants treated with DMSO, both on plates and in greenhouse conditions (Figure 11, E).

These results indicate that the nanobody-based knockout of TRBs appeared to be insufficient to fully deplete the supply of TRB1, leading to a failure to phenocopy the triple mutant. The plants instead exhibited an early flowering phenotype similar to the early flowering observed in some *trb* double mutants. While it would still be interesting to evaluate the effect of these knockdowns in certain tissues at certain developmental stages, the lack of complete knockout of TRB1 renders the system far less promising than expected and further experimentation will be necessary to assess the viability of post-translational knockout of TRBs.

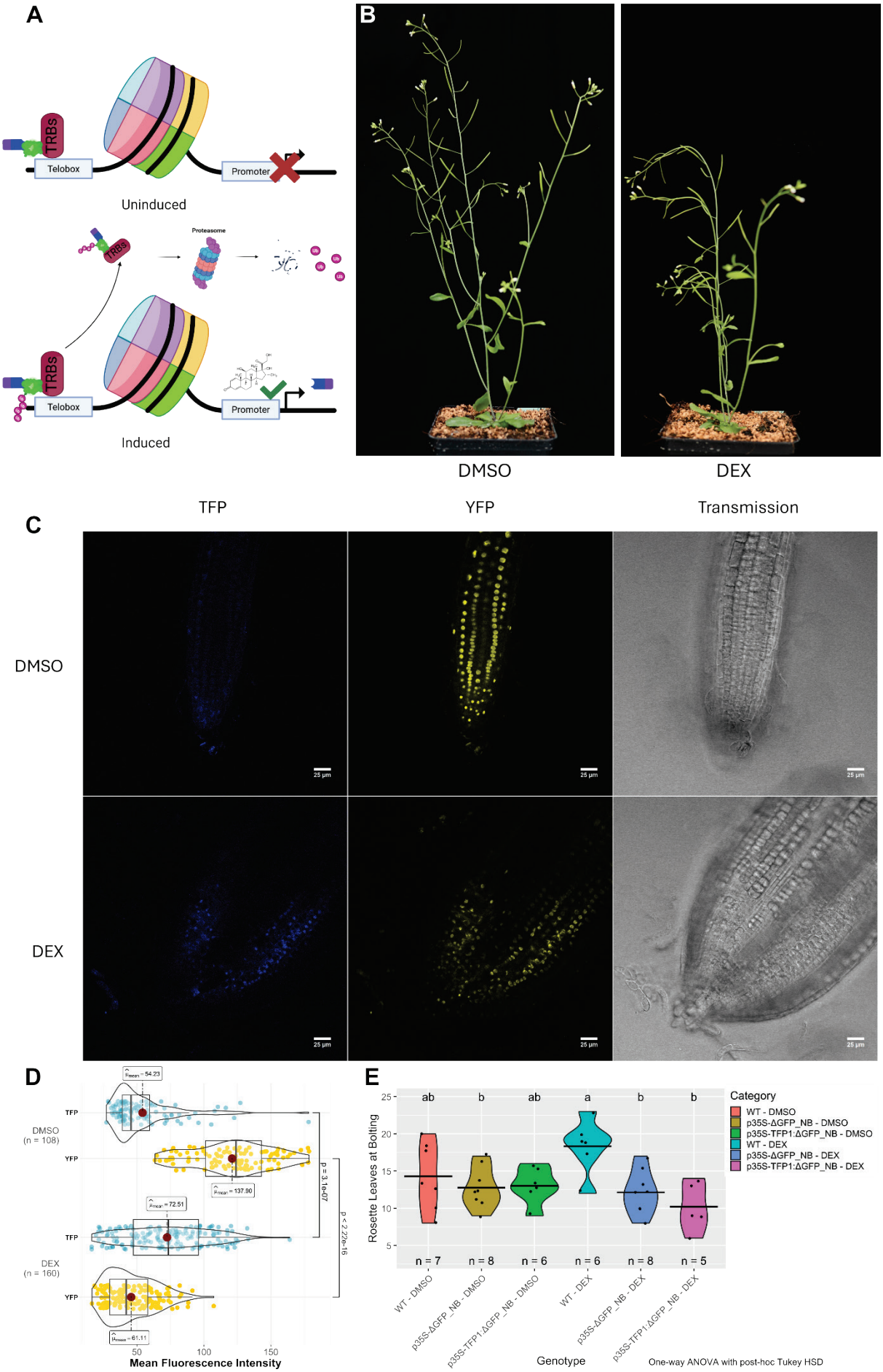
A
TRBs
Telobox
Promoter
Uninduced
Proteasome
Induced
B
DMSO
DEX
TFP
YFP
Transmission
C
DMSO
DEX
25 µm
D
DMSO
(n = 108)
DEX
(n = 160)
TFP
YFP
p = 3.1e-07
p < 2.22e-16
50
100
150
Mean Fluorescence Intensity
E
Rosette Leaves at Bolting
ab
b
ab
a
b
b
n = 7
n = 8
n = 6
n = 6
n = 8
n = 5
WT - DMSO
p35S-ΔGFP_NB - DMSO
p35S-TFP1:ΔGFP_NB - DMSO
WT - DEX
p35S-ΔGFP_NB - DEX
p35S-TFP1:ΔGFP_NB - DEX
Genotype
Category
One-way ANOVA with post-hoc Tukey HSD

*Figure 11, Anti-GFP Nanobody Proof of Concept. **A**, Concept of DEX-Inducible ΔGFP-Nanobody knockout. Top: Without induction, the GFP-tagged TRB protein functions normally and the nanobody is not expressed. Bottom: After induction with dexamethasone (DEX), the nanobody is expressed and binds to the GFP-tag of the TRB protein, leading to poly-ubiquitination and subsequent degradation of the nanobody-GFP-TRB complex in the proteasome. **B**, Phenotype of plants carrying pTRB1-TRB1:YFP in trb123 together with p35S-TFP1:ΔGFP-NB. Left: Mock treatment with DMSO, Right: Induced by watering three times per week with water containing 20 µM DEX. **C**, Confocal microscopy images of root tips of uninduced (top) and DEX-treated (bottom) plants of the same genotype as B. One channel each for TFP1 and YFP fluorescence signal, as well as transmission light. Scalebar equals 25 µm. **D**, Mean fluorescence intensity of the nuclei displayed in C for the YFP and TFP1 channel. **E**, Flowering time measured through number of rosette leaves at bolting of Col-0 or trb123 pTRB1-TRB1:YFP containing either p35S-ΔGFP_NB or p35S-TFP1: ΔGFP_NB. The first three categories show mock treatment with DMSO, the remaining three treatment with 20 µM DEX.*

5 Discussion

5.1 Traditional Methods of Protein Complex Discovery are Insufficient to Fully Capture TRB-Containing Complexes

Although the multi-faceted role of TRBs in epigenetic gene regulation had been known for multiple years (Tsuzuki and Wierzbicki 2018; Y. Zhou et al. 2018), recent discoveries have made it clear that we are far from understanding its full extend (Zheng et al. 2023; Ming Wang et al. 2023b). While protein-protein interaction studies can be a useful tool in the discovery of TRB-containing complexes (Q. Wang et al. 2025), the functional characterization of such complexes remains unresolved. Here I attempted to find evidence of a potential ICU11-associated TRB complex, derived from IP-MS data. In reverse genetics experiments I uncovered that loss-of-function alleles of *UTI1* can modulate the effect of *trb* double mutants on flowering time in either direction, depending on the TRB paralogs involved. This is emblematic for how the poorly understood divergence between TRB paralogs can impede inquiries into the general role of TRBs. While TRB1,2, and 3 were long thought to be redundant, it has now become clear that full redundancy of the three paralogs is not the case.

Analysis of the transcriptomes of the *uti1* and *trb* double mutant combinations suffered from the second major obstacle in TRB research: The dual-role of TRB mediated regulation. Since TRBs can take part in both activating and repressive complexes, many effects caused by TRB disruptions cannot easily be attributed to specific complexes. Nevertheless, using previously established lists and networks of flowering time genes (Bouché et al. 2016) allowed for efficient hypothesis development. One such hypothesis can be formed from the observation that multiple of the most misregulated genes with flowering time association were activators or repressors of *FLC*. Despite this, the expression levels of *FLC* at the time of harvesting did not appear to be severely affected, nor was there a notable effect on any of FLC's downstream targets. If this is due to compensatory effects or a more general loss of function of *FLC* remains to be investigated. Additionally, the role of SDG25 as potential antagonist of ICU11-mediated repression was discussed but not further investigated. The testing of these and other hypotheses will require more advanced genetics, which were outside of the scope of this work.

ChIP-Seq analysis of some of the components of the putative ICU11-containing complex proved to be more illuminating, particularly in combination with analysis of the effect of *trb123* on the involved histone marks. ChIP-Seq allows for a more in-depth examination of the overlap of putative complex components. This is vital when studying proteins that can form multiple distinct complexes with other proteins, as it allows to determine which complex is likely present at which

site. In combination with transcriptomic analysis, it can also be a useful tool to determine direct versus indirect effects TFs have on transcription. In the case of the putative PRC2-UTI-ICU11 complex, the association of TRBs with ICU11 could clearly be demonstrated by their significant overlap on genes. Furthermore, the change in H3K36me3 patterns observed in *trb123* is consistent with a lack of ICU11-mediated H3K36me3 demethylation in the TSS region. On the other hand, the strong hypermethylation observed in gene bodies hints towards a second, unknown effect of the absence of TRBs on H3K36me3 methylation. In addition to this, combining the ChIP-Seq and transcriptome analysis provided further insights. While only few sites changed histone marks either from H3K27me3 to H3K36me3 or *vice versa*, the few sites that did undergo this switch were significantly more likely to be targets of TRBs and ICU11. This overlap was more pronounced for flowering time regulating genes that were misregulated in *uti* mutants.

Overall, the ChIP-Seq data analysis provides evidence of both an ICU11 containing TRB complex, and of TRB-dependent H3K36me3 methylation patterns. It, however, also demonstrated that TRB-containing complexes are not solely responsible for either H3K36me3 deposition or removal. Taken together the RNA-Seq and ChIP-Seq data exhibited multiple signs compatible with the hypothetical PRC2-ICU11-TRB, but failed to fully capture all expected patterns.

5.2 The Role of TRB Paralogs is More Nuanced and Complex Than Previously Described

Research into the role of TRBs often treat TRB1, TRB2, and TRB3 as completely redundant for the sake of simplicity. Throughout this investigation, however, it has become clear that this is an oversimplification. While there is no doubt that this redundancy is observed in LD conditions, shorter photoperiod and/or lower temperature revealed clear divergent effects in *trb* mutants. This is especially clear in the opposing flowering time behavior observed in loss-of-function alleles of *UTI1* in different *trb* double mutants. Ultimately, the development of the large ChIP-Seq database in the submitted manuscript dispelled any doubt that the three TRB paralogs specialize in specific regulatory functions. It furthermore provides evidence of diversification of the three TRBs along activating/repressive lines. TRB1 appears to be more closely connected to activating complexes like PEAT and NuA4, while TRB2 and TRB3 seem to be more associated with repressive complexes like PRC2 and ICU11/JMJ14 demethylation complexes. The different specialized roles of TRB paralogs provide a good example of permanent heterozygous advantage, as introduced by Ohno (1970). By retaining multiple copies of TRBs, plants can profit from the advantages usually granted to heterozygous individuals (i.e., heterosis) while simultaneously allowing their offspring to fully inherit all advantageous alleles. According to Ohno, the biggest obstacle to retaining permanent

heterozygous advantage is the tightly regulated dose-dependency of most eucaryotic genes (Ohno 1970, Page 65). Even minor changes in expression levels can severely affect the balance of gene regulation or metabolic processes. This often renders the gene duplications, required to establish multiple paralogs, disadvantageous. It therefore comes as no surprise that TRBs appear to be relatively decoupled from dosage dependency. Neither the decrease of TRB abundance to a single allele, nor artificial reduction of TRBs through anti-GFP nanobodies severely affected plant development (Figure 11). Lastly, it should be mentioned that TRB4 and TRB5 are also closely related to TRB1, 2, and 3, albeit not as closely as the three paralogs among each other (Kusová et al. 2023). While the two additional TRBs were poorly studied for a long time, recent research has focused much more on their functions, including in epigenetic gene regulation (X. Wang et al. 2025; Amiard et al. 2024; Kusová et al. 2023). Future investigations into the roles of TRBs will therefore not be complete without the inclusion of TRB4 and TRB5, the latter of which has never been subject to ChIP-Seq studies.

5.3 Our Understanding of the Role of TRBs in Gene Regulation is Improving, but the Full Picture Remains Largely Unresolved

At the start of this project, TRBs were already implicated in two epigenetic regulatory complexes with opposing effects. The activating PEAT complex and the repressive PRC2 complex. Throughout this project evidence for multiple additional TRB complexes was uncovered (Manuscript Figure 7, B). Firstly, the IP-MS data generated in our group suggests the existence of a ICU11 containing TRB complex (Section 2.1, Figure 4). The connection between ICU11 and TRBs also appears in ChIP-Seq data, including the H3K36me3 methylation changes in *trb* triple mutants (Section 2.4, Figure 9 & Figure 10). During the drafting of our manuscript (Section 3.3), we learned that another group was working on a related publication (Q. Wang et al. 2025). Through a mix of TRB interactor studies and ChIP-Seq analysis, they were able to show that TRBs form at least two previously undescribed complexes. The first complex, named TRB1/2/3-HELIX-TURN-HELIX-PROTEIN (TRHT), involves UTI proteins, which they designated HELIX-TURN-HELIX (HTH). The second one involves JMJ14 and NAC50/52 TFs and was named TRB1/2/3-HISTONE-DEMETHYLASE (TRHD) complex. In their model, ICU11 occupies a central role within both complexes (Figure 12). Taken together, my ChIP-Seq analysis combined with their combination of ChIP-Seq and affinity purification provide a more complete picture of the ICU11-TRB relationship. This ultimately confirms the presence of a complex (TRHT) similar to the PRC2-ICU11 complex proposed in Section 2.1. The main difference between TRHT and the proposed PRC2-ICU11

complex is that Q. Wang et al. (2025) did not designate PRC2 components as part of TRHT. After adding their ICU11 and HTH1 (a.k.a. UTI3) ChIP-Seq data to the database I had constructed for the manuscript (Manuscript Figure 8, B), a cursory analysis confirmed that PRC2 and HTH1/ICU11 target sites did not correlate (Data not shown). A full evaluation of the relationship between TRHT and PRC2 will be required to fully falsify the proposed PRC2-ICU11 complex. Furthermore, my comparative analysis of 11 ChIP-Seq sets of various epigenetic regulatory complex components uncovered evidence of an additional complex. This complex is part of the activating NuA4 complex and uses TRBs as transcription factor component (Manuscript Figure 2).

Lastly, our newly generated TRB1, TRB2, and TRB3 ChIP-Seq dataset in combination with our *trb* mutants allowed for the first in depth analysis of the divergent roles of the paralogs. Through multiple different experimental approaches, I was able to determine which TRB paralog is specialized in each of the TRB-complexes (Manuscript Figure 9).

Despite these improvements in our understanding of TRB-mediated epigenetic gene regulation, many questions remain open. Chief among them is certainly the question of how TRBs stay as redundant as we can observe, despite showing divergent molecular behavior. While Ohno's concept of permanent heterozygous advantage provides an evolutionary explanation of why TRBs are largely redundant and dosage independent, the molecular mechanisms behind this remain elusive. Another question to which no satisfying answer has been produced yet is the targeting of TRB and their associated complexes. My analysis revealed that TRB complexes are largely mutually exclusive in their genomic binding sites, how this exclusivity is maintained, however, is unclear. DNA motif analysis provided evidence of some sequence specific complex recruitment but was not sufficient to fully explain or predict the presence of complexes at specific genomic sites (Manuscript Figure 4). Despite these open questions, the newly developed database containing genomic binding locations of TRB-related proteins will be a useful tool in subsequent investigation. The expansion of this database could provide even more insight into the role of TRBs in epigenetic regulation. Particularly the HTH1 and ICU11 ChIP-Seq data recently published by Q. Wang et al. (2025) will be a valuable addition. Furthermore, the direct effects of epigenetic regulatory complexes could be better understood through the inclusion of histone modification data and transcriptome changes into the same database. In the long term, developing a comprehensive database of the epigenetic regulatory landscape could contribute greatly to our understanding of how plants regulate gene expression.

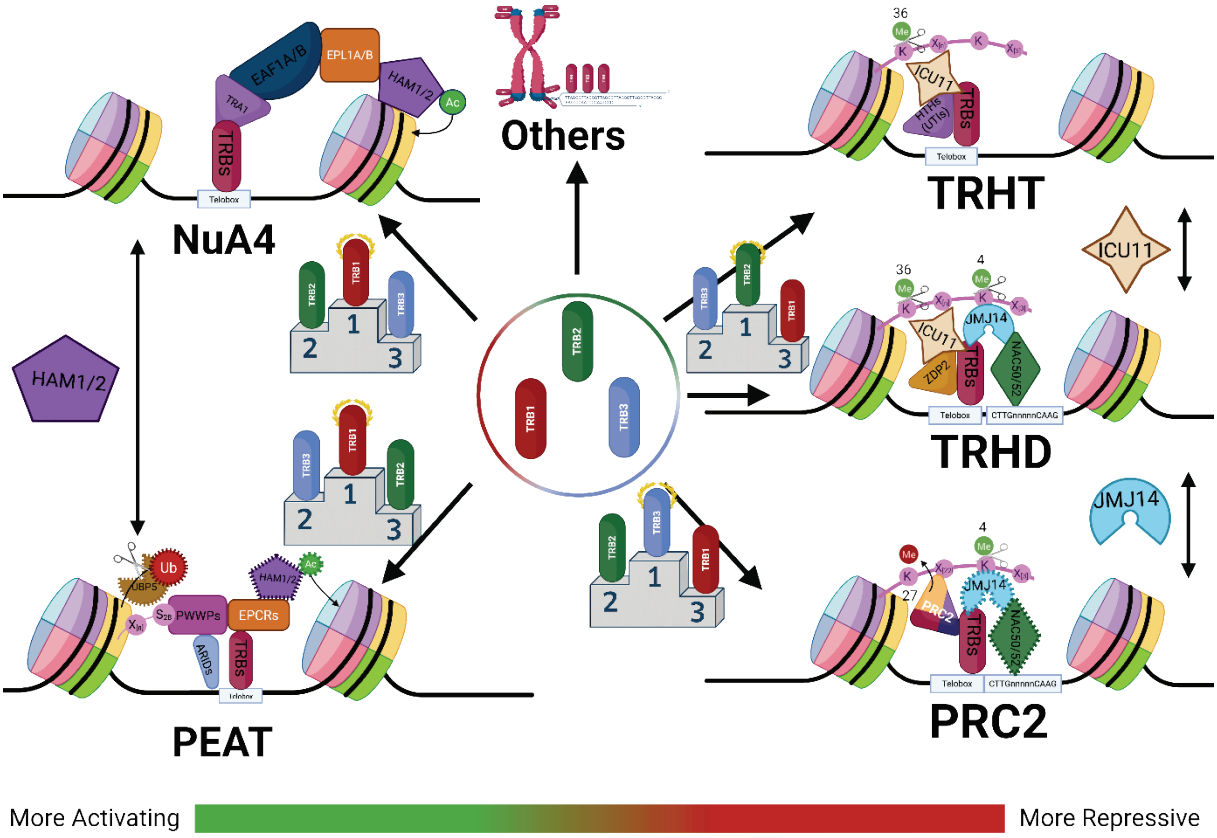

Figure 12, Current working model of TRB-mediated epigenetic gene regulation. Complex components which are not core to the TRB-containing complexes are indicated with dashed outlines. TRB-paralog specialization is conveyed via podiums, with red representing TRB1, green representing TRB2, and blue representing TRB3. HAM1/2 is shared between PEAT and NuA4, JMJ14 is shared between PRC2 and TRHD, and ICU11 is shared between TRHD and TRHT. The complexes on the left are assumed to be primarily activating, while the complexes on the right are assumed to be primarily repressive.

6 Materials and Methods

6.1 Plant Lines Used

For the transformation step of the reverse genetics approach, plants were grown in greenhouse conditions at 22 °C in LD photoperiod. Background lines for CRISPR transformation were: Col-0, *trb1-2 trb3-3* and *trb2-3 trb3-2*. For more details on the genotypes, see "Materials & Methods" in the manuscript provided in section 3.3.

The scoring of flowering time for the transformed plants was performed on plants grown in the indicated conditions in growth chambers. Flowering time was measured as the number of rosette leaves at time of bolting. Statistical analysis was performed through R (see 6.6).

For RNA-Seq, plants were grown in growth chambers at 22 °C with 12h photoperiod. Position of the genotypes in the trays was randomized. After seeds were stratified at 4 °C for 7 days, they were transferred into the growth chambers and after 14 days, ten seedlings per sample were harvested one hour before the start of the night cycle (at ZT11). Three biological replicates were taken one week apart, grown in the same chambers.

Plants for ChIP-Seq were grown in the same conditions as RNA-Seq by Marije Vos.

For the anti-GFP-Nanobody experiments, two lines of *trb123* mutant plants containing the YFP variant VENUS fused to TRB1 and under control of the native TRB1 promoter were used. Out of multiple *genTRB1-9ALA-VENUS trb1/2/3* lines provided by F. Turck, line 7-2-8 and 7-4-11 were chosen for the experiment based on the strength of their YFP-signal.

6.2 Analysis of the TRB Interaction Network

Analysis of the TRB interaction network was performed based on IP-MS, Y2H, and BiFC data generated by Zündorf (2022). The discovered interactions were used to build an interaction network in Cytoscape (Shannon et al. 2003). The full network was then collapsed into a minimal network by first merging paralogs into group nodes, followed by a second merge of known complex components into their respective complexes. The resulting overview network is displayed in Figure 4, A (with the "Demethylases" node expanded). The known (sub)-complexes discovered by Zheng et al. (2023) and Ming Wang et al. (2023b) were indicated in the network. The remaining interactions were then scanned for the presence of possible bi-functional complexes.

6.3 Reverse Genetics – CRISPR

For reverse genetics, the CRISPR/Cas based editing system described by Stuttmann et al. (2021) was utilized. sgDNAs against *UTI1* were designed using CRISPR-P 2.0 (H. Liu et al. 2017). The location of sgDNA sites in the genes can be found in Figure 5, A and more details regarding the generated alleles are listed in Supplementary Table 2. The cloning was performed according to the protocol published by Stuttmann et al. (2021), the sgDNAs were first hybridized and inserted into shuttle vectors pDGE331 - pDGE342. Subsequently, compatible shuttle vectors were assembled into expressions vectors pDGE347 through GoldenGate cloning. A schematic overview of the sgDNAs and the vector can be found in Figure 5, A+B. Shuttle and expression vectors were amplified by *Escherichia coli* transformation of the DH5α strain using a heat shock protocol (42 °C for 90 s) in LB-Medium containing the appropriate antibiotics. Subsequent plasmid preparation was performed using the NucleoSpin Plasmid Mini Kit (MACHEREY-NAGEL) according to the manufacturer's instructions. The fully assembled editing vectors were transformed into *Agrobacterium tumefaciens* strain GV3101 pSOUP through electroporation (1 pulse of 2.2 kV in a 0.1 cm cuvette). Transformed *A. tumefaciens* colonies were singled and plated with 300 µl of sterile water on LB medium containing appropriate antibiotics. After two days of incubation at 28 °C the bacterial lawn was resuspended in 1 ml of dipping solution (8% sucrose, 0.02% Silwet L-77). The resulting suspension was adjusted to a final OD600 of 1.9 using more dipping solution. For plant editing, the background plants described in 6.1 were transformed with pDGE347, harboring the appropriate sgDNAs *via* drop dipping: Plants that just started flowering (age dependent on genotype) were selected for transformation. First, all mature inflorescences were removed together with all but 5-10 immature inflorescences. The remaining un-opened flower buds were then dipped into the *A. tumefaciens* solution. After overnight incubation in darkness, the plants were transferred into the greenhouse and grown under LD conditions until ready for harvest. Transgenic plants of the following generation were selected based on seed fluorescence and grown on soil in the greenhouse. After 14 days of growth, one leaf of each T1 plant was harvested and its DNA extracted using BioSprint DNA Plant Kit (QIAGEN). The sgDNA target loci were amplified using PCR (see Supplementary Table 3). Samples with abnormal amplicon size were sent to Eurofins Genomics Europe for sequencing to verify full protein disruption. The same method was used to identify homozygous descendants in the following T2 generation. Lastly, the fluorescent seed marker was used again to select plants lacking the Cas9 construct. These plants constitute the transgene free, homozygously edited generation used for downstream experiments.

6.4 Transcriptome Analysis

6.4.1 RNA-Seq – Lab work

The plants were harvested as described in 6.1 and transferred into tubes containing two tungsten carbide beads. Immediately after, the tubes were frozen in liquid nitrogen and stored at -80 °C until RNA extraction. RNA extraction was performed using TRIzol reagent (Invitrogen). First, the frozen samples were homogenized in the TissueLyser III Bead Mill Homogenizer (QIAGEN) two times for one minute at 30hz. Afterwards 1 ml of TRIzol reagent was added to each tube. All subsequent steps were performed according to the manufacturer's instructions. The final RNA pellet was resuspended in 20 ml of RNAse-free water and RNA yield was determined using Qubit RNA assay (according to manufacturer's instructions). The extracted RNA was treated with DNAse using the DNA-free DNA Removal kit (Invitrogen), as described in the kit's instructions. Lastly, the RNA was sent to either the Genome Center at Max Planck Institute for Plant Breeding Research or Novogene for poly-A enrichment, library preparation, and paired-end short read cDNA sequencing (both on Illumina Platform).

6.4.2 RNA-Seq – Bioinformatics

Quality assessment of paired read sequences was performed using MultiQC (Ewels et al. 2016). Salmon (Patro et al. 2017) was used for the quantification of transcript reads and all subsequent steps were performed using R in R Studio (R Core Team 2021; Posit team 2025). Differential expression analysis started with generation of a SummerizedExperiment object containing the read quantifications. This was achieved through the use of Tximeta (Love et al. 2020) supplied with a custom *A. thaliana* transcriptome based on Araport11 (Cheng et al. 2017). The SummerizedExperiment was then used for differential expression analysis *via* the DESeq2 pipeline (Love, Huber, and Anders 2014). After initial PCA plotting, two replicates (one in each RNA-Seq experiment) were determined to be extreme outliers and therefore removed from the analysis. For subsequent analysis, the samples in both experiments were first combined into one SummerizedExperiment and then split into two sets: uti1trb13 (containing all samples of *uti1, trb1 trb3* and *uti1 trb1 trb3*), and uti1trb23 (containing the same *uti1* samples, together with *trb2 trb3* and *uti1 trb2 trb3*). Differentially expressed genes were visualized using the tools listed in 6.6. For the generation of heatmaps, DEGs were grouped into one of seven categories based on their expression patterns throughout the three genotypes in each set:

1. "Similar Effect", if the log2FoldChanges of all genotypes were within 10% from each other.

2. “uti-dominant”, if the log2FoldChange of *uti1 trb1/2 trb3* was within 10% of *uti1*, but not *trb1/2 trb3*.
3. “trb-dominant”, if the log2FoldChange of *uti1 trb1/2 trb3* was within 10% of *trb1/2 trb3*, but not *uti1*.
4. “Enhancing trb”, if the log2FoldChange of *uti1 trb1/2 trb3* was larger than the log2FoldChange of *trb1/2 trb3* and they shared the same sign.
5. “Rescuing trb”, if the log2FoldChange of *uti1 trb1/2 trb3* was smaller than the log2FoldChange of *trb1/2 trb3* and they shared the same sign.
6. “Counteracting – Both”, if the log2FoldChange of *uti1 trb1/2 trb3* had the opposite sign to both *uti1* and *trb1/2 trb3*.
7. “Counteracting - Only trb”, if the log2FoldChange of *uti1 trb1/2 trb3* had the opposite sign to *trb1/2 trb3*, but not to *uti1*.

Each DEG was assigned an expected effect on flowering time as well. First, FLOR-ID data published by Bouché et al. (2016) was used to filter the DEGs by genes with known impact on flowering time regulation. Within this list, each gene is assigned as having either a positive or negative effect on flowering time in WT conditions. This information was combined with transcription data to arrive at the expected effect of the differential gene expression:

Table 2, Decision Matrix for flowering time regulating DEGs

Effect on flowering time regulation according to FLOR-ID	Differential expression in my RNA-Seq analysis	Expected effect on flowering time
Positive	Higher expression levels	Expediting
Positive	Lower expression levels	Delaying
Negative	Higher expression levels	Expediting
Negative	Lower expression levels	Delaying

6.5 ChIP-Seq Analysis

6.5.1 ChIP-Seq – Lab work

ChIP-Seq lab work was provided by Marije Vos using a CUT&TAG approach. This description of the procedure was provided by Dr. Franziska Turck:

“Seeds of Col-0 and segregating *trb1/2/3* plants with one remaining wild-type allele of either TRB1, TRB2 or TRB3 were sterilized by two consecutive washes in 80% ethanol and plated on 10 cm square plates with GM media without sucrose. After placing 100 regularly spaced seeds, plates were sealed with microfilm, stratified for 2 days at 4°C in the dark and then grown for 2 weeks at 21°C in LD in a Percival chamber equipped with LED light. After 2-weeks, *trb/TRB* segregating

plates were screened under a binocular to identify individuals with typical trb1/2/3 triple mutant phenotype. The material was harvested into pre-weighted 1.5 ml Eppendorf tubes and fresh weight determined before snap-freezing the samples in liquid nitrogen. A similar amount of material (ca. 50 mg) was harvested for Col-0 controls.

Nuclei were prepared using Anti-Nucleus microbeads (Miltenyi Biotec) according to manufacturer's instructions with the following modification for plant material. Seedlings were added to 300 µl NSB buffer on a pre-cooled petri-dish on ice and the material was chopped with a sharp razor blade for 5 min. After adding an additional 300 µl NSB, the chopping was continued for 5 min, the suspension then filtered through a pre-wet 20µM into a tilted 50 ml Falcon tube. After centrifugation at 400g for 5 min at 4°C, the supernatant was discarded and the nuclei resuspended in 450 µl NSB buffer. After addition of 50 µl anti-nuclei beads and careful mixing, the samples were incubated for 15 min in the cold-room. During this time, an LS column (Miltenyi Biotec) was placed in the MACS separator in the cold room and rinsed with 3 ml NSB. After 15 min, 1 ml NSB was added to the sample, and the combined amount was supplied to the column. The column was rinsed twice with 1 ml NSB, then separated from the magnet and placed in a fresh 50 ml Falcon tube. Finally, 1 ml NSB was applied to the column and the liquid pushed out using the accessory plunger. A 25 µl aliquot of the nuclei suspension was removed to determine nuclei concentration after the addition of DAPI. CUT-and TAG was performed using 500000 nuclei using the iDeal CUT&TAG kit (Diagenode) according to manufacturer's instructions and CUT&TAG-grade anti-H3K36me3 antibodies (A1845P, Diagenode). Tagmented DNA was amplified for 18 cycles using Nextera barcoding oligonucleotides provided by Diagenode (C01011035) and libraries were sequenced by the Max Planck Genome Center Cologne (approximately 10 Mio paired end reads per library)."

6.5.2 ChIP-Seq – Bioinformatics

After quality control using MultiQC (Ewels et al. 2016), the generated paired-end reads were aligned to the TAIR10 reference genome through the bwa-mem2 aligner (Vasimuddin et al. 2019). From the alignments, BigWig files for genomic tracks were generated using the "bamCoverage" function of the deepTools2 package (Ramírez et al. 2016), using the parameters "binSize" 10, "normalizeUsing" RPKM, and "extendReads" 250. The tracks were visualized using IGV developed by Thorvaldsdóttir Robinson and Mesirov (2013). Subsequently, peaks were called using epic2 (Stovner and Sætrom 2019) with bin size 100 and fragment size 180. Replicates were compared using the Irreproducible Discovery Rate (IDR) framework with a threshold of 0.01 IDR, as well as filtered against a blacklist of known artefact sites.

The remaining peaks were read into R studio and analyzed using the ChIPseeker framework (G. Yu, Wang, and He 2015). Annotation of the peaks was performed within ChIPseeker using the *A. thaliana* reference object published by Thieffry (2021). Metagene plots were created using the plotPeakProf2 function of ChIPseeker. For the Venn diagrams, the data was combined with ChIP-Seq peaks for TRBs (see 3.3: Materials and Methods) and ICU11 ChIP-Seq peaks generated in Q. Wang et al. (2025). ChIP-Seq Data was additionally analyzed using the DiffBind package (Rory Stark 2017). Using the same peaks as in the ChIPseeker analysis, differentially bound sites were determined using the standard DiffBind pipeline and subsequently annotated using the same ChIPseeker annotatePeak function and reference object as above. Afterwards, statistical analysis and Venn diagrams were generated with the software listed in 6.6.

6.6 Statistical Analysis and Graph Plotting

All statistical analysis was performed in R (R Core Team 2021) using RStudio (Posit team 2025). General data handling was aided by the following packages: dplyr (Wickham et al. 2023), readr (Wickham, Hester, and Bryan 2024), readxl (Wickham and Bryan 2024), GenomicRanges (Lawrence et al. 2013), and stringr (Wickham 2023). Heatmaps were generated using the ComplexHeatmap package (Gu, Eils, and Schlesner 2016), Venn diagrams through VennDetail (Kai Guo 2019). Statistical analysis and visualization of multi-set interaction was performed *via* SuperExactTest (Minghui Wang, Zhao, and Zhang 2015). Further statistical analysis was performed within the package ggstatsplot, developed by Patil (2021). Due to the unequal variances present in the datasets, Welch's one way ANOVA was chosen as the initial analytical function. This was paired with a subsequent Games-Howell test for pairwise comparison using multiple comparison adjustments according to Holm (1979). All remaining plots were created using ggplot2 (Wickham 2016). Lastly, plots were exported using the svglite device (Wickham et al. 2025). Model representations of complexes and TRB functions were created using BioRender.

6.7 Anti-GFP-Nanobody-based Knockouts

E. coli cultures harboring two different plasmids containing the anti-GFP nanobody under control of the p35S promotor were provided by Dr. Martina Cerise. One contained the anti-GFP nanobody as published by Ma et al. (2019), the other was modified to include a mTFP1 (a cyan fluorescent protein) fusion to the nanobody. These cultures were grown overnight at 37 °C and the plasmids extracted using NucleoSpin Plasmid Mini Kit (MACHEREY-NAGEL). The plasmids were subsequently used to transform *Agrobacterium tumefaciens* strain GV3101 pSOUP via electroporation *(*1 pulse of 2.2 kV in a 0.1 cm cuvette). The transformed *Agrobacteria* were then

used to transform the background plants listed in 6.1 using drop-dipping as laid out in 6.3. Line 7-2-8 was transformed using the regular nanobody, while line 7-4-11 was transformed with the mTFP1-fused nanobody construct.

After transgenic plants were selected using antibiotic selection on GM medium, four independent lines (two with mTFP1-fused nanobodies, two without fusions) were selected for the induction experiment. Induction was conducted *via* dexamethasone (DEX) supplement. Seeds of homozygous nanobody lines were sterilized with ethanol and plated on selective GM plates containing 10 µM DEX or mock treatment containing 0.01% DMSO. After 3 days of stratification in dark, the plates were moved into a growth cabinet with 24 h light conditions. After three weeks (21 days) three seedlings per plate were randomly selected and their roots used for live fluorescence microscopy. Image acquisition was done on a Leica SP8 confocal laser scanning microscope. Subsequent image analysis and fluorescent quantification was performed in Fiji (Schindelin et al. 2012). After verification of the successful nanobody induction, the plants were transplanted into soil and moved into the greenhouse with LD (16h) photoperiod. After transplantation, the plants were watered with tap water containing 21 mM DEX in ethanol or 0.01% ethanol three times per week. The plants were allowed to grow until seed formation. Flowering time was determined through counting of rosette leaves at time of bolting. Statistical analysis was performed in R (see 6.6).

6.8 Data Availability

All raw data (except for raw sequencing reads), scripts used in the bioinformatic analysis, data imported from cited literature, and analysis results are contained in an Annotated Research Context (ARC) hosted at DataPLANT (Weil et al. 2023).

The ARC is accessible under: https://git.nfdi4plants.org/mmendler/PhD-Thesis

7 References

Adams, S P, T P Hartman, K Y Lim, M W Chase, M D Bennett, I J Leitch, and A R Leitch. 2001. “Loss and Recovery of Arabidopsis-Type Telomere Repeat Sequences 5’-(TTTAGGG)(n)-3’ in the Evolution of a Major Radiation of Flowering Plants.” *Proceedings. Biological Sciences / the Royal Society* 268 (1476): 1541–46. https://doi.org/10.1098/rspb.2001.1726.

Almeida, Mafalda, Joseph S Bowness, and Neil Brockdorff. 2020. “The Many Faces of Polycomb Regulation by RNA.” *Current Opinion in Genetics & Development* 61 (April): 53–61. https://doi.org/10.1016/j.gde.2020.02.023.

Amiard, Simon, Léa Feit, Emmanuel Vanrobays, Lauriane Simon, Samuel Le Goff, Loriane Loizeau, Léa Wolff, et al. 2024. “The TELOMERE REPEAT BINDING Proteins TRB4 and TRB5 Function as Transcriptional Activators of PRC2-Controlled Genes to Regulate Plant Development.” *Plant Communications* 5 (7): 100890. https://doi.org/10.1016/j.xplc.2024.100890.

Arico, Denise S, Paula Beati, Diego L Wengier, and Maria Agustina Mazzella. 2021. “A Novel Strategy to Uncover Specific GO Terms/Phosphorylation Pathways in Phosphoproteomic Data in Arabidopsis Thaliana.” *BMC Plant Biology* 21 (1): 592. https://doi.org/10.1186/s12870-021-03377-9.

Ariel, Federico, Leandro Lucero, Aurelie Christ, Maria Florencia Mammarella, Teddy Jegu, Alaguraj Veluchamy, Kiruthiga Mariappan, et al. 2020. “R-Loop Mediated Trans Action of the APOLO Long Noncoding RNA.” *Molecular Cell* 77 (5): 1055-1065.e4. https://doi.org/10.1016/j.molcel.2019.12.015.

Baile, Fernando, and Myriam Calonje. 2024. “Dynamics of Polycomb Group Marks in Arabidopsis.” *Current Opinion in Plant Biology* 80 (August): 102553. https://doi.org/10.1016/j.pbi.2024.102553.

Baile, Fernando, Ángeles Gómez-Zambrano, and Myriam Calonje. 2022. “Roles of Polycomb Complexes in Regulating Gene Expression and Chromatin Structure in Plants.” *Plant Communications* 3 (1): 100267. https://doi.org/10.1016/j.xplc.2021.100267.

Baile, Fernando, Wiam Merini, Inés Hidalgo, and Myriam Calonje. 2021. “EAR Domain-Containing Transcription Factors Trigger PRC2-Mediated Chromatin Marking in Arabidopsis.” *The Plant Cell* 33 (8): 2701–15. https://doi.org/10.1093/plcell/koab139.

Barrero-Gil, Javier, Laura Bouza-Morcillo, Loreto Espinosa-Cores, Manuel Piñeiro, and José A Jarillo. 2022. “H4 Acetylation by the NuA4 Complex Is Required for Plastid Transcription and Chloroplast Biogenesis.” *Nature Plants* 8 (9): 1052–63. https://doi.org/10.1038/s41477-022-01229-4.

Barrero-Gil, Javier, Alfonso Mouriz, Raquel Piqueras, Yingnan Tian, Juan A López, Jesús Vázquez, Pedro Crevillén, José A Jarillo, and Manuel Piñeiro. 2025. “Arabidopsis

INHIBITOR OF GROWTH 2 Promotes Flowering by Regulating NuA4-Dependent H4 Acetylation Levels at FT and SOC1." *Plant Physiology* 199 (3). https://doi.org/10.1093/plphys/kiaf511.

Bäurle, Isabel, Lisa Smith, David C Baulcombe, and Caroline Dean. 2007. "Widespread Role for the Flowering-Time Regulators FCA and FPA in RNA-Mediated Chromatin Silencing." *Science* 318 (5847): 109–12. https://doi.org/10.1126/science.1146565.

Bednar, Jan, Isabel Garcia-Saez, Ramachandran Boopathi, Amber R Cutter, Gabor Papai, Anna Reymer, Sajad H Syed, et al. 2017. "Structure and Dynamics of a 197 Bp Nucleosome in Complex with Linker Histone H1." *Molecular Cell* 66 (3): 384-397.e8. https://doi.org/10.1016/j.molcel.2017.04.012.

Berr, Alexandre, Lin Xu, Juan Gao, Valérie Cognat, Andre Steinmetz, Aiwu Dong, and Wen-Hui Shen. 2009. "SET DOMAIN GROUP25 Encodes a Histone Methyltransferase and Is Involved in FLOWERING LOCUS C Activation and Repression of Flowering." *Plant Physiology* 151 (3): 1476–85. https://doi.org/10.1104/pp.109.143941.

Bieluszewski, Tomasz, Weronika Sura, Wojciech Dziegielewski, Anna Bieluszewska, Catherine Lachance, Michał Kabza, Maja Szymanska-Lejman, et al. 2022. "NuA4 and H2A.Z Control Environmental Responses and Autotrophic Growth in Arabidopsis." *Nature Communications* 13 (1): 277. https://doi.org/10.1038/s41467-021-27882-5.

Bilaud, T, C E Koering, E Binet-Brasselet, K Ancelin, A Pollice, S M Gasser, and E Gilson. 1996. "The Telobox, a Myb-Related Telomeric DNA Binding Motif Found in Proteins from Yeast, Plants and Human." *Nucleic Acids Research* 24 (7): 1294–1303. https://doi.org/10.1093/nar/24.7.1294.

Blackledge, Neil P, Anca M Farcas, Takashi Kondo, Hamish W King, Joanna F McGouran, Lars L P Hanssen, Shinsuke Ito, et al. 2014. "Variant PRC1 Complex-Dependent H2A Ubiquitylation Drives PRC2 Recruitment and Polycomb Domain Formation." *Cell* 157 (6): 1445–59. https://doi.org/10.1016/j.cell.2014.05.004.

Bloomer, Rebecca H, Claire E Hutchison, Isabel Bäurle, James Walker, Xiaofeng Fang, Pumi Perera, Christos N Velanis, et al. 2020. "The Arabidopsis Epigenetic Regulator ICU11 as an Accessory Protein of Polycomb Repressive Complex 2." *Proceedings of the National Academy of Sciences of the United States of America* 117 (28): 16660–66. https://doi.org/10.1073/pnas.1920621117.

Bouché, Frédéric, Guillaume Lobet, Pierre Tocquin, and Claire Périlleux. 2016. "FLOR-ID: An Interactive Database of Flowering-Time Gene Networks in Arabidopsis Thaliana." *Nucleic Acids Research* 44 (D1): D1167-71. https://doi.org/10.1093/nar/gkv1054.

Bratzel, Fabian, Gema López-Torrejón, Marcus Koch, Juan C Del Pozo, and Myriam Calonje. 2010. "Keeping Cell Identity in Arabidopsis Requires PRC1 RING-Finger Homologs That Catalyze H2A Monoubiquitination." *Current Biology* 20 (20): 1853–59. https://doi.org/10.1016/j.cub.2010.09.046.

Broccoli, D, A Smogorzewska, L Chong, and T de Lange. 1997. “Human Telomeres Contain Two Distinct Myb-Related Proteins, TRF1 and TRF2.” *Nature Genetics* 17 (2): 231–35. https://doi.org/10.1038/ng1097-231.

Calonje, Myriam, Rosario Sanchez, Lingjing Chen, and Z Renee Sung. 2008. “EMBRYONIC FLOWER1 Participates in Polycomb Group-Mediated AG Gene Silencing in Arabidopsis.” *The Plant Cell* 20 (2): 277–91. https://doi.org/10.1105/tpc.106.049957.

Campbell, Neil A. 2008. *Biology [8th Edition] Volume 1, Custom Edition By Campbell & Reece, and Others*. Tenth. Pearson Custom Publishing.

Campi, Mabel, Lucio D’Andrea, Julia Emiliani, and Paula Casati. 2012. “Participation of Chromatin-Remodeling Proteins in the Repair of Ultraviolet-B-Damaged DNA.” *Plant Physiology* 158 (2): 981–95. https://doi.org/10.1104/pp.111.191452.

Cao, Ru, Yu-Ichi Tsukada, and Yi Zhang. 2005. “Role of Bmi-1 and Ring1A in H2A Ubiquitylation and Hox Gene Silencing.” *Molecular Cell* 20 (6): 845–54. https://doi.org/10.1016/j.molcel.2005.12.002.

Caussinus, Emmanuel, Oguz Kanca, and Markus Affolter. 2011. “Fluorescent Fusion Protein Knockout Mediated by Anti-GFP Nanobody.” *Nature Structural & Molecular Biology* 19 (1): 117–21. https://doi.org/10.1038/nsmb.2180.

Chahtane, Hicham, Xuelei Lai, Gabrielle Tichtinsky, Philippe Rieu, Moïra Arnoux-Courseaux, Coralie Cancé, Claudius Marondedze, and François Parcy. 2023. “Flower Development in Arabidopsis.” *Methods in Molecular Biology* 2686: 3–38. https://doi.org/10.1007/978-1-0716-3299-4_1.

Chanvivattana, Yindee, Anthony Bishopp, Daniel Schubert, Christine Stock, Yong-Hwan Moon, Z Renee Sung, and Justin Goodrich. 2004. “Interaction of Polycomb-Group Proteins Controlling Flowering in Arabidopsis.” *Development* 131 (21): 5263–76. https://doi.org/10.1242/dev.01400.

Charron, Jean-Benoit F, Hang He, Axel A Elling, and Xing Wang Deng. 2009. “Dynamic Landscapes of Four Histone Modifications during Deetiolation in Arabidopsis.” *The Plant Cell* 21 (12): 3732–48. https://doi.org/10.1105/tpc.109.066845.

Cheng, Chia-Yi, Vivek Krishnakumar, Agnes P Chan, Françoise Thibaud-Nissen, Seth Schobel, and Christopher D Town. 2017. “Araport11: A Complete Reannotation of the *Arabidopsis Thaliana* Reference Genome.” *The Plant Journal* 89 (4): 789–804. https://doi.org/10.1111/tpj.13415.

Chittuluru, Johnathan R, Yuriy Chaban, Julie Monnet-Saksouk, Michael J Carrozza, Vasileia Sapountzi, William Selleck, Jiehuan Huang, et al. 2011. “Structure and Nucleosome Interaction of the Yeast NuA4 and Piccolo-NuA4 Histone Acetyltransferase Complexes.” *Nature Structural & Molecular Biology* 18 (11): 1196–1203. https://doi.org/10.1038/nsmb.2128.

Costa, Silvia, and Caroline Dean. 2019. “Storing Memories: The Distinct Phases of Polycomb-Mediated Silencing of Arabidopsis FLC.” *Biochemical Society Transactions* 47 (4): 1187–96. https://doi.org/10.1042/BST20190255.

Crevillén, Pedro, Ángeles Gómez-Zambrano, Juan A López, Jesús Vázquez, Manuel Piñeiro, and José A Jarillo. 2019. “Arabidopsis YAF9 Histone Readers Modulate Flowering Time through NuA4-Complex-Dependent H4 and H2A.Z Histone Acetylation at FLC Chromatin.” *The New Phytologist* 222 (4): 1893–1908. https://doi.org/10.1111/nph.15737.

Derkacheva, Maria, Yvonne Steinbach, Thomas Wildhaber, Iva Mozgová, Walid Mahrez, Paolo Nanni, Sylvain Bischof, Wilhelm Gruissem, and Lars Hennig. 2013. “Arabidopsis MSI1 Connects LHP1 to PRC2 Complexes.” *The EMBO Journal* 32 (14): 2073–85. https://doi.org/10.1038/emboj.2013.145.

Dreissig, Steven, Simon Schiml, Patrick Schindele, Oda Weiss, Twan Rutten, Veit Schubert, Evgeny Gladilin, Michael F Mette, Holger Puchta, and Andreas Houben. 2017. “Live-Cell CRISPR Imaging in Plants Reveals Dynamic Telomere Movements.” *The Plant Journal* 91 (4): 565–73. https://doi.org/10.1111/tpj.13601.

Duc, Céline, Alexander Sherstnev, Christian Cole, Geoffrey J Barton, and Gordon G Simpson. 2013. “Transcription Termination and Chimeric RNA Formation Controlled by Arabidopsis Thaliana FPA.” *PLoS Genetics* 9 (10): e1003867. https://doi.org/10.1371/journal.pgen.1003867.

Durek, Pawel, Robert Schmidt, Joshua L Heazlewood, Alexandra Jones, Daniel MacLean, Axel Nagel, Birgit Kersten, and Waltraud X Schulze. 2010. “PhosPhAt: The Arabidopsis Thaliana Phosphorylation Site Database. An Update.” *Nucleic Acids Research* 38 (Database issue): D828-34. https://doi.org/10.1093/nar/gkp810.

Dvorácková, Martina, Pascale Rossignol, Peter J Shaw, Olga A Koroleva, John H Doonan, and Jirí Fajkus. 2010. “AtTRB1, a Telomeric DNA-Binding Protein from Arabidopsis, Is Concentrated in the Nucleolus and Shows Highly Dynamic Association with Chromatin.” *The Plant Journal* 61 (4): 637–49. https://doi.org/10.1111/j.1365-313X.2009.04094.x.

Earley, Keith W, Molly S Shook, Brent Brower-Toland, Leslie Hicks, and Craig S Pikaard. 2007. “In Vitro Specificities of Arabidopsis Co-Activator Histone Acetyltransferases: Implications for Histone Hyperacetylation in Gene Activation.” *The Plant Journal* 52 (4): 615–26. https://doi.org/10.1111/j.1365-313X.2007.03264.x.

Espinosa-Cores, Loreto, Laura Bouza-Morcillo, Javier Barrero-Gil, Verónica Jiménez-Suárez, Ana Lázaro, Raquel Piqueras, José A Jarillo, and Manuel Piñeiro. 2020. “Insights into the Function of the Nua4 Complex in Plants.” *Frontiers in Plant Science* 11 (February): 125. https://doi.org/10.3389/fpls.2020.00125.

Ewels, Philip, Måns Magnusson, Sverker Lundin, and Max Käller. 2016. “MultiQC: Summarize Analysis Results for Multiple Tools and Samples in a Single Report.” *Bioinformatics* 32 (19): 3047–48. https://doi.org/10.1093/bioinformatics/btw354.

Feng, Suhua, and Steven E Jacobsen. 2011. “Epigenetic Modifications in Plants: An Evolutionary Perspective.” *Current Opinion in Plant Biology* 14 (2): 179–86. https://doi.org/10.1016/j.pbi.2010.12.002.

Gerhold, Christian B, and Susan M Gasser. 2014. “INO80 and SWR Complexes: Relating Structure to Function in Chromatin Remodeling.” *Trends in Cell Biology* 24 (11): 619–31. https://doi.org/10.1016/j.tcb.2014.06.004.

Gu, Zuguang, Roland Eils, and Matthias Schlesner. 2016. “Complex Heatmaps Reveal Patterns and Correlations in Multidimensional Genomic Data.” *Bioinformatics* 32 (18): 2847–49. https://doi.org/10.1093/bioinformatics/btw313.

Helmlinger, Dominique, and László Tora. 2017. “Sharing the SAGA.” *Trends in Biochemical Sciences* 42 (11): 850–61. https://doi.org/10.1016/j.tibs.2017.09.001.

Hinsch, Valerie, Samuel Adkins, Darren Manuela, and Mingli Xu. 2021. “Post-Embryonic Phase Transitions Mediated by Polycomb Repressive Complexes in Plants.” *International Journal of Molecular Sciences* 22 (14). https://doi.org/10.3390/ijms22147533.

Hofr, Ctirad, Pavla Sultesová, Michal Zimmermann, Iva Mozgová, Petra Procházková Schrumpfová, Michaela Wimmerová, and Jirí Fajkus. 2009. “Single-Myb-Histone Proteins from Arabidopsis Thaliana: A Quantitative Study of Telomere-Binding Specificity and Kinetics.” *The Biochemical Journal* 419 (1): 221–28, 2 p following 228. https://doi.org/10.1042/BJ20082195.

Hohenstatt, Mareike L, Pawel Mikulski, Olga Komarynets, Constanze Klose, Ina Kycia, Albert Jeltsch, Sara Farrona, and Daniel Schubert. 2018. “PWWP-DOMAIN INTERACTOR OF POLYCOMBS1 Interacts with Polycomb-Group Proteins and Histones and Regulates Arabidopsis Flowering and Development.” *The Plant Cell* 30 (1): 117–33. https://doi.org/10.1105/tpc.17.00117.

Holm, Sture. 1979. “A Simple Sequentially Rejective Multiple Test Procedure.” *Scandinavian Journal of Statistics* 6 (2): 65. http://www.jstor.org/stable/4615733.

Hornyik, Csaba, Lionel C Terzi, and Gordon G Simpson. 2010. “The Spen Family Protein FPA Controls Alternative Cleavage and Polyadenylation of RNA.” *Developmental Cell* 18 (2): 203–13. https://doi.org/10.1016/j.devcel.2009.12.009.

Hu, Tieqiang, Darren Manuela, Valerie Hinsch, and Mingli Xu. 2022. “PICKLE Associates with Histone Deacetylase 9 to Mediate Vegetative Phase Change in Arabidopsis.” *The New Phytologist* 235 (3): 1070–81. https://doi.org/10.1111/nph.18174.

Kai Guo, Brett McGregor. 2019. “VennDetail.” *Bioconductor*. https://doi.org/10.18129/b9.bioc.venndetail.

Kalb, Reinhard, Sebastian Latwiel, H Irem Baymaz, Pascal W T C Jansen, Christoph W Müller, Michiel Vermeulen, and Jürg Müller. 2014. “Histone H2A Monoubiquitination Promotes Histone H3 Methylation in Polycomb Repression.” *Nature Structural & Molecular Biology* 21 (6): 569–71. https://doi.org/10.1038/nsmb.2833.

Karamysheva, Zemfira N, Yulia V Surovtseva, Laurent Vespa, Eugene V Shakirov, and Dorothy E Shippen. 2004. “A C-Terminal Myb Extension Domain Defines a Novel Family of Double-Strand Telomeric DNA-Binding Proteins in Arabidopsis.” *The Journal of Biological Chemistry* 279 (46): 47799–807. https://doi.org/10.1074/jbc.M407938200.

Kazda, Anita, Barbara Zellinger, Max Rössler, Elisa Derboven, Branislav Kusenda, and Karel Riha. 2012. “Chromosome End Protection by Blunt-Ended Telomeres.” *Genes & Development* 26 (15): 1703–13. https://doi.org/10.1101/gad.194944.112.

Kim, Jeongsik, Jin Hee Kim, Eric J Richards, Kyung Min Chung, and Hye Ryun Woo. 2014. “Arabidopsis VIM Proteins Regulate Epigenetic Silencing by Modulating DNA Methylation and Histone Modification in Cooperation with MET1.” *Molecular Plant* 7 (9): 1470–85. https://doi.org/10.1093/mp/ssu079.

Knutson, Bruce A, and Steven Hahn. 2011. “Domains of Tra1 Important for Activator Recruitment and Transcription Coactivator Functions of SAGA and NuA4 Complexes.” *Molecular and Cellular Biology* 31 (4): 818–31. https://doi.org/10.1128/MCB.00687-10.

Kralemann, Lejon E M, Shujing Liu, Minerva S Trejo-Arellano, Rafael Muñoz-Viana, Claudia Köhler, and Lars Hennig. 2020. “Removal of H2Aub1 by Ubiquitin-Specific Proteases 12 and 13 Is Required for Stable Polycomb-Mediated Gene Repression in Arabidopsis.” *Genome Biology* 21 (1): 144. https://doi.org/10.1186/s13059-020-02062-8.

Krause, Kristin, and Franziska Turck. 2018. “Plant H3K27me3 Has Finally Found Its Readers.” *Nature Genetics* 50 (9): 1206–8. https://doi.org/10.1038/s41588-018-0201-1.

Krause, Kristin. 2019. “The Role of TRB Proteins and Telobox Cis-Elements in Gene Regulation.”

Kuchar, Milan, and Jirí Fajkus. 2004. “Interactions of Putative Telomere-Binding Proteins in Arabidopsis Thaliana: Identification of Functional TRF2 Homolog in Plants.” *FEBS Letters* 578 (3): 311–15. https://doi.org/10.1016/j.febslet.2004.11.021.

Kusová, Alžbeta, Marcela Holá, Ivana Goffová Petrová, Jiří Rudolf, Dagmar Zachová, Jan Skalák, Jan Hejátko, et al. 2025. “TRB Proteins in Moss Reveal Their Evolutionarily

Conserved Roles in Plant Development and Telomere Maintenance." *The Plant Journal* 124 (3): e70574. https://doi.org/10.1111/tpj.70574.

Kusová, Alžbeta, Lenka Steinbachová, Tereza Přerovská, Lenka Záveská Drábková, Jan Paleček, Ahamed Khan, Gabriela Rigóová, et al. 2023. "Completing the TRB Family: Newly Characterized Members Show Ancient Evolutionary Origins and Distinct Localization, yet Similar Interactions." *Plant Molecular Biology* 112 (1–2): 61–83. https://doi.org/10.1007/s11103-023-01348-2.

Lagarou, Anna, Adone Mohd-Sarip, Yuri M Moshkin, Gillian E Chalkley, Karel Bezstarosti, Jeroen A A Demmers, and C Peter Verrijzer. 2008. "DKDM2 Couples Histone H2A Ubiquitylation to Histone H3 Demethylation during Polycomb Group Silencing." *Genes & Development* 22 (20): 2799–2810. https://doi.org/10.1101/gad.484208.

Lange, Titia de. 2005. "Shelterin: The Protein Complex That Shapes and Safeguards Human Telomeres." *Genes & Development* 19 (18): 2100–2110. https://doi.org/10.1101/gad.1346005.

Latrasse, David, Moussa Benhamed, Yves Henry, Séverine Domenichini, Wanhui Kim, Dao-Xiu Zhou, and Marianne Delarue. 2008. "The MYST Histone Acetyltransferases Are Essential for Gametophyte Development in Arabidopsis." *BMC Plant Biology* 8 (November): 121. https://doi.org/10.1186/1471-2229-8-121.

Lawrence, Michael, Wolfgang Huber, Hervé Pagès, Patrick Aboyoun, Marc Carlson, Robert Gentleman, Martin T Morgan, and Vincent J Carey. 2013. "Software for Computing and Annotating Genomic Ranges." *PLoS Computational Biology* 9 (8): e1003118. https://doi.org/10.1371/journal.pcbi.1003118.

Lee, Won Kyung, and Myeon Haeng Cho. 2016. "Telomere-Binding Protein Regulates the Chromosome Ends through the Interaction with Histone Deacetylases in Arabidopsis Thaliana." *Nucleic Acids Research* 44 (10): 4610–24. https://doi.org/10.1093/nar/gkw067.

Lee, Won Kyung, Ji-Hye Yun, Weontae Lee, and Myeon Haeng Cho. 2012. "DNA-Binding Domain of AtTRB2 Reveals Unique Features of a Single Myb Histone Protein Family That Binds to Both Arabidopsis- and Human-Type Telomeric DNA Sequences." *Molecular Plant* 5 (6): 1406–8. https://doi.org/10.1093/mp/sss063.

Lee, Woo Yong, Daeyoup Lee, Won-Il Chung, and Chang Seob Kwon. 2009. "Arabidopsis ING and Alfin1-like Protein Families Localize to the Nucleus and Bind to H3K4me3/2 via Plant Homeodomain Fingers." *The Plant Journal* 58 (3): 511–24. https://doi.org/10.1111/j.1365-313X.2009.03795.x.

Lim, Mi-Hye, Joonki Kim, Youn-Sung Kim, Kyung-Sook Chung, Yeon-Hee Seo, Ilha Lee, Jungmook Kim, Choo Bong Hong, Hie-Joon Kim, and Chung-Mo Park. 2004. "A New Arabidopsis Gene, FLK, Encodes an RNA Binding Protein with K Homology Motifs and Regulates Flowering Time via FLOWERING LOCUS C." *The Plant Cell* 16 (3): 731–40. https://doi.org/10.1105/tpc.019331.

Liu, Boyu, Alexandre Berr, Cheng Chang, Chunlin Liu, Wen-Hui Shen, and Ying Ruan. 2016. “Interplay of the Histone Methyltransferases SDG8 and SDG26 in the Regulation of Transcription and Plant Flowering and Development.” *Biochimica et Biophysica Acta* 1859 (4): 581–90. https://doi.org/10.1016/j.bbagrm.2016.02.003.

Liu, Hao, Yuduan Ding, Yanqing Zhou, Wenqi Jin, Kabin Xie, and Ling-Ling Chen. 2017. “CRISPR-P 2.0: An Improved CRISPR-Cas9 Tool for Genome Editing in Plants.” *Molecular Plant* 10 (3): 530–32. https://doi.org/10.1016/j.molp.2017.01.003.

Liu, Shiming, Yu Yu, Ying Ruan, Denise Meyer, Michel Wolff, Lin Xu, Ning Wang, Andre Steinmetz, and Wen-Hui Shen. 2007. “Plant SET- and RING-Associated Domain Proteins in Heterochromatinization.” *The Plant Journal* 52 (5): 914–26. https://doi.org/10.1111/j.1365-313X.2007.03286.x.

Liu, Yue, Tian Tian, Kang Zhang, Qi You, Hengyu Yan, Nannan Zhao, Xin Yi, Wenying Xu, and Zhen Su. 2018. “PCSD: A Plant Chromatin State Database.” *Nucleic Acids Research* 46 (D1): D1157–67. https://doi.org/10.1093/nar/gkx919.

Li, Zicong, Xing Fu, Yizhong Wang, Renyi Liu, and Yuehui He. 2018. “Polycomb-Mediated Gene Silencing by the BAH-EMF1 Complex in Plants.” *Nature Genetics* 50 (9): 1254–61. https://doi.org/10.1038/s41588-018-0190-0.

Love, Michael I, Wolfgang Huber, and Simon Anders. 2014. “Moderated Estimation of Fold Change and Dispersion for RNA-Seq Data with DESeq2.” *Genome Biology* 15 (12): 550. https://doi.org/10.1186/s13059-014-0550-8.

Love, Michael I, Charlotte Soneson, Peter F Hickey, Lisa K Johnson, N Tessa Pierce, Lori Shepherd, Martin Morgan, and Rob Patro. 2020. “Tximeta: Reference Sequence Checksums for Provenance Identification in RNA-Seq.” *PLoS Computational Biology* 16 (2): e1007664. https://doi.org/10.1371/journal.pcbi.1007664.

Luo, Yu-Xi, Xiao-Mei Hou, Cui-Jun Zhang, Lian-Mei Tan, Chang-Rong Shao, Rong-Nan Lin, Yin-Na Su, et al. 2020. “A Plant-Specific SWR1 Chromatin-Remodeling Complex Couples Histone H2A.Z Deposition with Nucleosome Sliding.” *The EMBO Journal* 39 (7): e102008. https://doi.org/10.15252/embj.2019102008.

Lupas, Andrei N, and Markus Gruber. 2005. “The Structure of Alpha-Helical Coiled Coils.” *Advances in Protein Chemistry* 70: 37–78. https://doi.org/10.1016/S0065-3233(05)70003-6.

Ma, Yanfei, Andrej Miotk, Zoran Šutiković, Olga Ermakova, Christian Wenzl, Anna Medzihradszky, Christophe Gaillochet, et al. 2019. “WUSCHEL Acts as an Auxin Response Rheostat to Maintain Apical Stem Cells in Arabidopsis.” *Nature Communications* 10 (1): 5093. https://doi.org/10.1038/s41467-019-13074-9.

Madrid, Eva, John W Chandler, and George Coupland. 2021. “Gene Regulatory Networks Controlled by FLOWERING LOCUS C That Confer Variation in Seasonal

Flowering and Life History." *Journal of Experimental Botany* 72 (1): 4–14. https://doi.org/10.1093/jxb/eraa216.

Marian, Calin O, Stefano J Bordoli, Marion Goltz, Rachel A Santarella, Leisa P Jackson, Olga Danilevskaya, Michael Beckstette, Robert Meeley, and Hank W Bass. 2003. "The Maize Single Myb Histone 1 Gene, Smh1, Belongs to a Novel Gene Family and Encodes a Protein That Binds Telomere DNA Repeats in Vitro." *Plant Physiology* 133 (3): 1336–50. https://doi.org/10.1104/pp.103.026856.

Mateo-Bonmatí, Eduardo, David Esteve-Bruna, Lucía Juan-Vicente, Riad Nadi, Héctor Candela, Francisca María Lozano, María Rosa Ponce, José Manuel Pérez-Pérez, and José Luis Micol. 2018. "INCURVATA11 and CUPULIFORMIS2 Are Redundant Genes That Encode Epigenetic Machinery Components in Arabidopsis." *The Plant Cell* 30 (7): 1596–1616. https://doi.org/10.1105/tpc.18.00300.

Merini, Wiam, and Myriam Calonje. 2015. "PRC1 Is Taking the Lead in PcG Repression." *The Plant Journal* 83 (1): 110–20. https://doi.org/10.1111/tpj.12818.

Merini, Wiam, Francisco J Romero-Campero, Angeles Gomez-Zambrano, Yue Zhou, Franziska Turck, and Myriam Calonje. 2017. "The Arabidopsis Polycomb Repressive Complex 1 (PRC1) Components AtBMI1A, B, and C Impact Gene Networks throughout All Stages of Plant Development." *Plant Physiology* 173 (1): 627–41. https://doi.org/10.1104/pp.16.01259.

Michaels, S D, and R M Amasino. 2001. "Loss of FLOWERING LOCUS C Activity Eliminates the Late-Flowering Phenotype of FRIGIDA and Autonomous Pathway Mutations but Not Responsiveness to Vernalization." *The Plant Cell* 13 (4): 935–41. https://doi.org/10.1105/tpc.13.4.935.

Mozgova, Iva, Claudia Köhler, and Lars Hennig. 2015. "Keeping the Gate Closed: Functions of the Polycomb Repressive Complex PRC2 in Development." *The Plant Journal* 83 (1): 121–32. https://doi.org/10.1111/tpj.12828.

Mozgová, Iva, Petra Procházková Schrumpfová, Ctirad Hofr, and Jirí Fajkus. 2008. "Functional Characterization of Domains in AtTRB1, a Putative Telomere-Binding Protein in Arabidopsis Thaliana." *Phytochemistry* 69 (9): 1814–19. https://doi.org/10.1016/j.phytochem.2008.04.001.

Ning, Yong-Qiang, Ze-Yang Ma, Huan-Wei Huang, Huixian Mo, Ting-ting Zhao, Lin Li, Tao Cai, She Chen, Ligeng Ma, and Xin-Jian He. 2015. "Two Novel NAC Transcription Factors Regulate Gene Expression and Flowering Time by Associating with the Histone Demethylase JMJ14." *Nucleic Acids Research* 43 (3): 1469–84. https://doi.org/10.1093/nar/gku1382.

Ogata, K, H Hojo, S Aimoto, T Nakai, H Nakamura, A Sarai, S Ishii, and Y Nishimura. 1992. "Solution Structure of a DNA-Binding Unit of Myb: A Helix-Turn-Helix-Related Motif with Conserved Tryptophans Forming a Hydrophobic Core." *Proceedings of the*

National Academy of Sciences of the United States of America 89 (14): 6428–32. https://doi.org/10.1073/pnas.89.14.6428.

Ohno, Susumu. 1970. *Evolution by Gene Duplication*. Berlin, Heidelberg: Springer Berlin Heidelberg. https://doi.org/10.1007/978-3-642-86659-3.

Patil, Indrajeet. 2021. "Visualizations with Statistical Details: The 'ggstatsplot' Approach." *The Journal of Open Source Software* 6 (61): 3167. https://doi.org/10.21105/joss.03167.

Patro, Rob, Geet Duggal, Michael I Love, Rafael A Irizarry, and Carl Kingsford. 2017. "Salmon Provides Fast and Bias-Aware Quantification of Transcript Expression." *Nature Methods* 14 (4): 417–19. https://doi.org/10.1038/nmeth.4197.

Peng, Ling, Longlong Wang, Yingpei Zhang, Aiwu Dong, Wen-Hui Shen, and Ying Huang. 2018. "Structural Analysis of the Arabidopsis AL2-PAL and PRC1 Complex Provides Mechanistic Insight into Active-to-Repressive Chromatin State Switch." *Journal of Molecular Biology* 430 (21): 4245–59. https://doi.org/10.1016/j.jmb.2018.08.021.

Peng, Maolin, Zepeng Li, Nana Zhou, Mengmeng Ma, Yupei Jiang, Aiwu Dong, Wen-Hui Shen, and Lin Li. 2018. "Linking PHYTOCHROME-INTERACTING FACTOR to Histone Modification in Plant Shade Avoidance." *Plant Physiology* 176 (2): 1341–51. https://doi.org/10.1104/pp.17.01189.

Pikaard, Craig S, and Ortrun Mittelsten Scheid. 2014. "Epigenetic Regulation in Plants." *Cold Spring Harbor Perspectives in Biology* 6 (12): a019315. https://doi.org/10.1101/cshperspect.a019315.

Posit team. 2025. *RStudio: Integrated Development Environment for R* (version 2025.9.1.401). Computer software. Boston, MA: Posit Software, PBC.

Potter, Bastiaan de, Maximilian W D Raas, Michael F Seidl, C Peter Verrijzer, and Berend Snel. 2023. "Uncoupled Evolution of the Polycomb System and Deep Origin of Non-Canonical PRC1." *Communications Biology* 6 (1): 1144. https://doi.org/10.1038/s42003-023-05501-x.

Pu, Li, and Zinmay Renee Sung. 2015. "PcG and TrxG in Plants - Friends or Foes." *Trends in Genetics* 31 (5): 252–62. https://doi.org/10.1016/j.tig.2015.03.004.

Qüesta, Julia I, Jie Song, Nuno Geraldo, Hailong An, and Caroline Dean. 2016. "Arabidopsis Transcriptional Repressor VAL1 Triggers Polycomb Silencing at FLC during Vernalization." *Science* 353 (6298): 485–88. https://doi.org/10.1126/science.aaf7354.

Radjacommare, Ramalingam, Shih-Yun Lin, Raju Usharani, Wen-Dar Lin, Guang-Yuh Jauh, Wolfgang Schmidt, and Hongyong Fu. 2023. "The Arabidopsis Deubiquitylase OTU5 Suppresses Flowering by Histone Modification-Mediated Activation of the Major

Flowering Repressors FLC, MAF4, and MAF5." *International Journal of Molecular Sciences* 24 (7). https://doi.org/10.3390/ijms24076176.

Ramakrishnan, V, J T Finch, V Graziano, P L Lee, and R M Sweet. 1993. "Crystal Structure of Globular Domain of Histone H5 and Its Implications for Nucleosome Binding." *Nature* 362 (6417): 219–23. https://doi.org/10.1038/362219a0.

R Core Team. 2021. *R: A Language and Environment for Statistical Computing* (version 4.5.0). Computer software. Vienna, Austria: R Foundation for Statistical Computing.

Ramírez, Fidel, Devon P Ryan, Björn Grüning, Vivek Bhardwaj, Fabian Kilpert, Andreas S Richter, Steffen Heyne, Friederike Dündar, and Thomas Manke. 2016. "DeepTools2: A next Generation Web Server for Deep-Sequencing Data Analysis." *Nucleic Acids Research* 44 (W1): W160-5. https://doi.org/10.1093/nar/gkw257.

Richards, E J, and F M Ausubel. 1988. "Isolation of a Higher Eukaryotic Telomere from Arabidopsis Thaliana." *Cell* 53 (1): 127–36. https://doi.org/10.1016/0092-8674(88)90494-1.

Richter, René, Atsuko Kinoshita, Coral Vincent, Rafael Martinez-Gallegos, He Gao, Annabel D van Driel, Youbong Hyun, Julieta L Mateos, and George Coupland. 2019. "Floral Regulators FLC and SOC1 Directly Regulate Expression of the B3-Type Transcription Factor TARGET OF FLC AND SVP 1 at the Arabidopsis Shoot Apex via Antagonistic Chromatin Modifications." *PLoS Genetics* 15 (4): e1008065. https://doi.org/10.1371/journal.pgen.1008065.

Rory Stark, Gord Brown. 2017. "DiffBind." *Bioconductor*. https://doi.org/10.18129/b9.bioc.diffbind.

Rosinski, J A, and W R Atchley. 1998. "Molecular Evolution of the Myb Family of Transcription Factors: Evidence for Polyphyletic Origin." *Journal of Molecular Evolution* 46 (1): 74–83. https://doi.org/10.1007/pl00006285.

Schindelin, Johannes, Ignacio Arganda-Carreras, Erwin Frise, Verena Kaynig, Mark Longair, Tobias Pietzsch, Stephan Preibisch, et al. 2012. "Fiji: An Open-Source Platform for Biological-Image Analysis." *Nature Methods* 9 (7): 676–82. https://doi.org/10.1038/nmeth.2019.

Schomburg, Fritz M., David A. Patton, David W. Meinke, and Richard M. Amasino. 2001. "*FPA* , a Gene Involved in Floral Induction in Arabidopsis, Encodes a Protein Containing RNA-Recognition Motifs." *The Plant Cell* 13 (6): 1427–36. https://doi.org/10.1105/TPC.010017.

Schrumpfová, Petra, Milan Kuchar, Gabriela Miková, Lenka Skrísovská, Tatiana Kubicárová, and Jirí Fajkus. 2004. "Characterization of Two Arabidopsis Thaliana Myb-like Proteins Showing Affinity to Telomeric DNA Sequence." *Genome* 47 (2): 316–24. https://doi.org/10.1139/g03-136.

Schrumpfová, Petra Procházková, Milan Kuchar, Jan Palecek, and Jirí Fajkus. 2008. "Mapping of Interaction Domains of Putative Telomere-Binding Proteins AtTRB1 and AtPOT1b from Arabidopsis Thaliana." *FEBS Letters* 582 (10): 1400–1406. https://doi.org/10.1016/j.febslet.2008.03.034.

Schrumpfová, Petra Procházková, Ivona Vychodilová, Martina Dvořáčková, Jana Majerská, Ladislav Dokládal, Sárka Schořová, and Jiří Fajkus. 2014. "Telomere Repeat Binding Proteins Are Functional Components of Arabidopsis Telomeres and Interact with Telomerase." *The Plant Journal* 77 (5): 770–81. https://doi.org/10.1111/tpj.12428.

Schrumpfová, Petra Procházková, Ivona Vychodilová, Jan Hapala, Šárka Schořová, Vojtěch Dvořáček, and Jiří Fajkus. 2016. "Telomere Binding Protein TRB1 Is Associated with Promoters of Translation Machinery Genes in Vivo." *Plant Molecular Biology* 90 (1–2): 189–206. https://doi.org/10.1007/s11103-015-0409-8.

Shafiq, Sarfraz, Alexandre Berr, and Wen-Hui Shen. 2014. "Combinatorial Functions of Diverse Histone Methylations in Arabidopsis Thaliana Flowering Time Regulation." *The New Phytologist* 201 (1): 312–22. https://doi.org/10.1111/nph.12493.

Shakirov, Eugene V, Yulia V Surovtseva, Nathan Osbun, and Dorothy E Shippen. 2005. "The Arabidopsis Pot1 and Pot2 Proteins Function in Telomere Length Homeostasis and Chromosome End Protection." *Molecular and Cellular Biology* 25 (17): 7725–33. https://doi.org/10.1128/MCB.25.17.7725-7733.2005.

Shannon, Paul, Andrew Markiel, Owen Ozier, Nitin S Baliga, Jonathan T Wang, Daniel Ramage, Nada Amin, Benno Schwikowski, and Trey Ideker. 2003. "Cytoscape: A Software Environment for Integrated Models of Biomolecular Interaction Networks." *Genome Research* 13 (11): 2498–2504. https://doi.org/10.1101/gr.1239303.

Shao, Z, F Raible, R Mollaaghababa, J R Guyon, C T Wu, W Bender, and R E Kingston. 1999. "Stabilization of Chromatin Structure by PRC1, a Polycomb Complex." *Cell* 98 (1): 37–46. https://doi.org/10.1016/S0092-8674(00)80604-2.

Shook, Molly S, and Eric J Richards. 2014. "VIM Proteins Regulate Transcription Exclusively through the MET1 Cytosine Methylation Pathway." *Epigenetics* 9 (7): 980–86. https://doi.org/10.4161/epi.28906.

Stovner, Endre Bakken, and Pål Sætrom. 2019. "Epic2 Efficiently Finds Diffuse Domains in ChIP-Seq Data." *Bioinformatics* 35 (21): 4392–93. https://doi.org/10.1093/bioinformatics/btz232.

Stuttmann, Johannes, Karen Barthel, Patrick Martin, Jana Ordon, Jessica L Erickson, Rosalie Herr, Filiz Ferik, et al. 2021. "Highly Efficient Multiplex Editing: One-Shot Generation of 8× Nicotiana Benthamiana and 12× Arabidopsis Mutants." *The Plant Journal* 106 (1): 8–22. https://doi.org/10.1111/tpj.15197.

Suzuki, Masaharu, Heidi H-Y Wang, and Donald R McCarty. 2007. “Repression of the LEAFY COTYLEDON 1/B3 Regulatory Network in Plant Embryo Development by VP1/ABSCISIC ACID INSENSITIVE 3-LIKE B3 Genes.” *Plant Physiology* 143 (2): 902–11. https://doi.org/10.1104/pp.106.092320.

Tamada, Yosuke, Jae-Young Yun, Seung Chul Woo, and Richard M Amasino. 2009. “ARABIDOPSIS TRITHORAX-RELATED7 Is Required for Methylation of Lysine 4 of Histone H3 and for Transcriptional Activation of FLOWERING LOCUS C.” *The Plant Cell* 21 (10): 3257–69. https://doi.org/10.1105/tpc.109.070060.

Tan, Lian-Mei, Cui-Jun Zhang, Xiao-Mei Hou, Chang-Rong Shao, Yu-Jia Lu, Jin-Xing Zhou, Yong-Qiang Li, Lin Li, She Chen, and Xin-Jian He. 2018. “The PEAT Protein Complexes Are Required for Histone Deacetylation and Heterochromatin Silencing.” *The EMBO Journal* 37 (19). https://doi.org/10.15252/embj.201798770.

Teano, Gianluca, Lorenzo Concia, Léa Wolff, Léopold Carron, Ivona Biocanin, Kateřina Adamusová, Miloslava Fojtová, et al. 2023. “Histone H1 Protects Telomeric Repeats from H3K27me3 Invasion in Arabidopsis.” *Cell Reports* 42 (8): 112894. https://doi.org/10.1016/j.celrep.2023.112894.

Thieffry, Axel. 2021. “TxDb.Athaliana.BioMart.Plantsmart51.” *Bioconductor*. https://doi.org/10.18129/b9.bioc.txdb.athaliana.biomart.plantsmart51.

Thorvaldsdóttir, Helga, James T Robinson, and Jill P Mesirov. 2013. “Integrative Genomics Viewer (IGV): High-Performance Genomics Data Visualization and Exploration.” *Briefings in Bioinformatics* 14 (2): 178–92. https://doi.org/10.1093/bib/bbs017.

Tresas, Theodoros, Ioannis Isaioglou, Andreas Roussis, and Kosmas Haralampidis. 2025. “A Brief Overview of the Epigenetic Regulatory Mechanisms in Plants.” *International Journal of Molecular Sciences* 26 (10). https://doi.org/10.3390/ijms26104700.

Tsuzuki, Masayuki, and Andrzej T Wierzbicki. 2018. “Buried in PEAT-Discovery of a New Silencing Complex with Opposing Activities.” *The EMBO Journal* 37 (19). https://doi.org/10.15252/embj.2018100573.

Umezawa, Taishi, Naoyuki Sugiyama, Fuminori Takahashi, Jeffrey C Anderson, Yasushi Ishihama, Scott C Peck, and Kazuo Shinozaki. 2013. “Genetics and Phosphoproteomics Reveal a Protein Phosphorylation Network in the Abscisic Acid Signaling Pathway in Arabidopsis Thaliana.” *Science Signaling* 6 (270): rs8. https://doi.org/10.1126/scisignal.2003509.

Vaquero-Sedas, María I, Chongyuan Luo, and Miguel A Vega-Palas. 2012. “Analysis of the Epigenetic Status of Telomeres by Using ChIP-Seq Data.” *Nucleic Acids Research* 40 (21): e163. https://doi.org/10.1093/nar/gks730.

Vasimuddin, Md., Sanchit Misra, Heng Li, and Srinivas Aluru. 2019. “Efficient Architecture-Aware Acceleration of BWA-MEM for Multicore Systems.” In *2019 IEEE International Parallel and Distributed Processing Symposium (IPDPS)*, 314–24. IEEE. https://doi.org/10.1109/IPDPS.2019.00041.

Wang, Duolin, Dongpeng Liu, Jiakang Yuchi, Fei He, Yuexu Jiang, Siteng Cai, Jingyi Li, and Dong Xu. 2020. “MusiteDeep: A Deep-Learning Based Webserver for Protein Post-Translational Modification Site Prediction and Visualization.” *Nucleic Acids Research* 48 (W1): W140–46. https://doi.org/10.1093/nar/gkaa275.

Wang, Liangjun, J Lesley Brown, Ru Cao, Yi Zhang, Judith A Kassis, and Richard S Jones. 2004. “Hierarchical Recruitment of Polycomb Group Silencing Complexes.” *Molecular Cell* 14 (5): 637–46. https://doi.org/10.1016/j.molcel.2004.05.009.

Wang, Ming, Zhenhui Zhong, Javier Gallego-Bartolomé, Suhua Feng, Yuan-Hsin Shih, Mukun Liu, Jessica Zhou, et al. 2023a. “Arabidopsis TRB Proteins Function in H3K4me3 Demethylation by Recruiting JMJ14.” *BioRxiv*, January. https://doi.org/10.1101/2023.01.10.523456.

———. 2023b. “Arabidopsis TRB Proteins Function in H3K4me3 Demethylation by Recruiting JMJ14.” *Nature Communications* 14 (1): 1736. https://doi.org/10.1038/s41467-023-37263-9.

Wang, Minghui, Yongzhong Zhao, and Bin Zhang. 2015. “Efficient Test and Visualization of Multi-Set Intersections.” *Scientific Reports* 5 (November): 16923. https://doi.org/10.1038/srep16923.

Wang, Qi, Dan-Yang Yuan, Yu-Jia Lu, Xin Wang, Hao Zheng, Lin Li, She Chen, and Xin-Jian He. 2025. “Arabidopsis TRB Proteins Form Two Closely Related Complexes to Mediate H3k4me3 Demethylation and Transcriptional Repression.” *Advanced Science (Weinheim, Baden-Wurttemberg, Germany)*, October, e03420. https://doi.org/10.1002/advs.202503420.

Wang, Xin, Zhen-Zhen Liu, Dan-Yang Yuan, Yu-Jia Lu, Lin Li, She Chen, and Xin-Jian He. 2025. “Nutrient-Driven TOR Signalling Controls a Chromatin-Associated Complex for Orchestrating Plant Growth and Stress Tolerance.” *Nature Plants*, September. https://doi.org/10.1038/s41477-025-02107-5.

Wang, Yizhong, Xiaofeng Gu, Wenya Yuan, Robert J Schmitz, and Yuehui He. 2014. “Photoperiodic Control of the Floral Transition through a Distinct Polycomb Repressive Complex.” *Developmental Cell* 28 (6): 727–36. https://doi.org/10.1016/j.devcel.2014.01.029.

Weil, Heinrich Lukas, Kevin Schneider, Marcel Tschöpe, Jonathan Bauer, Oliver Maus, Kevin Frey, Dominik Brilhaus, et al. 2023. “PLANTdataHUB: A Collaborative Platform for Continuous FAIR Data Sharing in Plant Research.” *The Plant Journal* 116 (4): 974–88. https://doi.org/10.1111/tpj.16474.

Wickham, Hadley, and Jennifer Bryan. 2024. “Readxl: Read Excel Files.” *The R Foundation*. https://doi.org/10.32614/cran.package.readxl.

Wickham, Hadley, Romain François, Lionel Henry, Kirill Müller, and Davis Vaughan. 2023. “Dplyr: A Grammar of Data Manipulation.” *The R Foundation*. https://doi.org/10.32614/cran.package.dplyr.

Wickham, Hadley, Lionel Henry, Thomas Lin Pedersen, T Jake Luciani, Matthieu Decorde, and Vaudor Lise. 2025. *Svglite: An “SVG” Graphics Device* (version 2.2.1.9000). Computer software. R package.

Wickham, Hadley, Jim Hester, and Jennifer Bryan. 2024. “Readr: Read Rectangular Text Data.” *The R Foundation*. https://doi.org/10.32614/cran.package.readr.

Wickham, Hadley. 2016. *Ggplot2 Elegant Graphics for Data Analysis*. 2nd ed. Cham: Springer.

———. 2023. *Stringr: Simple, Consistent Wrappers for Common String Operations* (version 1.5.1). Computer software. R package version 1.5.1, https://github.com/tidyverse/stringr.

Willbanks, Amber, Meghan Leary, Molly Greenshields, Camila Tyminski, Sarah Heerboth, Karolina Lapinska, Kathryn Haskins, and Sibaji Sarkar. 2016. “The Evolution of Epigenetics: From Prokaryotes to Humans and Its Biological Consequences.” *Genetics & Epigenetics* 8 (August): 25–36. https://doi.org/10.4137/GEG.S31863.

Woo, Hye Ryun, Travis A Dittmer, and Eric J Richards. 2008. “Three SRA-Domain Methylcytosine-Binding Proteins Cooperate to Maintain Global CpG Methylation and Epigenetic Silencing in Arabidopsis.” *PLoS Genetics* 4 (8): e1000156. https://doi.org/10.1371/journal.pgen.1000156.

Woo, Hye Ryun, Olga Pontes, Craig S Pikaard, and Eric J Richards. 2007. “VIM1, a Methylcytosine-Binding Protein Required for Centromeric Heterochromatinization.” *Genes & Development* 21 (3): 267–77. https://doi.org/10.1101/gad.1512007.

Wu, Chan-Juan, Zhen-Zhen Liu, Long Wei, Jin-Xing Zhou, Xue-Wei Cai, Yin-Na Su, Lin Li, She Chen, and Xin-Jian He. 2021. “Three Functionally Redundant Plant-Specific Paralogs Are Core Subunits of the SAGA Histone Acetyltransferase Complex in Arabidopsis.” *Molecular Plant* 14 (7): 1071–87. https://doi.org/10.1016/j.molp.2021.03.014.

Xiao, Jun, Run Jin, Xiang Yu, Max Shen, John D Wagner, Armaan Pai, Claire Song, et al. 2017. “Cis and Trans Determinants of Epigenetic Silencing by Polycomb Repressive Complex 2 in Arabidopsis.” *Nature Genetics* 49 (10): 1546–52. https://doi.org/10.1038/ng.3937.

Xiao, Jun, and Doris Wagner. 2015. “Polycomb Repression in the Regulation of Growth and Development in Arabidopsis.” *Current Opinion in Plant Biology* 23 (February): 15–24. https://doi.org/10.1016/j.pbi.2014.10.003.

Xu, Lin, and Wen-Hui Shen. 2008. “Polycomb Silencing of KNOX Genes Confines Shoot Stem Cell Niches in Arabidopsis.” *Current Biology* 18 (24): 1966–71. https://doi.org/10.1016/j.cub.2008.11.019.

Xu, Xin, and Xin-Jian He. 2025. “Plant Histone Acetyltransferase Complexes: Conserved and Plant-Specific Characteristics.” *Current Opinion in Plant Biology* 88 (December): 102815. https://doi.org/10.1016/j.pbi.2025.102815.

Yang, Chao, Fabian Bratzel, Nora Hohmann, Marcus Koch, Franziska Turck, and Myriam Calonje. 2013. “VAL- and AtBMI1-Mediated H2Aub Initiate the Switch from Embryonic to Postgerminative Growth in Arabidopsis.” *Current Biology* 23 (14): 1324–29. https://doi.org/10.1016/j.cub.2013.05.050.

Yang, Zhenlin, Shuiming Qian, Ray N Scheid, Li Lu, Xiangsong Chen, Rui Liu, Xuan Du, et al. 2018. “EBS Is a Bivalent Histone Reader That Regulates Floral Phase Transition in Arabidopsis.” *Nature Genetics* 50 (9): 1247–53. https://doi.org/10.1038/s41588-018-0187-8.

Yao, Qiuming, Huangyi Ge, Shangquan Wu, Ning Zhang, Wei Chen, Chunhui Xu, Jianjiong Gao, Jay J Thelen, and Dong Xu. 2014. “P^{3}DB 3.0: From Plant Phosphorylation Sites to Protein Networks.” *Nucleic Acids Research* 42 (Database issue): D1206-13. https://doi.org/10.1093/nar/gkt1135.

Yin, Xiaochang, Francisco J Romero-Campero, Pedro de Los Reyes, Peng Yan, Jing Yang, Guangmei Tian, XiaoZeng Yang, et al. 2021. “H2AK121ub in Arabidopsis Associates with a Less Accessible Chromatin State at Transcriptional Regulation Hotspots.” *Nature Communications* 12 (1): 315. https://doi.org/10.1038/s41467-020-20614-1.

Yuan, Wenya, Xiao Luo, Zicong Li, Wannian Yang, Yizhong Wang, Rui Liu, Jiamu Du, and Yuehui He. 2016. “A Cis Cold Memory Element and a Trans Epigenome Reader Mediate Polycomb Silencing of FLC by Vernalization in Arabidopsis.” *Nature Genetics* 48 (12): 1527–34. https://doi.org/10.1038/ng.3712.

Yun, Ji-Hye, Won Kyung Lee, Heeyoun Kim, Eunhee Kim, Chaejoon Cheong, Myeon Haeng Cho, and Weontae Lee. 2014. “Solution Structure of Telomere Binding Domain of AtTRB2 Derived from Arabidopsis Thaliana.” *Biochemical and Biophysical Research Communications* 452 (3): 436–42. https://doi.org/10.1016/j.bbrc.2014.08.095.

Yu, E Y, S E Kim, J H Kim, J H Ko, M H Cho, and I K Chung. 2000. “Sequence-Specific DNA Recognition by the Myb-like Domain of Plant Telomeric Protein RTBP1.” *The Journal of Biological Chemistry* 275 (31): 24208–14. https://doi.org/10.1074/jbc.M003250200.

Yu, Guangchuang, Li-Gen Wang, and Qing-Yu He. 2015. “ChIPseeker: An R/Bioconductor Package for ChIP Peak Annotation, Comparison and Visualization.” *Bioinformatics* 31 (14): 2382–83. https://doi.org/10.1093/bioinformatics/btv145.

Zachová, Dagmar, Miloslava Fojtová, Martina Dvořáčková, Iva Mozgová, Inna Lermontova, Vratislav Peška, Ingo Schubert, Jiří Fajkus, and Eva Sýkorová. 2013. “Structure-Function Relationships during Transgenic Telomerase Expression in Arabidopsis.” *Physiologia Plantarum* 149 (1): 114–26. https://doi.org/10.1111/ppl.12021.

Zellinger, Barbara, and Karel Riha. 2007. “Composition of Plant Telomeres.” *Biochimica et Biophysica Acta* 1769 (5–6): 399–409. https://doi.org/10.1016/j.bbaexp.2007.02.001.

Zhang, Xiaoyu, Oliver Clarenz, Shawn Cokus, Yana V Bernatavichute, Matteo Pellegrini, Justin Goodrich, and Steven E Jacobsen. 2007. “Whole-Genome Analysis of Histone H3 Lysine 27 Trimethylation in Arabidopsis.” *PLoS Biology* 5 (5): e129. https://doi.org/10.1371/journal.pbio.0050129.

Zhang, Yaru, Xuan Yu, and Sheng Zhang. 2025. “Analysis of the Relationships among Telomere–associated Protein–encoding Gene Expression, Tree Age and Telomere Length in Platycladus Orientalis (L.) Franco.” *Tree Genetics & Genomes* 21 (3): 15. https://doi.org/10.1007/s11295-025-01699-5.

Zheng, Si-Yao, Bin-Bin Guan, Dan-Yang Yuan, Qiang-Qiang Zhao, Weiran Ge, Lian-Mei Tan, Shan-Shan Chen, et al. 2023. “Dual Roles of the Arabidopsis PEAT Complex in Histone H2A Deubiquitination and H4K5 Acetylation.” *Molecular Plant* 16 (11): 1847–65. https://doi.org/10.1016/j.molp.2023.10.006.

Zhou, Jin-Xing, Xiao-Min Su, Si-Yao Zheng, Chan-Juan Wu, Yin-Na Su, Zhaodi Jiang, Lin Li, She Chen, and Xin-Jian He. 2022. “The Arabidopsis NuA4 Histone Acetyltransferase Complex Is Required for Chlorophyll Biosynthesis and Photosynthesis.” *Journal of Integrative Plant Biology* 64 (4): 901–14. https://doi.org/10.1111/jipb.13227.

Zhou, Yue, Benjamin Hartwig, Geo Velikkakam James, Korbinian Schneeberger, and Franziska Turck. 2016. “Complementary Activities of TELOMERE REPEAT BINDING Proteins and Polycomb Group Complexes in Transcriptional Regulation of Target Genes.” *The Plant Cell* 28 (1): 87–101. https://doi.org/10.1105/tpc.15.00787.

Zhou, Yue, Francisco J Romero-Campero, Ángeles Gómez-Zambrano, Franziska Turck, and Myriam Calonje. 2017. “H2A Monoubiquitination in Arabidopsis Thaliana Is Generally Independent of LHP1 and PRC2 Activity.” *Genome Biology* 18 (1): 69. https://doi.org/10.1186/s13059-017-1197-z.

Zhou, Yue, Emmanuel Tergemina, Haitao Cui, Alexander Förderer, Benjamin Hartwig, Geo Velikkakam James, Korbinian Schneeberger, and Franziska Turck. 2017. “Ctf4-Related Protein Recruits LHP1-PRC2 to Maintain H3K27me3 Levels in Dividing Cells in

Arabidopsis Thaliana." *Proceedings of the National Academy of Sciences of the United States of America* 114 (18): 4833–38. https://doi.org/10.1073/pnas.1620955114.

Zhou, Yue, Yuejun Wang, Kristin Krause, Tingting Yang, Joram A Dongus, Yijing Zhang, and Franziska Turck. 2018. "Telobox Motifs Recruit CLF/SWN-PRC2 for H3K27me3 Deposition via TRB Factors in Arabidopsis." *Nature Genetics* 50 (5): 638–44. https://doi.org/10.1038/s41588-018-0109-9.

Zündorf, Simone. 2022. "The Role of TRB Interaction Partners in Epigenetic Gene Repression," August.

8 Supplemental Data

Supplementary Table 1, Relevant Genes

Gene Identifier	Gene Symbol	Gene Name
Various	*AL*	*ALFIN1-LIKE*
Various	*ARID*	*AT-RICH INTERACTIVE DOMAIN PROTEIN*
AT3G18610	*ATNUC-L2*	*NUCLEOLIN LIKE 2*
AT2G30580/ AT1G06770/ AT3G23060	*BMI1A, BMI1B, BMI1C*	*BMI1-like genes*
AT2G23380	*CLF*	*CURLY LEAF*
AT2G17290	*CPK6*	*CALCIUM-DEPENDENT PROTEIN KINASE 6*
AT4G14385/ AT1G26470	*EAF6/7*	*ESA1-ASSOCIATED FACTOR 6/7*
AT4G22140	*EBS*	*EARLY BOLTING IN SHORT DAYS*
AT5G11530	*EMF1*	*EMBRYONIC FLOWER 1*
AT5G51230	*EMF2*	*EMBRYONIC FLOWER 2*
Various	*EPCR*	*ENHANCER OF POLYCOMB RELATED PROTEIN*
AT1G16690/ AT1G79020	*EPL1A/B*	*ENHANCER OF POLYCOMB-LIKE 1 A/B*
AT3G20740	*FIE*	*FERTILIZATION-INDEPENDENT ENDOSPERM*
AT2G35670	*FIS2*	*FERTILIZATION-INDEPENDENT SEED 2*
AT5G10140	*FLC*	*FLOWERING LOCUS C*
AT3G04610	*FLK*	*FLOWERING LOCUS K HOMOLOGY DOMAIN*
AT2G43410	*FPA*	*FPA*
AT1G65480	*FT*	*FLOWERING LOCUS T*
AT5G60910	*FUL*	*FRUITFULL*
AT5G64610/ AT5G09740	*HAM1/2*	*Histone acetyltransferases of the MYST family*
AT5G63110	*HDA6*	*HISTONE DEACETYLASE 6*
AT2G27840	*HDT4*	*Histone deacetylase-related protein*
AT1G22950	*ICU11*	*INCURVATA 11*
AT3G24010/ AT1G54390	*ING1/2*	*INHIBITOR OF GROWTH 1/2*
AT4G20400	*JMJ14*	*JUMONJI 14*
AT5G61850	*LFY*	*LEAFY*
AT5G17690	*LHP1*	*LIKE-HETEROCHROMATIN PROTEIN 1*
Various	*MAF1-5*	*MADS AFFECTING FLOWERING 1-5*
AT1G02580	*MEA*	*MEDEA*
AT4G37280/ AT1G02740	*MRG1/2*	*MORF RELATED GENE 1/2*
AT5G58230	*MSI1*	*MULTICOPY SUPPRESSOR OF IRA 1*
AT3G10480/ AT3G10490	*NAC50/52*	*NAC domain containing TF 50/52*
AT5G06310	*POT1b*	*PROTECTION OF TELOMERES 1b*
Various	*PWWP*	*PWWP-DOMAIN INTERACTOR OF POLYCOMB*
AT5G44280/ AT1G03770	*RING1A/RING1B*	*ARABIDOPSIS THALIANA RING 1A/1B*
AT5G42400	*SDG25*	*SET DOMAIN PROTEIN 25*

AT4G39100	*SHL*	*SHORT LIFE*
AT4G0202	*SWN*	*SWINGER*
AT5G16850	*TERT*	*TELOMERASE REVERSE TRANSCRIPTASE*
AT2G17930/ AT4G36080	*TRA1A/B*	*Proteins homologous to Tra1*
AT1G49950	*TRB1*	*TELOMERE REPEAT BINDING FACTOR 1*
AT5G67580	*TRB2*	*TELOMERE REPEAT BINDING FACTOR 2*
AT3G49850	*TRB3*	*TELOMERE REPEAT BINDING FACTOR 3*
AT1G17520	*TRB4*	*TELOMERE REPEAT BINDING FACTOR 4*
AT1G72740	*TRB5*	*TELOMERE REPEAT BINDING FACTOR 5*
Various	*TRFL1-10*	*TRF-LIKE 1-10*
AT2G40930	*UBP5*	*UBIQUITIN-SPECIFIC PROTEASE 5*
AT5G66000	*UTI1/HTH3*	*UNSTRUCTURED TRB INTERACTOR 1 / HELIX-TURN-HELIX 3*
AT4G35510	*UTI2/HTH2*	*UNSTRUCTURED TRB INTERACTOR 2 / HELIX-TURN-HELIX 2*
AT2G17540	*UTI3/HTH1*	*UNSTRUCTURED TRB INTERACTOR 3 / HELIX-TURN-HELIX 1*
AT2G30470/ AT4G32010	*VAL1/2*	*VIVIPAROUS1/ABI3-LIKE 1/2*
AT1G57820/ AT1G66050/ AT5G39550	*VIM1/VIM2/VIM3*	*VARIANT IN METHYLATION 1/2/3*
AT4G16845	*VRN2*	*VERNALIZATION 2*

Supplementary Table 2, Generated Alleles

Gene	AGI	Background	sgDNA(s)	Edit	Allele	Effect
UTI1	AT5G66000	Col-0	sgUTI1-1 sgUTI1-2	+14 bp @ sgUTI1-2	*uti1-3*	Frameshift
UTI1	AT5G66000	Col-0	sgUTI1-1 sgUTI1-2	+14 bp @ sgUTI1-2	*uti1-4*	Frameshift
UTI1	AT5G66000	*trb1-2 trb3-2*	sgUTI1-1 sgUTI1-2	-5 bp @ sgUTI1-2	*uti1-8*	Frameshift
UTI1	AT5G66000	*trb1-2 trb3-2*	sgUTI1-1 sgUTI1-2	+1 bp @ sgUTI1-2	*uti1-9*	Frameshift
UTI1	AT5G66000	*trb1-2 trb3-2*	sgUTI1-1 sgUTI1-2	+1 bp @ sgUTI1-2	*uti1-10*	Frameshift
UTI1	AT5G66000	*trb2-3 trb3-2*	sgUTI1-1 sgUTI1-2	-31 bp @ sgUTI1-2	*uti1-11*	Frameshift
UTI1	AT5G66000	*trb2-3 trb3-2*	sgUTI1-1 sgUTI1-2	+118 bp @ sgUTI1-2 +1 @ sgUTI1-1	*uti1-12*	Frameshift + Disruption
UTI1	AT5G66000	*trb2-3 trb3-2*	sgUTI1-1 sgUTI1-2	-35 bp @ sgUTI1-2 +1 @ sgUTI1-1	*uti1-13*	Frameshift + Disruption
UTI1	AT5G66000	*trb1-2*	sgUTI1-1 sgUTI1-2	-56 bp @ sgUTI1-2	*uti1-15*	Frameshift
UTI1	AT5G66000	*trb3-2*	sgUTI1-1 sgUTI1-2	-4 bp @ sgUTI1-1 +5 bp @ sgUTI1-1	*uti1-16*	Frameshift

Supplementary Table 3, List of Oligonucleotides

Primer Name	Sequence	Use
SZ_456 - seqUTI1-F	CGCGTAAGATCTGATAGGGT	Genotyping of UTI1
SZ_390 - seqCRISPR-66R	CCAAATCATTTGGACTTTGG	Genotyping of UTI1
FT1056 – TRB2 WT	ACTTCCCCCGGAGGTTCTG	Genotyping of WT TRB2
Krause-249 - dCAPS_TRB2_R1	ATTGCCTCAAAGATGATCTTATCC	Genotyping of WT TRB2 and trb2-3
FT1057 – trb2-3	ACTTCCCCCGGAGGTTCTTG	Genotyping of trb2-3
SZ_387 - trb3-2_LP	ATGGTTCACGAGAAACCTGTG	Genotyping of WT TRB3
SZ_388 - trb3-2_RP	AGGACAACAGATTGATGCACC	Genotyping of WT TRB3 and trb3-2
SZ_001 - SALK_LBb1.3	ATTTTGCCGATTTCGGAAC	Genotyping of trb3-2 and trb1-2
YZhou-041 - SALK_001540 RP	ATGCCACCACAATAAATCTCG	Genotyping of WT TRB1 and trb1-2
YZhou-040 - SALK_001540 LP	TTAGCGGAGTCTTGTACCTGC	Genotyping of WT TRB1
sgUTI1-1	ATTGAAGCATCTGCAATCTCCTGAGTTT	Guide DNA targeting *UTI1*
sgUTI1-2	ATTGGCCTCCTTTCCTCCTAACCAGTTT	Guide DNA targeting *UTI1*